Optimization of PHB production in *Methylosinus trichosporium* OB3b

by

Jorge Adalberto Zaldívar Carrillo

A thesis submitted in partial fulfillment of the requirements for the degree of

Master of Science

in

Chemical Engineering

Department of Chemical and Materials Engineering
University of Alberta

Abstract

The utilization of waste materials to generate value-added products is an appealing prospect that can generate economic and environmental benefits. When the end product of this process is itself environmentally friendly, the benefits escalate. Such is the case of the present work. *M. trichosporium* OB3b is a bacterium that can metabolize methane—a potent greenhouse gas and common industrial waste—and methanol—another common industrial waste—to produce polyhydroxybutyrate (PHB)—a naturally occurring polymer. PHB is the focus of intense research because it is completely biodegradable into harmless compounds and exhibits properties similar to those of other relevant polymers.

The growth of *Methylosinus trichosporium* OB3b and its production of PHB was studied and characterized. Empirical second order response surface models were developed to predict three responses—cell dry weight, PHB concentration and PHB cell content—as a function of three independent variables—the carbon source, the nitrogen source and the nitrogen-to-carbon ratio. Methane, methanol and mixtures of them were investigated as carbon sources. Ammonium, nitrate and mixtures of them were investigated as nitrogen sources. Nitrogen-to-carbon ratios in the molar range from 0.005 to 1.0 were investigated. The effect of oxygen was also assessed. A maximum response for PHB concentration was predicted at a composition of 30%mol of methane and 70%mol of methanol as carbon source, 100% nitrate as nitrogen source, and a 0.017 nitrogen-to-carbon ratio, with a predicted concentration of 40 mg/L of PHB. The prediction was confirmed experimentally obtaining a PHB concentration of 48.7 ± 8.3 mg/L, with a PHB cell content of 52.5% ± 6.3%. The predictions of the models for cell dry weight and for PHB cell content failed experimental confirmation due to the low signal-to-noise ratio that resulted from the low cell densities worked with, but important behavioural trends were predicted and confirmed. Greater cell dry weights were predicted and observed with ammonium at high nitrogen-to-carbon ratios. The cell dry weight was predicted and observed to be independent of the

carbon source used when the nitrogen source was nitrate. On the other hand, the preferred nitrogen source for PHB accumulation was found to vary depending on the carbon source used. For methane, ammonium was preferred; for methanol, nitrate was preferred. Nitrogen-to-carbon ratios of 0.017 were also found to promote PHB accumulation. A synergistic effect of the carbon source was found on PHB concentration, in that certain mixtures of methane and methanol resulted in greater accumulation of PHB than when either of the carbon sources was used separately. An important effect of oxygen was found, in that the availability of a great stoichiometric excess of it favored the accumulation of PHB. In the absence of this excess, accumulated PHB was metabolized and depleted to various levels.

Acknowledgements

First and foremost, to God, for the gift of life and love. You speak in many ways to each of us, so that we, through our personal journey of discovery, may marvel in the wonders of Your creation and come to You.

To my supervisor, Prof. Dominic Sauvageau. Thank you for your patience, guidance and support, and for believing in me in the first place and welcoming me into your research group.

To my co-supervisor, Prof. Lisa Stein. Thank you for your time, support and commitment.

To the Sauvageau's lab group. Thank you, guys, I learned a lot from you. Special thanks to Matthew Teel. Your idea for sealing the threads was great and your help with the experiments is appreciated. Thanks also to Preetam Anbukarasu for kindly providing me with purified PHB, and to Dimitri Kits, whose comment on the impossibility of having two limiting conditions at once started me on the track of the oxygen effects. Good luck to you all.

To the National Council of Science and Technology, Mexico (CONACyT), the Mexican Secretariat of Public Education (SEP), the Government of Mexico, the Biorefining Conversions Network, Alberta Innovates Bio Solutions, Ms. Flora Greenghalgh (through the Captain Thomas Farrell Greenhalgh Memorial Graduate Scholarship), the Faculty of Graduate Studies and Research of the University of Alberta and the Graduate Student's Association of the University of Alberta for their financial support.

To all the good people that selflessly helped us during our stay in Canada, especially to Cloribel Santiago, Cecilia Guzmán, Monica Patarroyo and Dr. Jorge Perez-Parada.

To my extended family, my parents, brothers and sisters, in-laws, nephews and nieces, for their love and support.

To my daughters, both Lucero who accompanied me to these Northern latitudes in this adventure as well as Georgis that always kept in touch, for their love and support, for their tenderness that often lightened the load, for cheering me up. You are really a blessing. I love you.

Y muy en especial a ti, Minita, mi amada esposa, compañera de mi vida y mi más grande bendición. Gracias por apoyarme y por creer en mí, por animarme y acompañarme siempre y, especialmente, durante este posgrado. Este logro es tan tuyo como mío. Gracias por tu entrega

generosa y sin medida. Gracias por tu amor incondicional. Gracias por estar siempre presente para mí, incluso en el tiempo y en la distancia. Realmente no habría podido hacer esto sin ti. *Juntos para siempre… para siempre juntos.*

Table of contents

List of tables

List of figures

List of abbreviations

A.	Alcaligenes
AMS	ammonium mineral salts
ANOVA	analysis of variance
atm	atmosphere
C	carbon
°C	degree Celsius
CDW	cell dry weight
CH_3OH	methanol
CH_4	methane
d	day
Da	dalton
EDTA	ethylenediaminetetraacetic acid
EPA	Environmental Protection Agency, USA
Eq.	equation
F	Fisher's F
FID	flame ionization detector
g	gram
h	hour
ICI	Imperial Chemical Industries
K	kelvin

kPa	kilopascal
kt	kilotonne
L	litre
m	metre
M.	Methylosinus, Methylocystis
MDH	methanol dehydrogenase
mg	milligram
min	minute
mL	millitre
mM	millimolar
MMO	methane monooxygenase
mmol	millimole
µm	micrometre
µM	micromolar
mol	mole
Mt	megatonne
N	nitrogen
NH_4^+	ammonium
nlMS	nitrogenless mineral salts
nm	nanometre
NMS	nitrate mineral salts

NO_3^-	nitrate
O_2	oxygen
OD	optical density
OMeGA	Organization of Methanotroph Genome Analysis
P4HB	poly-4-hydroxybutyrate
PHB	polyhydroxybutyrate
PHBV	poly(3-hydroxybutyrate-co-3-hydroxyvalerate)
PHV	polyhydroxyvalerate
rpm	revolutions per minute
RSM	response surface methodology
SFCA	surfactant-free cellulose acetate
sym.	symmetric
t	Student's t, tonne, time
USA	United States of America
WTE	Whittenbury trace elements
yr	year

1 Introduction

Our world is subject to a multitude of environmental stresses due to the polluting activities of the human race: land, water, air pollution; industrial, agricultural, domestic discharges. Among the air contaminants released daily into the Earth's atmosphere is the potent greenhouse gas methane. Produced both by human activities and by natural means, it is second in prevalence as a greenhouse gas only to carbon dioxide. Its lifetime in the atmosphere is twelve years, but methane's impact on climate change is over twenty times greater than carbon dioxide's over a period of one hundred years (EPA 2014).

Other important contaminants are plastics. In 2013, almost 300 million metric tonnes were produced worldwide (Statista 2014). Much of that production ends up in our land, rivers and oceans. Biodegradable alternatives are much needed: plastics that would not only break down into smaller particles of the same material but that would actually decompose changing its chemical composition to yield innocuous final degradation products.

Bacteria—and archaea—are ubiquitous and numerous; it is estimated that $4\text{-}6 \times 10^{30}$ inhabit Earth (Whitman et al. 1998). Evolution has doted them with an assortment of survival strategies and versatile metabolism and we can find them thriving in the more remote areas and feeding from a wide variety of substrates. The idea of using the metabolic versatility that bacteria have evolved through millions of years to somehow eliminate these environmental problems is attractive. As it turns out, there exist bacteria — methanotrophs — that can use methane as their feedstock to produce biodegradable plastics.

The object of study of this work is one such bacteria, *Methylosinus trichosporium* OB3b, that not only can consume methane but that can also produce the biodegradable polymer polyhydroxybutyrate (PHB). The focus will be on optimizing conditions to lead to greater biomass concentrations and PHB production levels. This study will provide valuable information for the development of industrial processes for the conversion of methane to PHB.

2 Literature review

2.1 Polyhydroxyalkanoates and polyhydroxybutyrate

Polyhydroxyalkanoates (PHAs) are biopolymers synthesized by a range of bacteria. They accumulate inside the cellular body to function as a reserve of carbon, energy and reducing equivalents. Polyhydroxybutyrate (PHB) was the first PHA discovered (Lemoigne 1926 cited by Luengo et al. 2003) and is the most widely studied and characterized (Khosravi-Darani et al. 2013). Chemically, it is a polyester and has properties similar to those of polypropylene (Madison and Huisman 1999). Schematics of the chemical structure of PHB and a few selected PHAs are depicted in Figure 2-1.

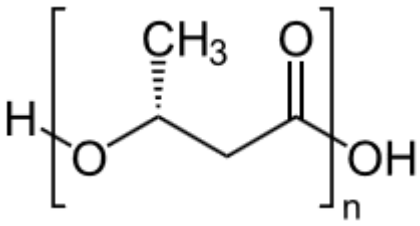

polyhydroxybutyrate (PHB)

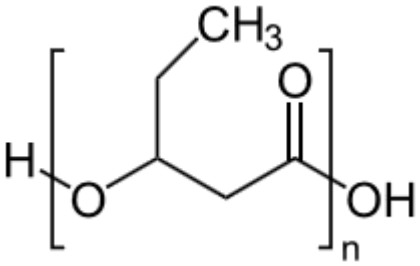

polyhydroxyvalerate (PHV)

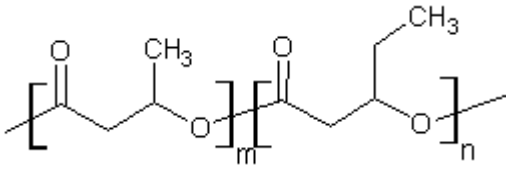

poly(3-hydroxybutyrate-co-3-hydroxyvalerate) (PHBV)

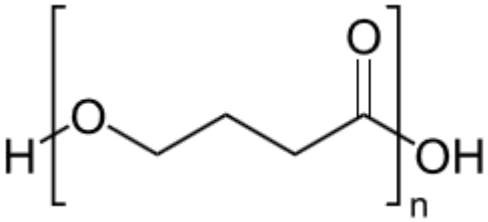

poly-4-hydroxybutyrate (P4HB)

Figure 2-1. Chemical structures of some PHAs.

More than 300 microorganisms synthesizing PHAs have been identified, among them hydrogen-oxidizing bacteria, nitrogen-fixing bacteria, pseudomonades and methyloprophs (Volova 2004). These which synthesize PHAs of molecular weights ranging from 10^3 to $>10^6$ Da (Anderson and Dawes 1990; Lee 1996). PHB is produced by many different bacteria from substrates as diverse as carbohydrates, ethanol, acetate, methane and mixtures of hydrogen and carbon dioxide, among others (Holmes 1988).

After being extracted and purified from biomass, PHB can be processed by conventional extrusion and moulding methods (Byrom 1987) since it behaves as a normal crystalline thermoplastic. In addition, it is completely biodegradable into nontoxic compounds (Khanna and Srivastava 2005). This property makes it desirable for uses in general disposable products but also in medical, veterinary and horticultural applications (Holmes 1988).

PHB was first commercially produced by ICI in 1982, using *A. eutrophus* grown heterotrophically using carbohydrates as substrate. It was commercialized under the trademark Biopol (Anderson and Dawes 1990). Nowadays, various companies produce PHB using carbohydrates as substrate. Barriers to further its commercialization and expansion of its applications include the relatively high costs of the fermentation and product recovery processes, and the costs of the sugar substrates (Lenz and Marchessault 2005; Marvi and Mahdi 2011). In fact, the cost of the sugars used as feedstock can amount up to 30% of the total cost of PHB production (Choi and Lee 1997). Consequently, alternatives substrates are the focus of much research (Lenz and Marchessault 2005; Marvi and Mahdi 2011).

World production of PHAs has been consistently increasing in recent years, going from an estimated 3 kt/yr in 2000 (Lichtenthaler 2000) to 34 kt/yr of production capacity in 2013 (Institute for Bioplastics and Biocomposites 2014). In fact, PHAs now represent 2.1% of the global biopolymer annual production capacity of 1.622 Mt (Institute for Bioplastics and Biocomposites 2014). Production is expected to continue to increase significantly, quadrupling between 2011 and 2020 and surpassing the expected growth of 300% for bioplastics as a whole (nova Institute for Ecology and Innovation 2013).

2.2 Methylotrophs and methanotrophs

Methylotrophs form a varied group of bacteria that can grow on single-carbon compounds as their sole source of carbon and energy. The most simple of the single-carbon compounds is methane, and the subset of methylotrophs that can grow on it are called methanotrophs. Methylotrophs have been found in marine and fresh waters environments, tundra permafrost, hot springs, plants and even the human body (as opportunistic pathogens) (Kelly and Wood 2010).

Several methylotrophs, specifically α-proteobacteria, accumulate PHB and/or other PHAs. It has been reported that deprivation of one or several nutrients—such as oxygen, nitrogen, phosphorous or

magnesium—can boost PHB production in different microorganisms (Doronina et al. 2008; Wendlandt et al. 2001).

2.2.1 *Methylosinus trichosporium* OB3b

Methylosinus trichosporium OB3b—first isolated in 1970 (Whittenbury et al. 1970)—is a methylotrophic bacterium from the Methylocystaceae family (Murrell 2010). These Gramm negative, α-proteobacteria are obligate methylotrophs that can use either methane or methanol as their carbon and energy source (Bowman 2005). Park et al. (1991) reported optimal growth of *M. trichosporium* OB3b to occur between 30 to 34°C, at pH ranging from 6.0 to 7.0, and a phosphate concentration from 10-40 mM. In their study, the authors also observed a long lag phase preceding the exponential growth phase, and reported that it was shortened by the supplementation of carbon dioxide.

M. trichosporium OB3b has received attention for its uses in bioremediation of sites contaminated with halogenated hydrocarbons (Lontoh and Semrau 1998; Murrell 2010; Park et al. 1991), single-cell protein production (Murrell 2010), and PHB production. It is also considered one of the best characterized methanotrophs (Murrell 2010) and a model microorganism for research on methanotrophy (Rostkowski et al. 2013).

Carbon assimilation in *M. trichosporium* OB3b occurs when methane is first oxidized to methanol via the methane monooxygenase (MMO) enzyme. The use of methanol as carbon source precludes the first oxidation step of methane to methanol and can lead to suppression of the expression of MMO, which is recovered upon liquid culturing on methane (Adegbola 2008). Methanol is further oxidized to formaldehyde, in a reaction catalyzed by methanol dehydrogenase (MDH). MDH can be inhibited by phosphate, cyclopropanol, high concentrations of sodium chloride or carbon dioxide. In these cases, methanol accumulates in the culture (Duan et al. 2011). Formaldehyde enters the serine cycle where the carbon is assimilated (Murrell 2010). Alternatively to enter the serine cycle for assimilation, formaldehyde can be further oxidized to formic acid and all the way to carbon dioxide for energy production.

2.2.1.1 Methanol as carbon source

Methanol is generally regarded as an inhibitory substrate (Hou 1984). Accordingly, for most cell types, high cell densities, which require high amounts of carbon source, are not possible in batch cultures. To circumvent this problem, strategies such as feed batch cultivation are used to limit the instantaneous concentration of methanol below inhibitory levels (Kim et al. 2003).

Although *M. trichosporium* OB3b has been shown to be able to grow on methanol at concentrations reaching up to 40 g/L (initial concentration of batch), growth was only seen after a long lag phase (Yu et al. 2009). In addition, the authors reported significant metabolic inhibition for methanol concentrations exceeding 3 g/L.

Adegbola (2008) reported obtaining a cell dry weight of 62 g/L in fed-batch cultivation of *M. trichosporium* OB3b when using methanol as substrate, with a biomass yield of 0.3 g dry weight per g of methanol.

2.2.1.2 Methane as carbon source

On the other hand, methane is a gas and its rate of consumption is limited by its mass transfer from the gas phase into the liquid phase and into the cells. This also impacts the attainment of high cell densities in cultures.

The growth yield of *M. trichosporium* OB3b growing on methane has been reported to range between 0.4-0.5 g cells dry weight per g of methane (Bowman and Sayler 1994).

In his review, Murrell (2010) reported cell dry weights of 1-5 g/L when growing on methane in batch or continuous cultures, while Shah et al. (1996), on their part, reported a maximum cell density of 18 g/L for batch cultures, also when growing on methane.

Lontoh and Semrau (1998) grew batch liquid cultures of *M. trichosporium* OB3b on methane with cell densities, measured by the concentration of protein, from 0.035 to 0.1 mg of protein per mL. They reported no mass transfer limitation when the headspace concentration of methane was such as to maintain a calculated methane concentration of 32 µM in the liquid phase.

Doronina et al. (2008) reported a dry biomass yield of 20 g/L after 120 h of culture. In addition, a PHB content of 30% was obtained when growing the culture in two stages: biomass growth and PHB biosynthesis under nitrogen deficiency. These cultures were grown with methane under normal atmospheric conditions of pressure.

2.2.2 Nitrogen source

2.2.2.1 Fixation of nitrogen gas

Under low oxygen conditions, *M. trichosporium* OB3b can fix atmospheric nitrogen (Bowman 2005). Vorob'ev and Dedysh (2008) reported this process occurred only when the partial pressures of oxygen in the gas phase ranged from 0.05 to 0.15 bar. However, even if *M. trichosporium* OB3b could fix nitrogen at higher oxygen partial pressures—0.15 to 0.17 bar—, it grew only after multiple transfers in nitrogen-free medium. Additionally, the greatest specific growth rates were obtained when the oxygen partial pressures was below 0.02 bar (Dedysh et al. 2004). Rostkowski et al. (2013) also found that oxygen at partial pressures at or in excess of 0.3 atm inhibited the assimilation of gaseous nitrogen.

2.2.2.2 Nitrate

The medium typically recommended for growing *M. trichosporium* OB3b is nitrate mineral salts (NMS) or, which contains potassium nitrate at a concentration of 10 mM (Whittenbury et al. 1970; Bowman 2005). Asenjo and Suk (1986) reported no PHB accumulation after 340 h of culture when using 0.85 g/L of sodium nitrate with methane as the carbon source. Reducing the sodium nitrate concentration to 0.2125 g/L still resulted in no accumulation after 90 and 190 h of culture, but at 310 h the PHB accumulation was 0.08 g/L for a cell dry weight of 3.0 g/L.

Two phases of different growth rate were observed by Park et al. (1991) when continuously adding methane to cultures of *M. trichosporium* OB3b grown in NMS: a fast phase followed by a slow phase. The cell density at the transition from the fast growth phase to the slow one was proportional to the initial concentration of nitrate in the culture medium and the transition time was coincident with the depletion of nitrate in the medium. This relationship held for nitrate concentrations in the range of 5-20 mM. This diauxic growth was attributed to a metabolic switch in nitrogen source from nitrate to atmospheric nitrogen.

2.2.2.3 Ammonium

Ammonium can also be used as a nitrogen source, although it is an inhibitor of methane oxidation since it competes with methane for the active sites of MMO (Dunfield and Knowles 1995). Furthermore, the oxidation products of ammonium, hydroxylamine and nitrite, are toxic to methanotrophic bacteria. Moreover, a high concentration of ammonium salts can result in osmotic stress to the cells (Bodelier and Laanbroek 2004).

Veillette et al. (2011) reported that an increase in ammonium concentration decreased biooxidation of methane. When using total nitrogen fixed at 0.5 g/L in a mixed culture containing methanotrophs and methylotrophs as well as nitrifying and denitrifying bacteria, a "tolerance limit" of 0.1-0.2 g/L of ammonium nitrogen was observed.

When growing *M. trichosporium* OB3b on ammonium as the nitrogen source (and methane as the carbon source), Doronina et al. (2008) reported two distinct phases in the cultures: biomass growth and PHB accumulation, the last one triggered by the "abrupt decrease in ammonium nitrogen concentration" when switching the pH control from ammonium hydroxide to sodium hydroxide. A 30% content of PHB in biomass was reported for cultures in batch fermenters (6 g PHB/L in 20 g CDW/L cultures). PHB contents of the biomass were reported as 3-5% in the log growth phase, and 15-20% in the polymer biosynthesis phase; but no time profile of PHB content or concentration was provided.

Serafim et al. (2004) reported that, for a mixed culture of non-methanotrophs, cell growth and PHB accumulation occurred simultaneously until depletion of nitrogen, after which carbon uptake was accumulated as PHB. But the authors were also quick to point out that different bacteria have different PHB storage mechanisms. It was also reported that in the absence of ammonium, the degradation of the accumulated PHB was slower than when nitrogen was present. On the other hand, (Pieja et al. 2011) reported rapid PHB depletion, leading to cell growth and replication in *M. parvus* OBBP, when both nitrogen and carbon were externally supplied, but not when only nitrogen and no additional carbon was supplied; theorizing co-metabolism of PHB and the exogenous carbon source was at cause. Introducing cyclic limitations of nitrogen, nitrogen and methane, and nitrogen and oxygen, in mixed-methanotroph cultures produced similar results: accumulated PHB from the previous cycle was consumed when fresh nitrogen source, in the form of nitrate, was added, and accumulation resumed once the additional nitrogen was depleted (Pieja et al. 2012).

Rostkowski et al. (2013) encountered more variability in their results when changing the nitrogen source from nitrate to ammonium. They attributed the increased variability to the reducing equivalents necessary for the reduction of hydroxylamine to ammonium in a hypothesized "futile" cycle of hydroxylamine detoxification suggested by the presence of gene clusters in *M. trichosporium* OB3b that would make this cycle possible (Stein et al. 2010).

2.2.3 Methylotroph stoichiometry

Table 2-1 provides the stoichiometry of methane utilization by methanotrophic bacteria, depending on the nitrogen source (Rostkowski et al. 2013).

Table 2-1. Stoichiometric equations used to describe methanotrophic growth and PHB production (Rostkowski et al. 2013, used with permission).

Nitrogen source	Total reaction
Growth phase	
Nitrate (NO_3^-)	$\frac{1}{4}\mathrm{CH_4} + \left(\frac{1}{4}+\frac{f_e}{4}\right)\mathrm{O_2} + \frac{f_s}{28}\mathrm{NO_3^-} + \left(\frac{29f_s}{28}+f_e-1\right)\mathrm{H^+} \longrightarrow \left(\frac{1}{4}-\frac{5f_s}{28}\right)\mathrm{CO_2} + \left(\frac{f_e}{2}+\frac{11f_s}{28}\right)\mathrm{H_2O} + \frac{f_s}{28}\mathrm{C_5H_7O_2N}$
Ammonium (NH_4^+)	$\frac{1}{4}\mathrm{CH_4} + \left(\frac{1}{4}+\frac{f_e}{4}\right)\mathrm{O_2} + \frac{f_s}{23}\mathrm{HCO_3^-} + \frac{f_s}{23}\mathrm{NH_4^+} + \left(\frac{20f_s}{23}+f_e-1\right)\mathrm{H^+} \longrightarrow \left(\frac{1}{4}-\frac{4f_s}{23}\right)\mathrm{CO_2} + \left(\frac{f_e}{2}+\frac{9f_s}{23}\right)\mathrm{H_2O} + \frac{f_s}{23}\mathrm{C_5H_7O_2N}$
Nitrogen gas (N_2)	$\frac{1}{4}\mathrm{CH_4} + \left(\frac{1}{4}+\frac{f_e}{4}\right)\mathrm{O_2} + \frac{f_s}{50}\mathrm{N_2} \longrightarrow \left(\frac{1}{4}-\frac{f_s}{5}\right)\mathrm{CO_2} + \left(\frac{f_e}{2}+\frac{8f_s}{25}\right)\mathrm{H_2O} + \frac{f_s}{25}\mathrm{C_5H_7O_2N}$
PHB production phase	
No nitrogen	$\frac{1}{4}\mathrm{CH_4} + \left(\frac{1}{4}+\frac{f_e}{4}\right)\mathrm{O_2} \longrightarrow \left(\frac{1}{4}-\frac{4f_s}{18}\right)\mathrm{CO_2} + \left(\frac{f_e}{2}+\frac{f_s}{3}\right)\mathrm{H_2O} + \frac{f_s}{18}\mathrm{C_4H_6O_2}$

In the table, f_e and f_s are the substrate partitioning parameters; f_e is the fraction of the reducing equivalents (electrons) available from the carbon source (electron donor) that is used for energy production while f_s is the fraction of the reducing equivalents that is used for cell synthesis. The cell synthesis material is biomass (with an empirical formula $C_5H_7O_2N$) during the growth phase and PHB (with an empirical formula $C_4H_6O_2$) during the PHB producing phase. These fractions add to one, as per Eq. 2-1.

$$f_e + f_s = 1 \qquad \text{Eq. 2-1}$$

The oxygen-to-carbon ratio stemming from this equations is dependent on the equilibrium between f_e and f_s and is given by $(1 + f_e)$, for both growth and PHB synthesis. This contrasts with the statement by Asenjo and Suk (1986) that this ratio is constant and equal to 1.50. Rostkowski et al. (2013) listed values of 0.66 ± 0.03 and 0.56 ± 0.17 for f_s for nitrate and ammonium as the nitrogen source, respectively, with methane as the carbon source. These values would yield oxygen-to-carbon ratios close to 1.50.

Similar equations for growth on methanol are not provided, but they can be calculated by the method outlined by McCarty (1975) to produce the equations shown in Table 2-2.

Table 2-2. Stoichiometry of *M. trichosporium* OB3b growth using methanol as the carbon source.

Nitrogen source	Total reaction
Growth phase	
Nitrate (NO_3^-)	$\frac{1}{6}CH_3OH + \frac{f_e}{4}O_2 + \frac{f_s}{28}NO_3^- + \left(\frac{29f_s}{28} + f_e - 1\right)H^+ \longrightarrow \left(\frac{1}{6} - \frac{5f_s}{28}\right)CO_2 + \left(\frac{f_e}{2} + \frac{11f_s}{28} - \frac{1}{6}\right)H_2O + \frac{f_s}{28}C_5H_7O_2N$
Ammonium (NH_4^+)	$\frac{1}{6}CH_3OH + \frac{f_e}{4}O_2 + \frac{f_s}{20}NH_3 + \left(\frac{20f_s}{23} + f_e - 1\right)H^+ \longrightarrow \left(\frac{1}{6} - \frac{f_s}{4}\right)CO_2 + \left(\frac{f_e}{2} + \frac{2f_s}{5} - \frac{1}{6}\right)H_2O + \frac{f_s}{20}C_5H_7O_2N$

2.3 Response surface methodology

Response surface methodology (RSM) is an incremental optimization strategy used to explore the space of two or more explanatory or independent variables by statistically approximating a model of the relationship between them and one or more independent variables or responses within a properly delimited region (Myers et al. 2009; NIST/SEMATECH 2013; Mason et al. 2003; Cornell 2002).

2.3.1 Modelling

To model the response, an empirical model is built to approximate the true functional relationship between the dependent and independent variables. The approximating function usually takes the form of a polynomial. That is, the true relationship is an unknown function f of the natural variables ξ_i

$$y = f(\xi_1, \xi_2, \dots, \xi_k) + \epsilon \qquad \text{Eq. 2-2}$$

The ξ_i variables are called natural because they are expressed in natural units. It is customary, in response surface methodology to use coded variables, that is, to transform the natural variables, by simple mathematical manipulations, so that all the independent variables are dimensionless, and have a mean of zero and the same standard deviation. This makes the comparison of the magnitude of the effects of the variables easier by just comparing the magnitude of the estimated coefficients.

If $\xi_{i,min}$ and $\xi_{i,max}$ are the extreme values that the natural variable ξ_i would take in the experimental space, a standard transformation, or coding, would be to subtract the mean and divide the difference by half the span of the experimental range

$$x_i = \frac{(\xi_i - \frac{\xi_{i,min} + \xi_{i,max}}{2})}{\frac{\xi_{i,max} - \xi_{i,min}}{2}} \qquad \text{Eq. 2-3}$$

This would result in extreme values for the coded variable x_i of $x_{i,min} = -1$ and $x_{i,max} = +1$.

The true relationship can now be written in terms of the coded variables x_i as

$$y = g(\mathrm{x}_1, x_2, \dots, x_k) + \epsilon \qquad \text{Eq. 2-4}$$

which would still be unknown. Independently of the complexity this true relationship may have, it is usually modelled, over a relatively small region, by a low order polynomial. The use of first order, first order with interaction, or second order polynomials is frequent.

The form of the first order model is

$$\hat{y} = b_0 + b_1 x_1 + b_2 x_2 + \cdots + b_k x_k \qquad \text{Eq. 2-5}$$

If terms are added to account for interaction among the variables, the model takes the form

$$\hat{y} = b_0 + b_1 x_1 + b_2 x_2 + \cdots + b_k x_k + b_{12} x_1 x_2 + \cdots + b_{1k} x_1 x_k + b_{23} x_2 x_3 + \cdots + b_{(k-1)k} x_{k-1} x_k \qquad \text{Eq. 2-6}$$

which can also be written as

$$\hat{y} = b_0 + \sum_{i=1}^{k} b_i x_i + \sum_{i=1}^{k} \sum_{j>i}^{k} b_{ij} x_i x_j \qquad \text{Eq. 2-7}$$

If the curvature is considerable enough not to be captured by a first order polynomial, even with interaction terms, a second order model can be used

$$\hat{y} = b_0 + \sum_{i=1}^{k} b_i x_i + \sum_{i=1}^{k} b_{ii} x_i^2 + \sum_{i=1}^{k} \sum_{j>i}^{k} b_{ij} x_i x_j \qquad \text{Eq. 2-8}$$

A second order model is, in many cases, a good enough approximation since it can represent a versatile variety of shapes with different curvatures.

The rationale behind the use of a polynomial as an approximating function is that it is equivalent to the truncation of the Taylor series expansion of the unknown function g at the first or second order terms, depending on the model selected. In all cases, the parameters b_i are estimated from the experimental results by means of linear regression.

2.3.2 Optimization

Since the second order model provides surfaces with curvature, there is the possibility that a local maximum or minimum—the stationary point—occurs within the experimental region. Another possibility is that the stationary point is neither a local maximum nor a local minimum, in which case, it is called a saddle point. One of the goals of response surface methodology is the localization and identification of the stationary point.

The stationary point, if it exists, would be located at the solution to the system of equations

$$\frac{\partial y}{\partial \mathbf{x}} = 0 \qquad \text{Eq. 2-9}$$

Eq. 2-8 can be rewritten as:

$$\hat{y} = b_0 + \mathbf{x'b} + \mathbf{x'}\widehat{\mathbf{B}}\mathbf{x} \qquad \text{Eq. 2-10}$$

where $\mathbf{x'b}$ represents the summation of the first order terms in matrix form

$$\mathbf{x'b} = \begin{bmatrix} x_1 & x_2 & \cdots & x_k \end{bmatrix} \begin{bmatrix} b_1 \\ b_2 \\ \vdots \\ b_k \end{bmatrix} \qquad \text{Eq. 2-11}$$

and $\widehat{\mathbf{B}}$ is the symmetric matrix

$$\widehat{\mathbf{B}} = \begin{bmatrix} b_{11} & b_{12}/2 & \cdots & b_{1k}/2 \\ & b_{22} & \cdots & b_{2k}/2 \\ & & \ddots & \vdots \\ \text{sym.} & & & b_{kk} \end{bmatrix} \qquad \text{Eq. 2-12}$$

so that in $\mathbf{x'}\widehat{\mathbf{B}}\mathbf{x}$ the diagonals elements contribute with the quadratic terms, and the off-diagonal elements with the interaction terms.

Combining Eq. 2-9 and Eq. 2-10 and solving yields the position of the stationary point:

$$\mathbf{x}_s = -\frac{1}{2}\widehat{\mathbf{B}}^{-1}\mathbf{b} \qquad \text{Eq. 2-13}$$

The analysis of the eigenvalues of matrix $\widehat{\mathbf{B}}$—$\lambda_1, \lambda_2, \ldots, \lambda_k$—gives an indication of the nature of the stationary point, specifically, the signs determine whether the stationary point is a minimum (all λ_i positive), a maximum (all λ_i negative), or a saddle point (λ_i with mixed signs). If the stationary point does not exist, is located outside of the experimental region, or is a saddle point, the optimum would be located along a boundary of the design region and can be determined by numerical methods.

2.3.3 Experimental designs for response surfaces

There are numerous experimental designs appropriate for fitting response surfaces, in particular for second order models. Only three popular designs will be mentioned herein.

The **central composite design** (Figure 2-2a) is formed by the combination of a factorial design (usually a fractional factorial) augmented with several replicates of the center point, and a set of axial (or "star") points. It provides the minimum of three levels for each variable necessary for the fitting of a second order model. The factorial points are located on the vertices of the cube and represent combinations of the factors at the ±1 levels in coded units. There is a point at the center of the design region where all the coded variables assume the value of 0. Projected through this central point and extending equally in both directions through the centres of the cube faces are the axial points at a distance $\alpha > 1$ from the centre. These points have the values $\pm\alpha$ for one of the variables and 0 for the others. The central composite design provides good predictions over the entire design space but five levels are required for each of the variables and the axial range extends beyond the range of the original factorial, such that in some cases it would not be practical, or even possible, to operate at those levels. The central composite can be scaled down in such a form that the axial points fall within the design region (inscribed central composite); in this case, the factorial points fall inside the design region and prediction power is lost at the corners.

The **face-centered central composite design** (Figure 2-2b) is a special case of the central composite design in which $\alpha = 1$, and the axial points lay on the centres of the faces of the cube (or hypercube if there are more than three independent variables).

The face centered central composite design can also provide predictions of good quality over the entire experimental region. It is not rotatable, as opposed to the central composite design, meaning that the variance of the predictions is not a function only of the distance from the centre of the design. All the points fall within the range of the original factorial and information on the combination of extreme factor levels at the corners of the design region is gathered.

Another popular design for response surfaces is the **Box-Behnken design (**Figure 2-2c). The design points fall on the centres of the edges of the cube, where one of the variables assumes the value of 0 and the others occur at the ±1 levels. A central point is also part of the design.

The Box-Behnken design is rotatable. It contains regions of poor prediction power (as with the inscribed central composite design), due to the lack of points at the corners of the design region. Those missing corners are convenient when the combination of extreme levels of factors is undesirable or impossible.

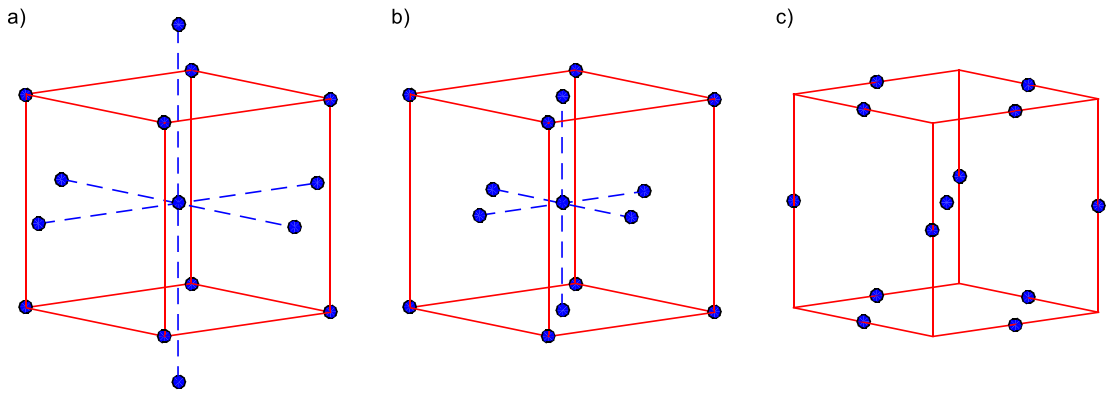

Figure 2-2. Example visualization of three experimental designs for response surfaces of three independent variables. (a) Central composite design. (b) Face-centered central composite design. (c) Box-Behnken design.

Some combinations of variables produce, by their own nature, a region of interest that is cuboidal, that is, the limits on the range of the variables are strict and operating outside them may be even physically impossible: there is a flat plane delimiting the operative region. Special care should be given to guarantee both that the whole region of interest is sampled with the experimental design and that no inferences are implied in the model for points outside of the operability region.

The central composite and the Box-Behnken design are a good fit when the region of interest is spherical in nature while the face-centered central composite design is appropriate for cuboidal regions.

2.3.4 Experiments with mixtures

When the variables x_i represent compositions of a mixture, some complications arise, since they are not independent but related. For a mixture of q components, the relationship is given by

$$\sum_{i=1}^{q} x_i = 1 \qquad \text{Eq. 2-14}$$

For this reason, they require special treatment and there are specific designs, different to those given in section 2.3.3, for dealing with them. Also, the behaviour of mixtures can be complicated and it is not unusual to fit third of even fourth order models. Additional complications arise when the values of some or all of the components' proportions are subject to lower and/or upper bounds.

Also, when working with mixtures, it is customary to express the model as a Scheffé polynomial with no independent term, so that each coefficient b_i is a direct measure of the effect of the i-th component. So, for a second order model

$$\hat{y} = \sum_{i=1}^{q} b_i x_i + \sum_{i=1}^{q} \sum_{j>i}^{q} b_{ij} x_i x_j \qquad \text{Eq. 2-15}$$

However, some transformations of the variables are possible to come up with a model with $(q-1)$ independent variables, whose analysis can be approached using the designs and strategies outlined in sections 2.3.1, 2.3.2 and 2.3.3.

3 Hypothesis and objectives

It is hypothesized that the growth of *M. trichosporium* OB3b and its production of PHB can be independently optimized by changing the environmental conditions in which the cells are cultured. These conditions include the source of carbon (methane, methanol, or a blend of the two), the source of nitrogen (ammonium, nitrate, or a blend of the two), the molar ratio of nitrogen to carbon, the oxygen level and the history of the inoculum used for culture.

The main objectives of the present study were to:

- characterize the growth of *Methylosinus trichosporium* OB3b in response to changes in culture conditions;
- characterize its production of polyhydroxybutyrate (PHB) as affected by those changes;
- describe these responses using a second order interaction model;
- use the model to evaluate and optimize growth and PHB production by *M. trichosporium* OB3b;
- experimentally confirm predictions obtained from the model.

4 Materials and methods

4.1 Microorganism

Methylosinus trichosporium OB3b was obtained from the Organization of Methanotroph Genome Analysis (OMeGA) culture bank. For long term preservation of the cells, they were maintained as methane-grown liquid cultures kept at room temperature. These cultures were found to remain indefinitely viable and were used to prepare working inocula by subculturing into media supplemented with the desired carbon source.

4.2 Solutions and media

The media used in this works were modified formulations of nitrate mineral salts (NMS) and ammonium mineral salts (AMS) solutions (Whittenbury et al. 1970). The modifications consisted in varying amounts of the nitrogen compound, potassium nitrate or ammonium chloride, for NMS and AMS, respectively.

Table 4-1. Compositions per litre of (unmodified) nitrate mineral salts (NMS) and ammonium mineral salts (AMS) solutions.

	NMS	AMS
$MgSO_4 \cdot 7H_2O$	10.00 g	10.00 g
KNO_3	10.00 g	
NH_4Cl		5.00 g
$CaCl_2 \cdot 2H_2O$	2.28 g	2.28 g
WTE solution	10 mL	10 mL
0.1% Na2MoO4 solution	5 mL	5 mL
3.8% Fe EDTA solution	1 mL	1 mL
100 mM $CuSO_4$ solution	0.5 mL	0.5 mL

Whittenbury Trace Elements (WTE) solution was prepared dissolving 0.5 g of iron (II) sulphate heptahydrate (Acros Organics, USA), 0.4 g of zinc (II) sulphate heptahydrate (Fisher Scientific, USA), 0.02 g of manganese (II) chloride tetrahydrate (Sigma-Aldrich, USA), 0.05 g of cobalt (II) chloride hexahydrate (Sigma-Aldrich, USA), 0.01 g of nickel (II) chloride hexahydrate (Acros Organics, USA), 0.015 g of boric acid (Sigma-Aldrich, USA), and 0.25 g of disodium EDTA (J.T. Baker) in 1 L of deionized water.

Phosphate stock solution was prepared dissolving 26 g of potassium phosphate monobasic (Fisher Scientific, USA) and 33 g of sodium phosphate dibasic (Fisher Scientific, USA) in 1 L of deionized water.

10X nitrogenless mineral salts (nIMS) stock solution was prepared dissolving 10.00 g of magnesium sulphate heptahydrate (Fihser Scientific, USA) and 2.28 g of calcium chloride dihydrate (Fisher Scientific, USA) in 800 mL of deionized water, adding 10 mL WTE solution, 5 mL of 0.1% sodium molibdate (Terochem Laboratories, Canada) solution, 1 mL of 3.8% iron EDTA (Fisher Scientific, USA) solution, 0.5 mL of 100 mM copper (II) sulphate (Fisher Scientific, USA) solution, and completing the volume to 1 L with deionized water.

Separate 99 mM solutions of **potassium nitrate** (Fisher Scientific, USA) and **ammonium chloride** (Fisher Scientific, USA) were also prepared.

4.3 Culture media and inoculation

For the preparation of the culture medium, 10X nIMS stock solution was diluted ten times with deionized water in 250-mL Wheaton or 1-L Kimax bottles and autoclaved. Upon cooling, 1.5% of filter-sterilized (SFCA, 0.2 µm, 26 mm, Corning, USA) phosphate stock solution and a volume of sterilized nitrogen source solution (base on final concentration desired) were added. The bottles were capped with septum crew caps. The actual volumes of the bottles were 311 mL for the 250-mL bottles, and 1.19 L for the 1-L bottles. Table 4-2 lists the headspace volume for the bottles for different volumes of liquid culture.

Table 4-2. Headspace volumes for different volumes of liquid cultures.

	Headspace in bottles	
Liquid culture volume	250-mL bottles	1-L bottles
25 mL	286 mL	1.17 L
50 mL	261 mL	1.14 L
100 mL	211 mL	1.09 L

Methanol (Fisher Scientific, USA) and a methane mixture with 5% carbon dioxide (Praxair, Canada) were used as carbon sources.

When methanol was used as carbon source, it was added as a filter-sterilized measured amount of liquid before capping the bottles. Typical methanol concentrations were 10 mmol/L and 20 mmol/L. When methane was used as carbon source, it was injected sterilely into the headspace through the septum, as a measured amount of gas, after the extraction of variable amounts of air, as will be indicated below. Typical carbon loads of methane were 20 mmol and 21.7 mmol of methane per L of liquid. (Given that methane was partitioned between the liquid and gas phases, predominantly present in the gas phase, the term "carbon load", meaning the total supplied amount of carbon source per volume of liquid culture, is better suited than "concentration" to describe the situation. In the case of methanol, this carbon load is equivalent to concentration. This terminology will be used throughout this work.)

The cultures were inoculated with 1-4% of a liquid preculture injected through the septum. Cultures were then incubated at 30°C and 150 rpm in an incubation shaker (Ecotron, Infors MT, Canada).

4.4 Air extractions and additions

In all cases, the gases (methane and air) were injected sterilely through a 0.22 µm filter (Corning, USA).

For the initial experiments (Section 5.1), 50 mL of air were extracted through the septum prior to the addition of 60 mL of methane in order to keep the internal pressure from increasing significantly. The internal pressure in the bottles after the extraction of air and the injection of methane was calculated as

$$P_f = P_0 \left(\frac{V_{hs}}{V_{hs} - V_w^0} + \frac{V_{CH4}^0}{V_{hs}} \right) \qquad \text{Eq. 4-1}$$

where P_f is the final internal pressure, in kPa; P_0 is the atmospheric pressure, which is equal to the initial pressure inside the bottle, in kPa; V_{hs} is the headspace volume, in mL; $V_w^0 = 50\ \mathrm{mL}$ is the volume of air that was withdrawn from the bottles, and $V_{CH4}^0 = 60\ \mathrm{mL}$ is the volume of methane that was injected to the bottles.

For the experiments in Section 5.2.1, two sets of bottles were prepared. One was set to have the same initial internal pressure as the bottles from Section 5.1. Since more methane would be added,

more air had to be extracted. The air was extracted in consecutive withdrawals of the same volume calculated as

$$V_w = V_{hs}\left[\left(\frac{P_0}{P_f - \frac{P_0 V_{CH4}^T}{V_{hs}}}\right)^{\frac{1}{n_w}} - 1\right] \quad \text{Eq. 4-2}$$

where V_w is the volume of air to be withdrawn from the bottle each time, in mL; n_w is the number of consecutive withdrawals of volume V_w; V_{CH4}^T is the total volume of methane that would be injected after the air is withdrawn, in mL; and P_f is the internal pressure of the bottles in Section 5.1, in kPa, calculated with Eq. 4-1. An extra bottle was prepared to have a reduced pressure ($\frac{2}{3}P_f$) and the air extractions were calculated with Eq. 4-2.

For the second set of bottles of Section 5.2.1, no attempt was made to have the same initial internal pressure as in the experiments in Section 5.1, only to have the same initial pressure within the bottles in this set. This was accomplished by injecting the same volume of gas, supplementing the bottles to which less methane was added with additional injections of air.

Thus, to the bottles with a carbon load of 21.7 mmol of methane per L of liquid, 60 mL of methane (at ambient temperature and pressure) and 120 mL of air (at ambient temperature and pressure) were added; to the bottles with a carbon load of 43.4 mmol of methane per L of liquid, 120 mL of methane and 60 mL of air (both at ambient temperature and pressure) were added, and to the bottles with a carbon load of 65.0 mmol of methane per L of liquid, 180 mL of methane (at ambient temperature and pressure) and no air were added. As per the standard procedure, 50 mL of air were extracted from the bottles before the additions of methane. The internal pressure was calculated with Eq. 4-1, changing the value of V_{CH4}^0 accordingly.

For the analysis of both sets, the amount of oxygen injected was calculated as:

$$n_{O2}^{inj} = \frac{P_0 V_{air}^{inj} y_{O2}}{RT} \quad \text{Eq. 4-3}$$

where n_{O2}^{inj} is the amount of oxygen injected, in moles; V_{air}^{inj} is the volume of air injected, in mL; y_{O2} is the molar fraction of oxygen in air; $R = 8.314 \times 10^{-3}$ mL kPa mol^{-1} K^{-1} is the gas constant; and T is the room temperature, in K.

To get the total amount of oxygen, this value needed to be added to the amount of oxygen already present in the bottle headspace, which was calculated as:

$$n_{O2}^{0} = \frac{P_0 V_{hs} y_{O2}}{RT} \cdot \left(\frac{V_{hs}}{V_{hs} + V_w}\right)^{n_w} \quad \text{Eq. 4-4}$$

where n_{O2}^{0} is the amount of oxygen already present in the bottle headspace, in moles.

4.5 Cell dry weight measurement

20- to 30-mL samples of cultures were centrifuged at 10,000 × g and 4°C for 10 min (Sorvall RC 6 Plus equipped with a Sorvall SS-34 rotor, Thermo Scientific, USA). The supernatant was removed, and the pellet was resuspended in 10 mL of deionized water and transferred to a tared weigh dish. The dish was placed in an oven (Isotemp 500 Series, Fisher Scientific, USA) at 60°C for drying to constant mass. The remaining mass was then converted to a cell dry weight, with units of mg/L by dividing by the sample volume.

4.6 Optical density measurement

Optical density of 1-mL culture samples was measured at a wavelength of 540 nm using a spectrophotometer (Biochrom Ultrospec 50). A calibration curve (Figure 4-1) was prepared to convert these measurements to equivalent cell dry weights.

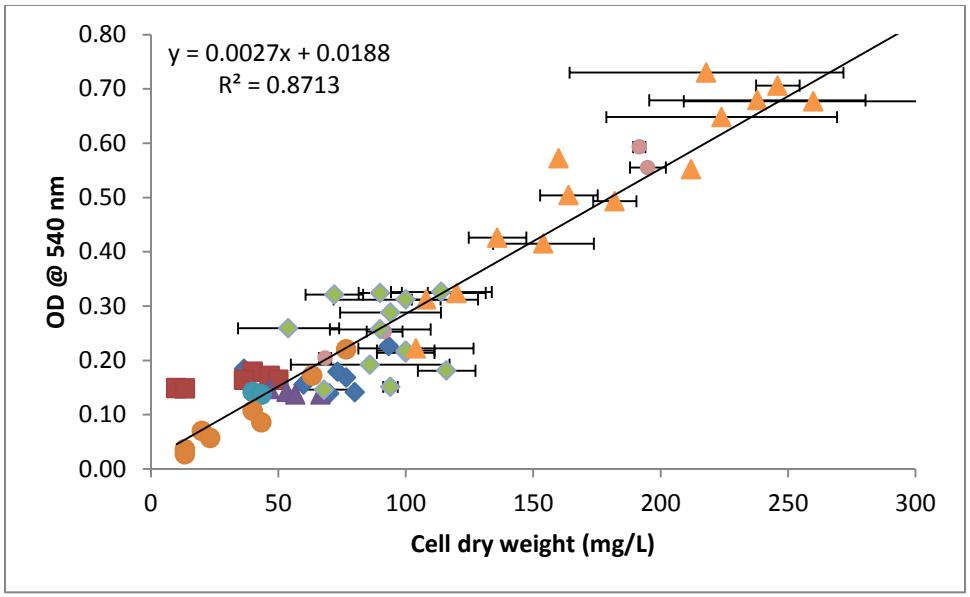

Figure 4-1. Calibration curve for cell dry weight and optical density at 540 nm. Inset are the regression equation and its coefficient of determination.

4.7 PHB content measurement

The quantification of PHB was performed using a modified methodology from Braunegg et al. (1978) and Oehmen et al. (2005). A 7-10 mL sample of the culture was centrifuged in a screw-capped glass vial (Kimble Chase, USA) 2,988 × g for 30 min (Sorvall RC 6 Plus equipped with a Sorvall SS-34 rotor, Thermo Scientific, USA). The supernatant was removed and replaced by 2 mL of chloroform and 2 mL of a 40-mg/L benzoic acid (Fisher Scientific, USA) solution in methanol that had been acidified with 3% concentrated sulfuric acid (Sigma-Aldrich, USA), before resuspension of the pellet. The sample was then digested for 5 h by placing the capped glass vial in a boiling water bath. After cooling, 1 mL of deionized water was added and the sample was vortexed (LSE vortex mixer, Corning, USA) for 20 s and let to stand for phase separation. The organic phase was kept for quantitative analysis by gas chromatography. The goal of the digestion was to depolymerize the PHB to its monomer, 3-hydroxybutyric acid, and methylate the monomer to the more volatile methyl 3-hydroxybutyrate. The added benzoic acid underwent methylation to methyl benzoate, which was used as an internal standard in the analysis described below.

A gas chromatograph (7890A, Agilent Technologies, USA) equipped with an autosampler (G4513A, Agilent Technologies, USA), and combined to a 30 m × 250 µm column with a 0.25 µm film

thickness (DB-5ms, Agilent Technologies, USA) was used. The injector temperature was held at 250°C, and 3 µL of sample were injected at a split ratio of 1:10. A flame ionization detector (FID) at 300°C was used for detection. The initial oven temperature was 80°C, held for 1 min, and then raised at a rate of 10°C/min to 120°C, and then to 270°C at 30°C/min, before being held for 3 min. Helium was used as the carrier gas at a flow of 1.5 mL/min.

An example of a resulting chromatogram is seen in Figure 4-2. The methyl 3-hydroxybutyrate peak was seen at 2.8 min. The methyl benzoate peak, used as an internal standard, was observed at 5.4 min. Standard solutions of purified PHB at different concentrations were subjected to the same treatment for construction of a calibration curve (Figure 4-3). The ratio of the area of the methyl 3-hydroxybutyrate peak divided by the area of the internal standard peak was multiplied by the concentration of the internal standard solution to use as the response factor for the calibration curve.

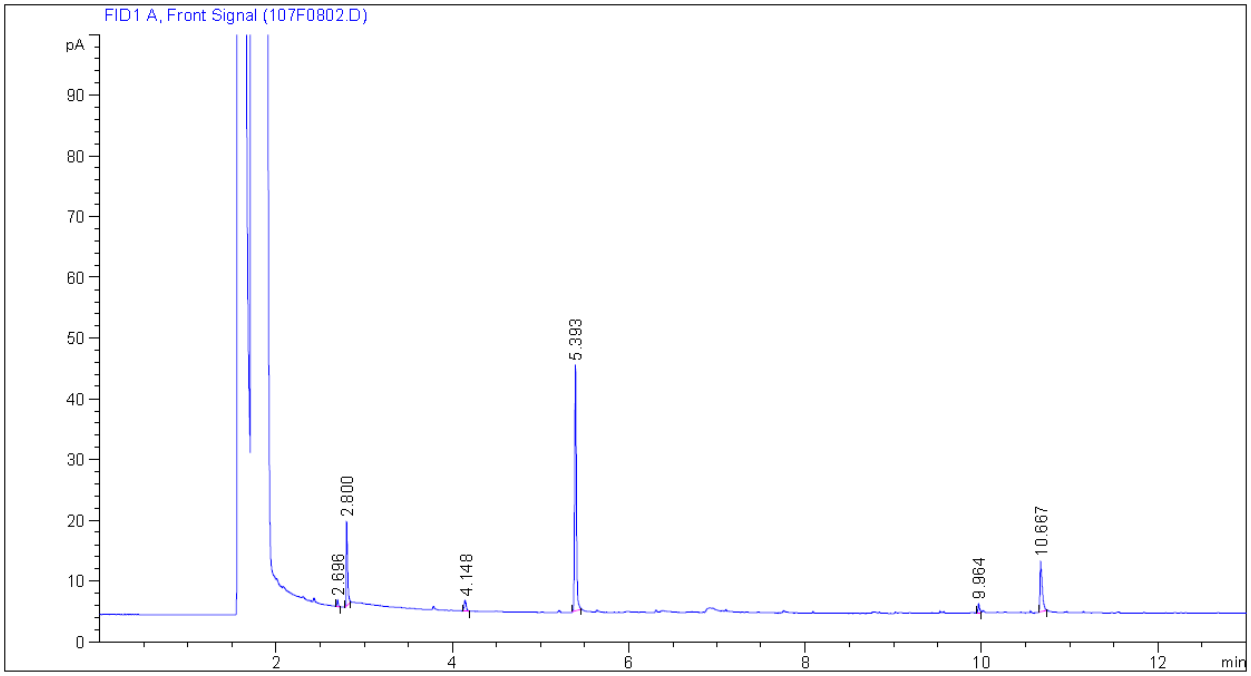

Figure 4-2. Example gas chromatogram for PHB determination.

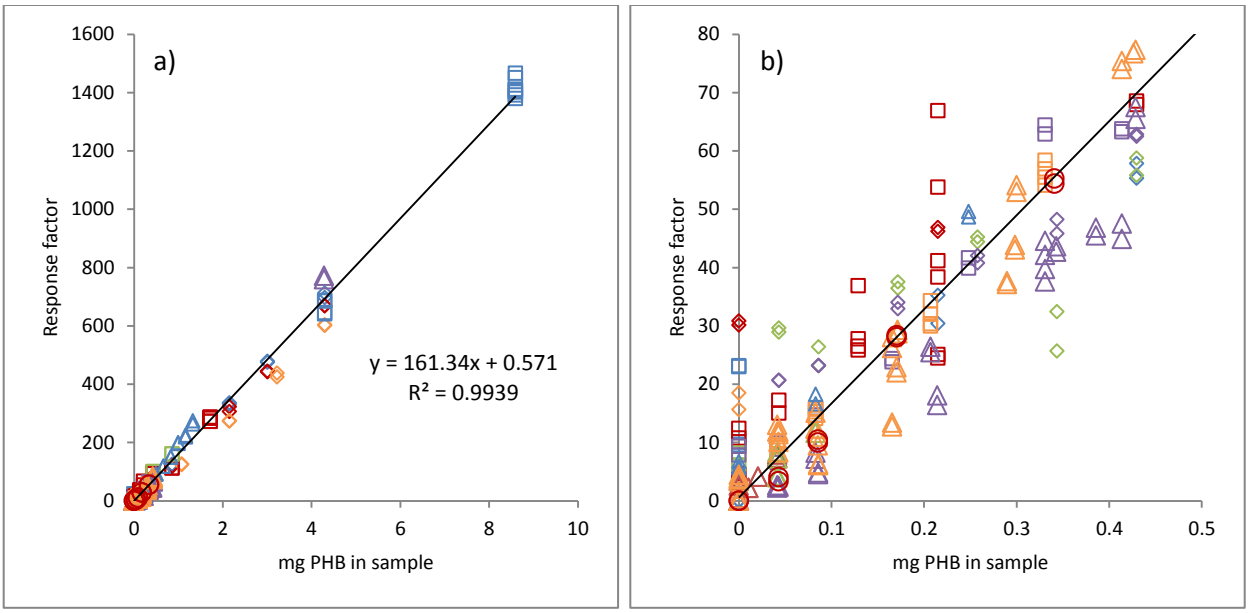

Figure 4-3. Calibration curve for the determination of PHB. Inset are the regression equation and its coefficient of determination. (a) Calibration curve over the whole range. (b) Detail of the low concentration region of the calibration curve; most samples fell in this region.

5 Results

5.1 *M. trichosporium* OB3b growth

The growth of *M. trichosporium* OB3b and its production of PHB are expected to change depending on the specific conditions under which the cells are cultured. Four factors were selected for the investigation of *M. trichosporium* OB3b's growth: the carbon source, the nitrogen source, the nitrogen-to-carbon ratio and the history of the inoculum. A 2^4 full factorial experiment design was performed in which each of the four factors had two levels (Table 5-1).

Table 5-1. Factors and level for the factorial experiment on *M. trichosporium* OB3b growth.

Factor	Levels
Carbon source	Methane (CH_4) or methanol (CH_3OH)
Nitrogen source	Ammonium (NH_4^+) or nitrate (NO_3^-)
Nitrogen-to-carbon ratio	Low[(1)] or high[(2)]
Inoculum history	Fresh or aged methane-grown; fresh or aged methanol-grown[(3)]

[(1)] The low level of N:C ratio was 0.046 for methane and 0.1 for methanol.
[(2)] The high level of N:C ratio was 0.46 for methane and 1.0 for methanol .
[(3)] Methane-grown inocula were used to start both methane- and methanol-grown cultures; methanol-grown inocula were used to start only methanol-grown cultures.

The carbon source used was either methane or methanol. The nitrogen source was either ammonium, in the form of ammonium chloride, or nitrate, in the form of potassium nitrate. For methane the nitrogen-to-carbon ratios used were 0.046:1 and 0.46:1, while for methanol they were 0.1:1 and 1:1. These ratios differed due to the different amounts of methane (gas phase) and methanol (liquid phase) added to the system. Since methane-grown, aged inocula were planned to be used for the experiments, there was an interest in determining whether the history of the inoculum had any effect on growth. Fresh methane-grown inocula were between four and eight weeks old at the time of inoculation, and were grown with ammonium as nitrogen source. Aged methane-grown inocula, grown with nitrate as nitrogen source, were between 5.5 and 6.3 months old at the time of inoculation. Preliminary experiments showed interactions between inoculum history and the carbon source used for the preculture, and prohibitive lag times for cultures grown with methanol. Hence, the design was augmented with a 2^3 factorial to include methanol-grown cultures initiated from fresh and aged methanol-grown inocula. Fresh methanol-grown inocula were between 2.1 and 2.3 weeks old while

aged methanol-grown inocula were between 3.1 and 3.3 weeks old. All methanol-grown inocula used ammonium as nitrogen source. Each factor had 2 levels, except for the inoculum history which had four levels. In total, $2^4 + 2^3 = 24$ treatments were investigated (see Table 5-1 and Table B-1 in Appendix B for the experimental conditions tested). All experiments were performed in triplicates, except for the augmented conditions (methanol-grown inocula) which were conducted in duplicates. It should also be noted that the initial factorial experiments and the augmented experiments were treated as different blocks, since they were performed at different times.

Methanol was used at a concentration of 9.9 mmol/L, the culture volume was 100 mL. The carbon load of methane was 21.7 mmol of methane per L of liquid, with the same liquid volume. These values were taken from standard in-house protocols previously developed and did not account for mass transfer limitations encountered when using methane as a carbon source (it being a gas and having to diffuse from the headspace into the liquid). Examples of typical growth curves are shown in Figure 5-1 for cultures grown on either methane (Figure 5-1a) or methanol (Figure 5-1b), using ammonium as nitrogen source, a low N:C ratio and initiated with aged, methane-grown inocula. The growth curves for the other conditions tested are available in Appendix B, Figure B-1 to Figure B-3. As can be observed, the growth curves adopt a typical pattern, showing a lag phase followed by rapid growth in the exponential phase, and stabilization of the biomass in the stationary phase. An interesting point was that the lag phase was always shorter for cultures grown with methane. It is also interesting to note a peculiar behaviour for the cultures grown with methanol as the carbon source. At the end of the exponential growth phase, a maximum in optical density was reached, followed by a rapid but short decline and then a steady decrease at a slower rate.

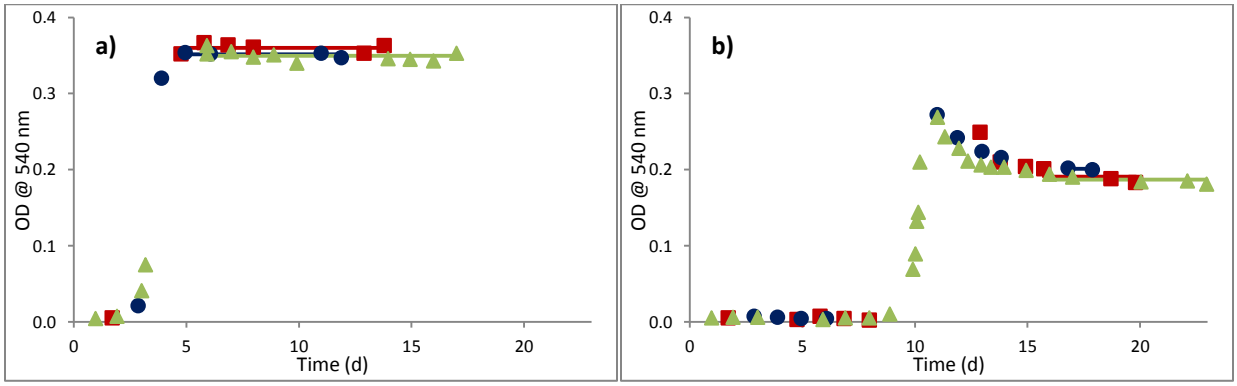

Figure 5-1. Growth curves for cultures grown on methane (a) and methanol (b) as carbon source, ammonium as nitrogen source, a low N:C ratio and initiated with an aged inoculum. Each symbol and color represents a different replicate. The horizontal lines in matching colors represent the average final optical density calculated from the corresponding data points.

The final biomass yield was obtained from these curves by taking the average optical density of the measurements made in the stabilized sections of the stationary phase (as shown by the colored horizontal lines in Figure 5-1, and Figure B-1 to Figure B-3 in Appendix B). From the examples shown in Figure 5-1, the cultures grown on methane had a lag phase of 2.5 days and reached a final optical density of 0.35, while the methanol-grown cultures had longer lag phase of 9 days and grew to a maximum optical density of 0.27 to finally decrease to 0.19 in the stationary phase.

The graphs for all 64 cultures of the 24 treatments are shown in Appendix B, Figure B-1 to Figure B-3. The average final optical densities are reported in Table 5-2 for each of the 24 treatments tested. The culture conditions and the individual final OD values are listed in Table B-1 in Appendix B.

The length of the lag phases is given in Table 5-3. The shorter lag phases (1—1.5 d) correspond to methane-grown cultures initiated from fresh methane-grown inocula. The use of aged-methane-grown inocula increases the lag phase of the methane-grown cultures to 2.5 d. The duration of the lag phase in methanol-grown cultures ranged from 4.5 d to 14 d, always shorter when initiated from fresh methanol-grown inocula, and usually shorter when initiated from methanol-grown inocula than when initiated from methane-grown inocula, except for the case of cultures grown from methanol and ammonium at a high N:C ratio. The shorter lag phase for a methanol-grown culture was 4.5 d for cultures grown on nitrate at both high and low N:C ratio. When initiated from methane-grown cultures, the methanol cultures had a longer lag phase of up to 14 d, usually longer when using fresh inocula.

Table 5-2. Final optical densities for the *M. trichosporium* OB3b growth experiment. Values are reported as mean ± standard deviation of three (methane-grown inocula) or two (methanol-grown inocula) replicates.

			CH_4-grown inocula		CH_3OH-grown inocula	
C source	N source	N:C ratio	fresh	aged	fresh	aged
CH_4	NH_4^+	low	0.346 ± 0.009	0.354 ± 0.006		
CH_4	NH_4^+	high	0.336 ± 0.013	0.331 ± 0.020		
CH_4	NO_3^-	low	0.270 ± 0.030	0.291 ± 0.007		
CH_4	NO_3^-	high	0.275 ± 0.018	0.291 ± 0.008		
CH_3OH	NH_4^+	low	0.225 ± 0.012	0.193 ± 0.007	0.240 ± 0.016	0.190 ± 0.014
CH_3OH	NH_4^+	high	0.183 ± 0.010	0.193 ± 0.014	0.223 ± 0.009	0.174 ± 0.015
CH_3OH	NO_3^-	low	0.197 ± 0.017	0.173 ± 0.016	0.208 ± 0.000	0.170 ± 0.005
CH_3OH	NO_3^-	high	0.156 ± 0.021	0.160 ± 0.007	0.182 ± 0.014	0.163 ± 0.007

Table 5-3. Approximate lag phase times in days according to history of inoculum.

			CH_4-grown inocula		CH_3OH-grown inocula	
C source	N source	N:C ratio	fresh	aged	fresh	aged
CH_4	NH_4^+	low	1	2.5		
CH_4	NH_4^+	high	1.5	2.5		
CH_4	NO_3^-	low	1.5	2.5		
CH_4	NO_3^-	high	1.5	2.5		
CH_3OH	NH_4^+	low	12—14	9	5—5.5	9.5—10.5
CH_3OH	NH_4^+	high	10—13	12—13	5.5	9—11
CH_3OH	NO_3^-	low	12—14	10.5	4.5—5	9—11.5
CH_3OH	NO_3^-	high	10.5—11	9	4.5	8.5

Table 5-4. Analysis of variance for factor effects on growth experiments. The response factor is optical density at 540 nm, as a measure of biomass concentration. Significant effects are highlighted in bold red.

Source	Sum of squares	Degrees of freedom	Mean square	F	*p*-Value
C source	**0.228220**	**1**	**0.228220**	**950.07**	**9.66e-34**
N source	**0.027938**	**1**	**0.027938**	**116.30**	**1.55e-14**
N:C ratio	**0.002988**	**1**	**0.002988**	**12.44**	**0.000923**
Inoculum	0.000517	1	0.000517	2.15	0.148820
C source*N source	**0.004228**	**1**	**0.004228**	**17.60**	**0.000114**
C source*N:C ratio	0.000761	1	0.000761	3.17	0.081334
C source*Inoculum	**0.003801**	**1**	**0.003801**	**15.82**	**0.000229**
N source*N:C ratio	0.000192	1	0.000192	0.80	0.375320
N source*Inoculum	0.000633	1	0.000633	2.64	0.110810
N:C ratio*Inoculum	0.000254	1	0.000254	1.06	0.308830
C source*N source*N:C ratio	0.000470	1	0.000470	1.96	0.168090
C source*N source*Inoculum	0.000056	1	0.000056	0.23	0.630220
C source*N:C ratio*Inoculum	**0.001030**	**1**	**0.001030**	**4.29**	**0.043683**
N source*N:C ratio*Inoculum	0.000006	1	0.000006	0.02	0.880010
Error	0.011771	49	0.000240		
Total	0.281490	63			

Constrained (Type III) sums of squares.

To better understand the effects of each factor, an analysis of variance (ANOVA) was performed for the results obtained from the experiments (Table 5-4). Three main effects – the carbon source, the nitrogen source and the N:C ratio –, two two-way interaction effects – the carbon source combined to the nitrogen source, the carbon source combined to the inoculum history – and one three-way interaction effect – carbon source combined to N:C ratio and inoculum history – were found to be significant.

To aid in the visualization of the impact of these factors and relationships, a series of graphs was built (Figure 5-2 to Figure 5-5). In these, clusters of data were created according to the experimental variables. The mean of the cluster is shown as a dark red horizontal line and is surrounded by a light red rectangle that spans 1.96 times the standard error both above and below the mean. The value of plus/minus one standard deviation is also shown as blue rectangles. Typically, when the red areas of two clusters do not overlap, the factors or treatments are considered to have a significant difference. However, the criteria for significance was taken from the ANOVA, which considers all the interactions, not taken into account in the clustering of Figure 5-2 to Figure 5-5.

In quantitative terms, the single most important effect was observed for carbon source (see Figure 5-2a). Greater growth was obtained when using methane, with an average optical density of 0.31, over methanol, with an average optical density of 0.19.

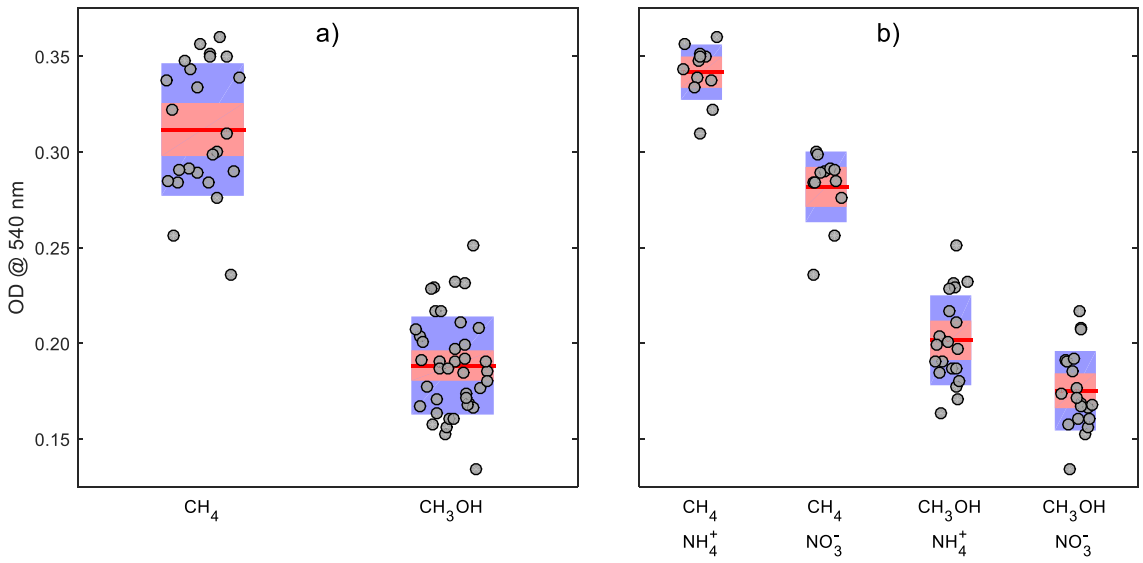

Figure 5-2. Effect of carbon source (a) and combined carbon and nitrogen sources (b) on biomass concentration of *M. trichosporium* OB3b. The red lines represent the mean. The red areas represent 1.96 times the standard error above and below the mean, and the blue areas represent one standard deviation in either direction. For the generation of these graphs, the program nonBoxPlot was used (Campbell 2010).

Similarly, the use of ammonium produced higher yields as compared to nitrate (Figure 5-2b). This effect was more noticeable when using methane as the carbon source. Thus, the difference of 0.06 units between the average optical densities obtained with the two different nitrogen sources when the carbon source was methane was reduced by half for cultures grown on methanol. However, in both cases, the biomass yield was greater in cultures grown using ammonium.

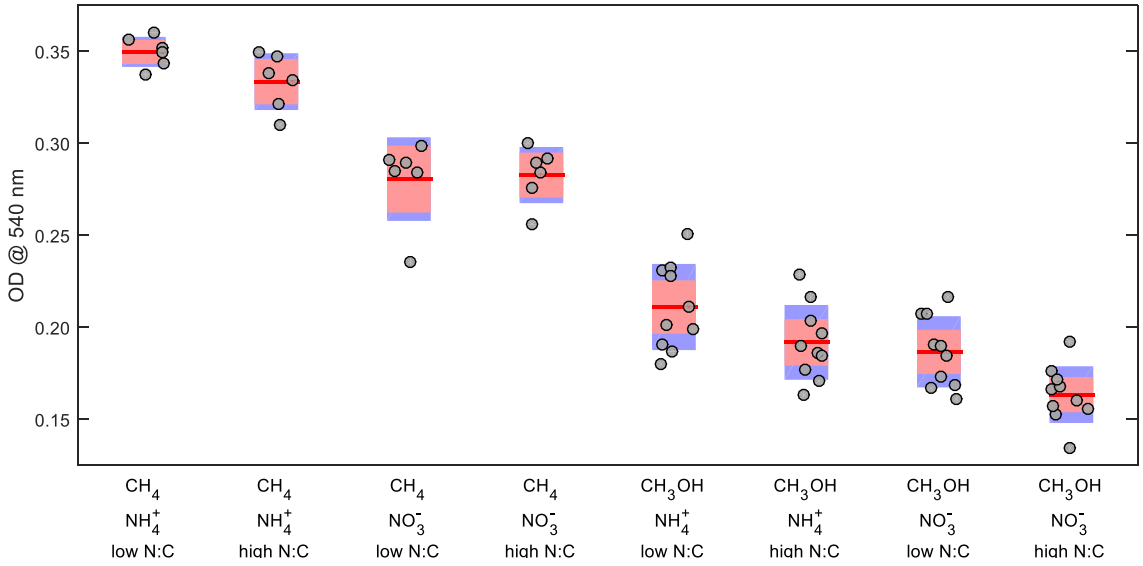

Figure 5-3. Effect of combined carbon source, nitrogen source and nitrogen-to-carbon ratio on biomass concentration of *M. trichosporium* OB3b. Symbols as explained in caption of Figure 5-2.

Figure 5-3 introduces the effect of nitrogen-to-carbon ratio. The four clusters on the left represent methane-grown cultures and the four on the right are for methanol-grown cultures. For each carbon source, the first pair of clusters is for ammonium-grown cultures and the second pair for nitrate-grown ones. Finally, the left cluster of each pair represents the culture grown on low nitrogen-to-carbon ratio while the right cluster of each pair corresponds to high nitrogen-to-carbon ratio. It can first be observed that the differences in average optical density within each pair, around 0.02 units, were lower than in previous observations (Figure 5-2); and in some cases they were not significant – such as in the second pair of clusters, corresponding to methane with nitrate. Surprisingly, it can also be observed that, with the exception of this combination of methane with nitrate, lower nitrogen-to-carbon ratios consistently resulted in increased biomass yields.

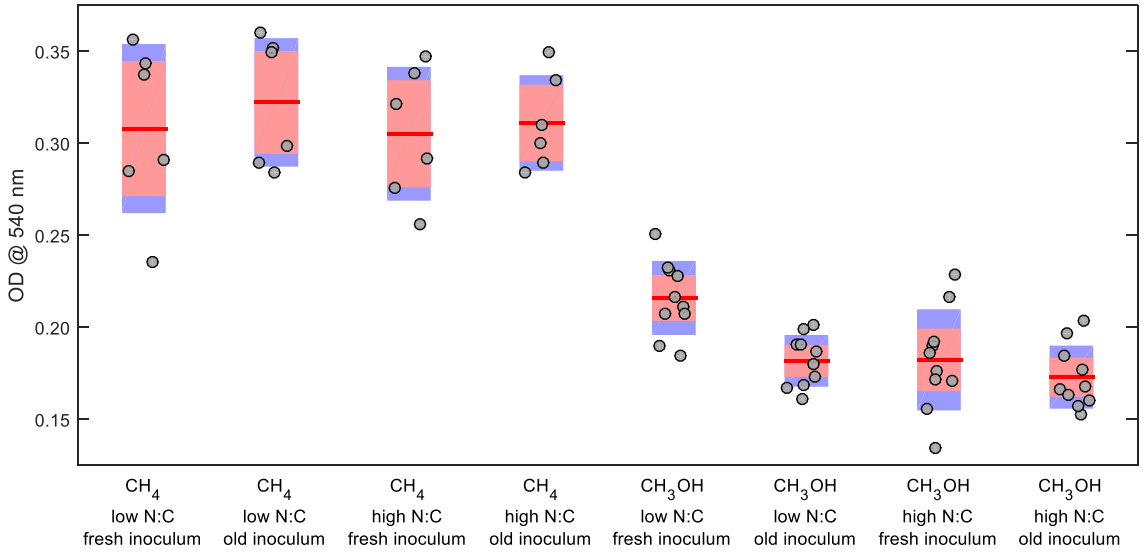

Figure 5-4. Three-way interaction of carbon source, nitrogen-to-carbon ratio and inoculum history on biomass concentration of *M. trichosporium* OB3b. Symbols as explained in caption of Figure 5-2.

As mentioned before, inoculum history, of itself, had no significant effect on biomass concentration. However, it participated in two interactions. In particular, its three-way interaction with carbon source and nitrogen-to carbon ratio is depicted in Figure 5-4. Again the clusters can be divided in two groups based on the carbon source used: methane for the leftmost four clusters and methanol for the rightmost four. The average optical densities of the clusters on the methane group (left) were not significantly different to each other. The group average was 0.31 units, the value already reported for methane as carbon source. Similarly, there was no significant difference between three of the methanol clusters (rightmost group), namely the second, third and fourth clusters. However, the first cluster of the rightmost group—corresponding to methanol as the carbon source at low nitrogen-to-carbon ratio and using fresh inoculum—sets itself apart from the other three. It had a significantly higher average optical density, at 0.22 units, compared to the average of 0.18 for the other three clusters in the group. Thus higher biomass yields were obtained when a fresh inoculum was used to initiate a culture grown on methanol under low nitrogen-to-carbon ratio conditions.

Continuing with the exploration of the effects of inoculum history—in particular, its interaction with carbon source—the methanol-grown cultures inoculated with methanol-grown inocula were specifically investigated. In this case, not only was there a significant effect on biomass yield, but it was also the most important both in terms of significance and of magnitude. Effectively, Table 5-5 shows the

ANOVA for cultures grown under these conditions. Of importance, it should be noted that the *p*-value for the history of the inoculum was the smallest at 2.2×10^{-5}. It should also be noted that for the conditions tested, all factors were significant.

Table 5-5. Analysis of variance for main factor effects for methanol-grown cultures from methanol-grown inocula.

Source	Sum of squares	Degrees of freedom	Mean square	F	*p*-Value
N source	0.002680	1	0.0026802	19.8626	0.000783
N:C ratio	0.001079	1	0.0010794	7.9992	0.015224
Inoculum	0.006035	1	0.0060353	44.7267	0.000022
Error	0.001619	1	0.0016193		
Total	0.011414	15			

Constrained (Type III) sums of squares.

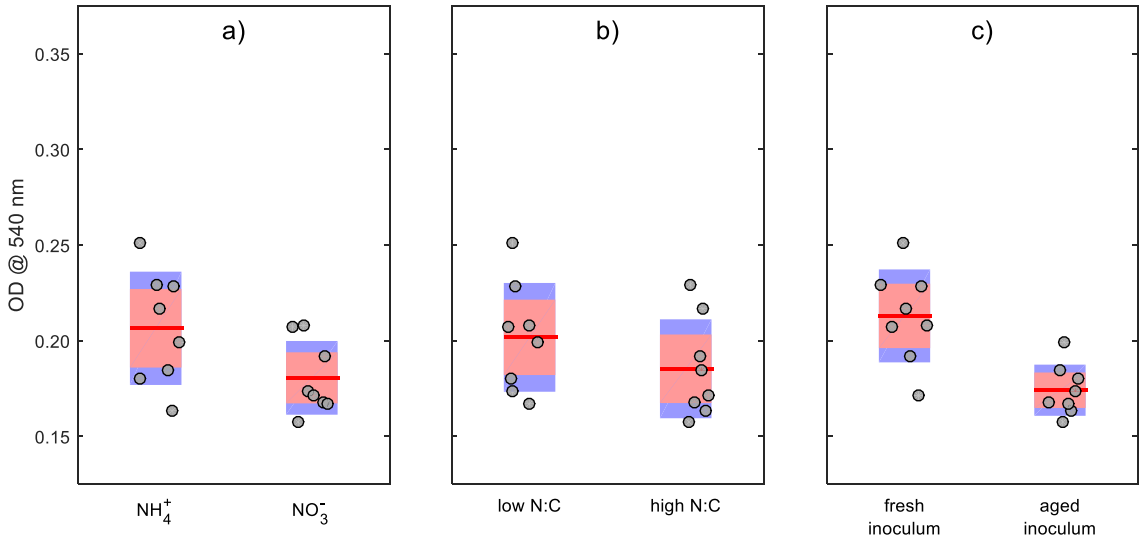

Figure 5-5. Main factor effects on biomass concentration for methanol-grown *M. trichosporium* OB3b cultures inoculated from methanol-grown inocula. (a) Nitrogen source; (b) N:C ratio; (c) inoculum history. Symbols as explained in caption of Figure 5-2.

In terms of magnitude of effects, the difference between the average optical densities between both types of inocula (0.039 units) was greater than the average of the differences generated by the nitrogen source (0.026 units) and by the nitrogen-to-carbon ratio (0.016 units) (Figure 5-5).

Given the significance of the carbon source effect and the fact that the carbon loads of the two carbon sources was not the same, the optical density was normalized dividing it by the moles of carbon and the ANOVA repeated with the results shown in Table 5-6. The differences with the previous ANOVA—effects that were found to be significant in the analysis in Table 5-4 but not in Table 5-6 and vice versa—are indicated with a yellow background.

There is no difference with respect to the effects of the carbon source, the nitrogen source and the nitrogen-to-carbon ratio, the two-way interaction of the carbon source with the inoculum history and the three-way interaction of the carbon source, the nitrogen-to-carbon ratio and the inoculum: they are significant in both analyses. In the analysis of the normalized optical density, two new significant effects appear: the inoculum history and the interaction of the carbon source with the nitrogen-to-carbon ratio. As well, the two-way interaction of carbon source and nitrogen source, previously found to be significant, was not significant when using the normalized data. Figure 5-6 displays a representation of the four main effects after the normalization of the OD data.

Table 5-6. Analysis of variance or the normalized response for factor effects on growth experiments. The normalized response factor is the optical density at 540 nm divided by the number of millimoles of carbon source supplied. Significant effects are highlighted in bold red, and the differences with the previous analysis of variance (Table 5-4), highlighted with a yellow background.

Source	Sum of squares	Degrees of freedom	Mean square	F	*p*-Value
C source	**0.032167**	**1**	**0.032167**	**182.07**	**4.00e-18**
N source	**0.011024**	**1**	**0.011024**	**62.40**	**2.72e-10**
N:C ratio	**0.002277**	**1**	**0.002277**	**12.89**	**0.000763**
Inoculum	**0.001128**	**1**	**0.001128**	**6.39**	**0.014784**
C source*N source	0.000004	1	0.000004	0.02	0.881290
C source*N:C ratio	**0.001242**	**1**	**0.001242**	**7.03**	**0.010778**
C source*Inoculum	**0.002655**	**1**	**0.002655**	**15.03**	**0.000316**
N source*N:C ratio	0.000018	1	0.000018	0.10	0.750540
N source*Inoculum	0.000270	1	0.000270	1.53	0.222160
N:C ratio*Inoculum	0.000420	1	0.000420	2.38	0.129440
C source*N source*N:C ratio	0.000147	1	0.000147	0.83	0.365780
C source*N source*Inoculum	0.000002	1	0.000002	0.01	0.917930
C source*N:C ratio*Inoculum	**0.000781**	**1**	**0.000781**	**4.42**	**0.040684**
N source*N:C ratio*Inoculum	0.000000	1	0.000000	0.00	0.964450
Error	0.008657	49	0.000177		
Total	0.064121	63			

Constrained (Type III) sums of squares.

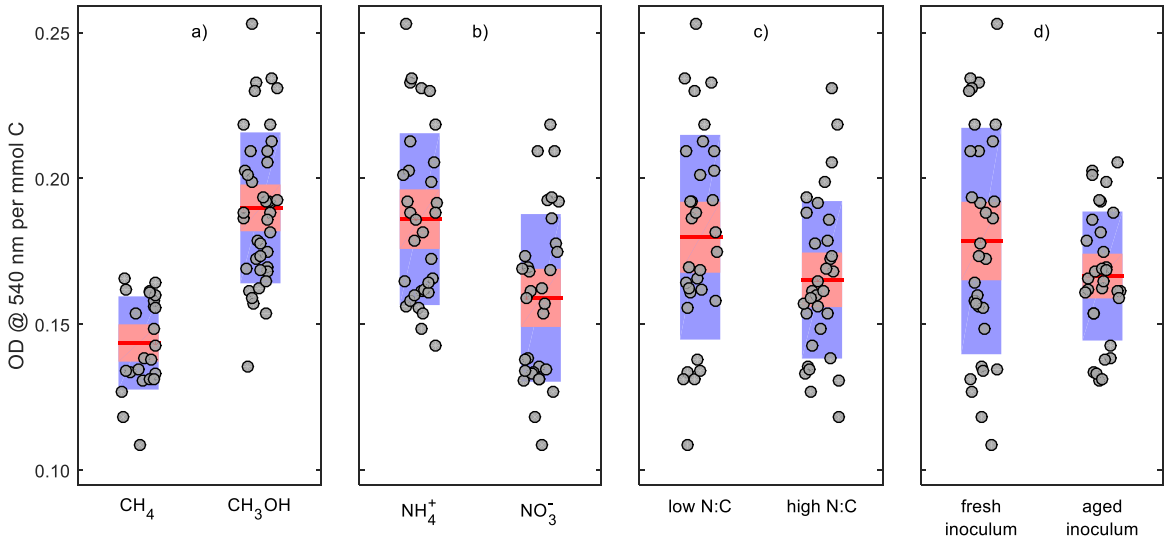

Figure 5-6. Main factor effects on normalized biomass concentration for *M. trichosporium* OB3b cultures. (a) Carbon source; (b) nitrogen source; (c) N:C ratio; (d) inoculum history. Symbols as explained in caption of Figure 5-2.

The PHB content of these cultures was too low to be reported with any significance (data not shown). Accordingly, additional experiments were conducted to explore both increased amounts of carbon source, to get higher growth, and further nitrogen limitation, to promote a higher accumulation of PHB.

5.2 Growth with increased amounts of carbon source

The prospects of increasing the cell densities of the cultures (beyond the maximum optical density obtained in the preliminary studies of 0.36, equivalent to a dry cell weight of approximately 130 mg/L) were investigated by increasing the amount of carbon source supplied.

5.2.1 Methane

Based on the experiments described above, the condition selected for this experiment was ammonium as nitrogen source with a high nitrogen-to-carbon ratio, and varying carbon loads of methane (21.7 mmol/L, 32.5 mmol/L, 43.4 mmol/L and 65.0 mmol/L for 100 mL of liquid medium). It should be noted that the headspace volume to liquid volume ratio was 2.1 (210 mL of headspace), and that the initial overhead pressure was kept the same at 103 kPa for all experiments, except for an additional experiment performed at 32.5 mmol/L with a reduced pressure of 69 kPa. The resulting growth curves are shown to the left of the first arrow in Figure 5-7. It can be observed that the higher the amount of methane, the lower the resulting cell density. The final optical density obtained for the culture with a methane load of 21.7 mmol/L was 0.31 units. In contrast, optical densities of 0.25, 0.20 and 0.12 were observed for the cultures with methane loads of 32.5, 43.4, and 65.0 mmol per L of liquid, respectively. The culture with a carbon load of 32.5 mmol of methane per L of liquied with a reduced total pressure showed an optical density of 0.12, the same as the culture grown at 103 kPa with a methane load of 65.0 mmol/L. These two cultures followed the same growth behaviour throughout the experiment.

Lack of growth was suspected to be due to a lack of oxygen and additional air was injected in 60-mL portions until the internal pressure made sampling and further additions too difficult. The time points of the air additions are indicated by the green, upward-pointing arrows in Figure 5-7. Additional growth was observed in every case after each addition of air, except for the final two additions to the

21.7 mmol of methane per L of liquid condition. This culture showed no more growth after reaching a maximum optical density of 0.64, a little more than double the value obtained before any addition of oxygen. The final oxygen-to-methane ratio at which no more additional growth was observed was 1.5. Otherwise, in general, the behaviour observed at the start of the experiment continued to be observed. That is, cultures with higher amounts of methane showed lower growth, however the spread between the cultures had a tendency to decrease with each further addition of oxygen. It should be noted that beside the culture with a carbon load of 21.7 mmol of methane per L of liquid, no other culture reached a ratio of oxygen to methane of 1.5.

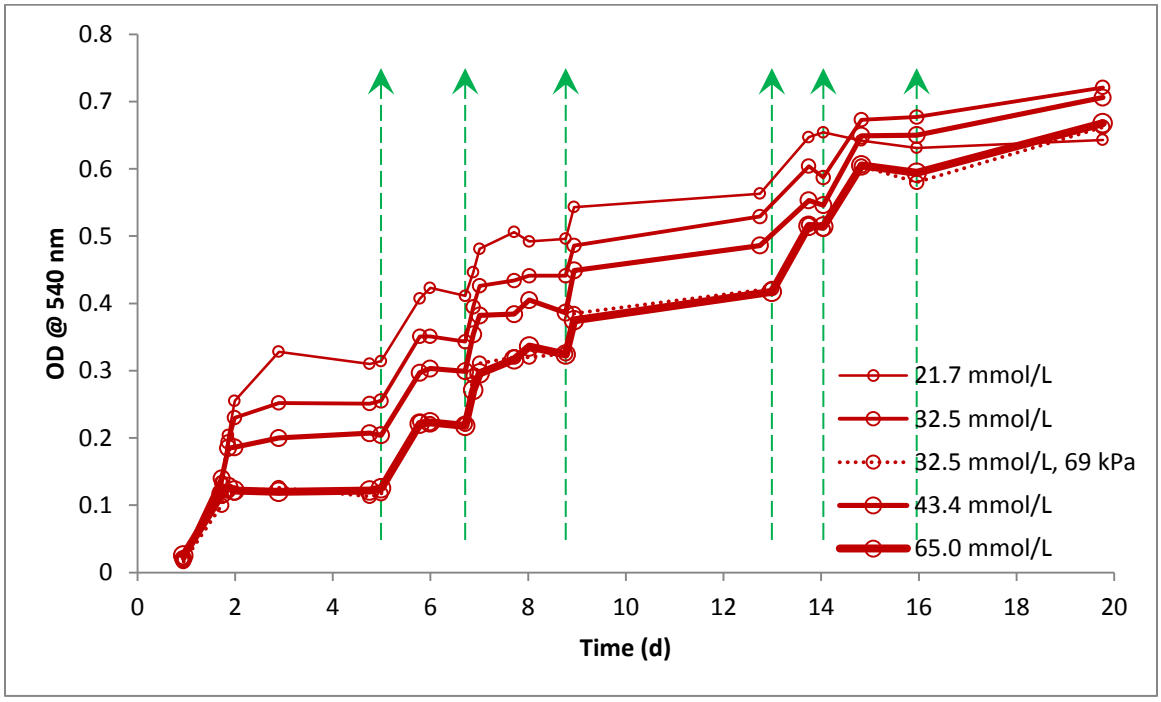

Figure 5-7. Growth of *M. trichosporium* OB3b with different amounts of methane. Each green arrow corresponds to the addition of 60 mL of air.

Additional experiments were performed with loads of 21.7, 43.4, and 65.0 mmol of methane per L of liquid in which different amounts of air were added before inoculation to obtain the same internal pressure in all the bottles (157 kPa). The resulting growth curves from these cultures are shown in Figure 5-8. Again, greater cell densities were achieved in the cultures with lower amounts of methane and, correspondingly, higher amounts of oxygen. The cultures grown on 21.7 mmol of methane per L of liquid

reached a final optical density of 0.50. Similarly, the cultures grown on 43.4 mmol of methane per L of liquid reached a final optical density of 0.42. A final optical density of 0.32 was obtained in the cultures grown on 65.0 mmol of methane per L of liquid.

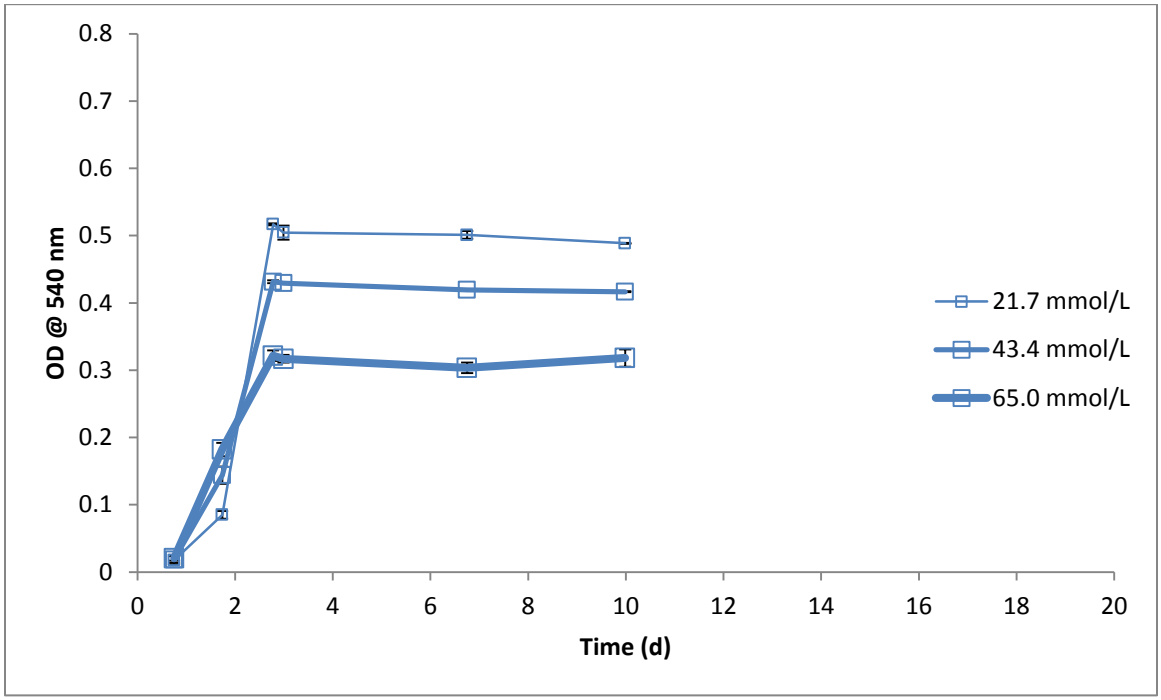

Figure 5-8. Growth with different amounts of methane. Air and methane were injected into the bottles in a proportion such as to maintain the total gaseous volume added (and thus the initial internal pressure) the same. Error bars represent standard deviation of two replicates.

Combining the data from all the experiments, both the ones with successive additions of air (Figure 5-7) and the ones in which all the air was present before inoculation (Figure 5-8), it can be observed from Figure 5-9 that, in fact, the growth that was obtained was linearly dependent on the total amount of oxygen added in all cases.

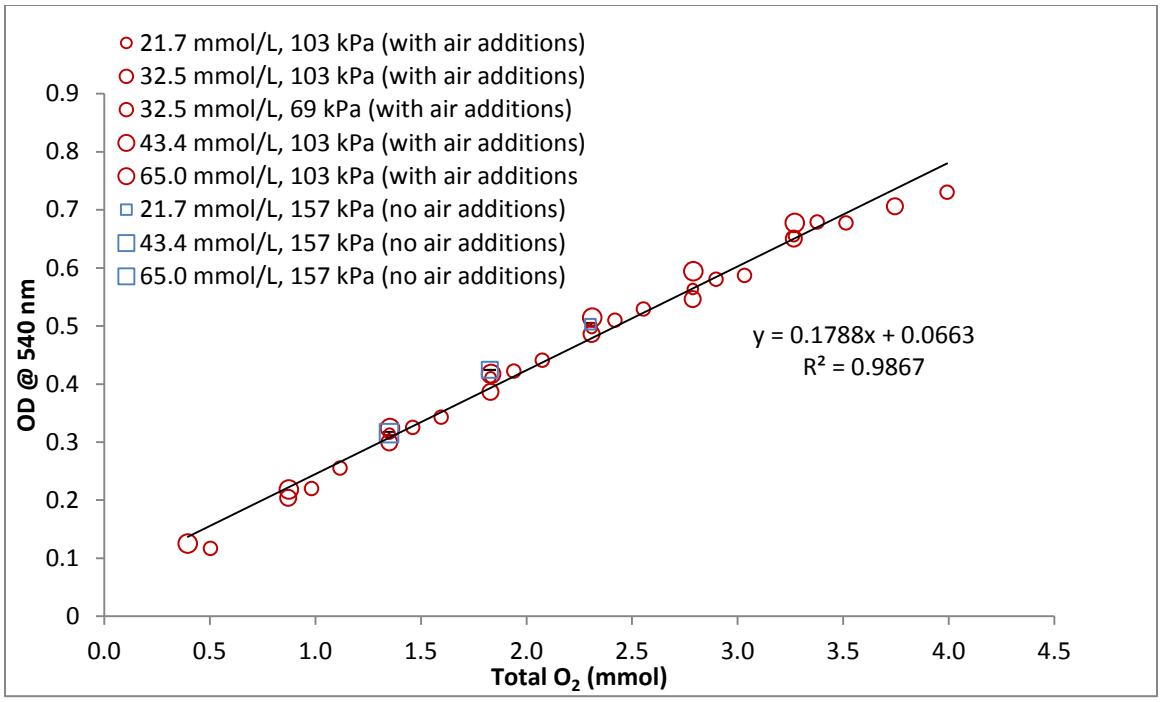

Figure 5-9. Final OD vs. total amount of oxygen added. Red circles represent the experiment with successive additions of air to the bottles (seen in Figure 5-7). Blue squares represent the experiments in which all air was injected at the beginning with no further injections (seen in Figure 5-8). Error bars for this series (too small to be seen) represent standard deviation of two replicates. Inset are shown the regression line equation and its coefficient of determination.

Form Figure 5-9, it can be seen that each additional mmol of oxygen increased the OD by 0.18 units, equivalent to 6.7 mg of dry weight of biomass (67 mg/L).

5.2.2 Methanol

As with methane, it was desired to assess the possibility of increased cell densities in cultures of *M. trichosporium* OB3b by using increased concentrations of methanol. To this end, media containing 9.9 mmol/L, 19.8 mmol/L and 29.7 mmol/L were prepared, inoculated and incubated. Again, as when using methane as carbon source, ammonium, at a high nitrogen-to-carbon ratio, was used as the nitrogen source. After reaching stationary phase, 60 mL of air (at ambient temperature and pressure) were injected into each bottle. The growth curves obtained are shown in Figure 5-10, on which solid lines represent the growth before the addition of air, and the dashed lines, that after the addition of air.

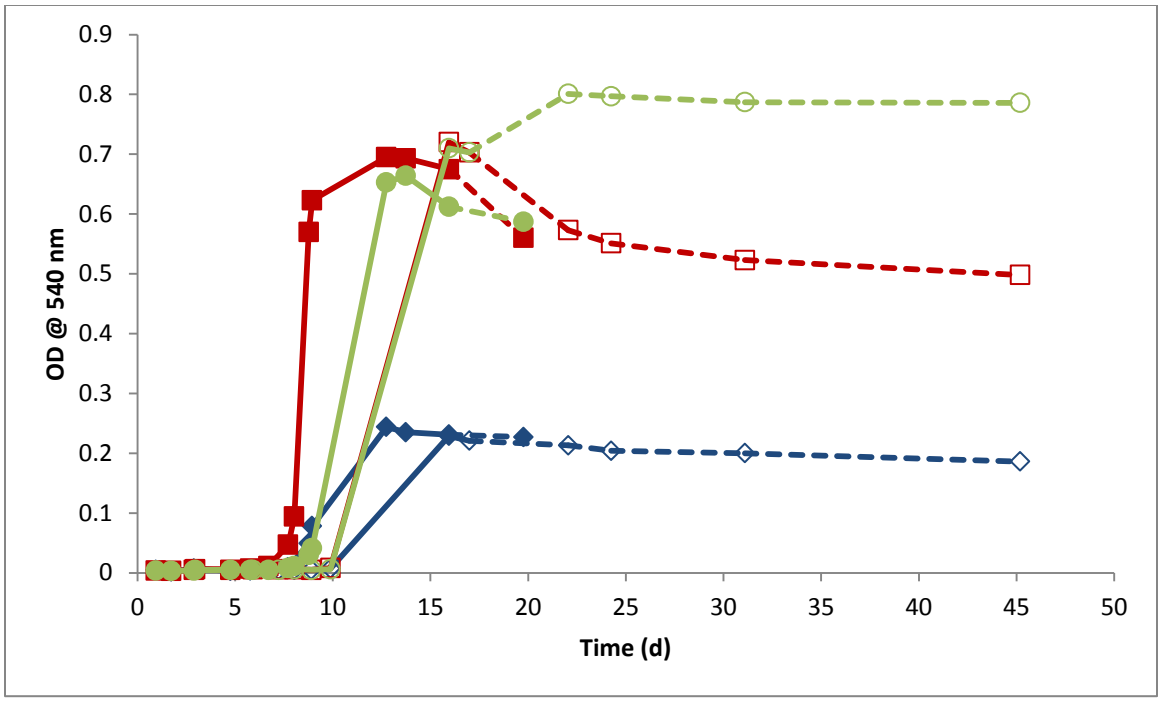

Figure 5-10. Growth curves for *M. trichosporium* OB3b growing on methanol: 9.9 mmol/L (♦,◇), 19.8 mmol/L (■,□), and 29.7 mmol/L (●,○). Replicates are shown. Dashed lines represent the growth after the addition of 60 mL of air.

Table 5-7 summarizes the maximum and final OD values for the cultures and Table 5-8 compares the growth observed as multiples of that of the lower concentration.

Table 5-7. Maximum and final ODs of *M. trichosporium* OB3b cultures using different concentrations of methanol as carbon source. Results are reported as mean ± RSD of two replicates, except as noted.

Methanol concentration	OD @ 540 nm	
	Maximum	Final
9.9 mmol/L	0.236 ± 4.5%	0.224 ± 4.4%
19.8 mmol/L	0.708 ± 2.5%	0.542 ± 4.7%
29.7 mmol/L		
- before air addition	0.687 ± 4.7%	0.587[(1)]
- after air addition	0.801[(2)]	0.790[(2)]

[(1)] First replicate only, second replicate's OD had just started to decrease.
[(2)] Only the second replicate showed additional growth after air addition.

The growth observed for cultures grown on 9.9 mmol/L of methanol was consistent with what had been observed in previous experiments, reaching a final optical density of 0.22 and was unaffected by the subsequent addition of air. The use of double the concentration of carbon source resulted more

than 2-fold increases in biomass yields, reaching a final optical density of 0.54. Here again, the culture was unaffected by the injection of additional air. On the other hand, when using triple the concentration of methanol, the replicates behaved slightly differently after the injection of more air. With the first one, the behaviour was very similar to that obtained for the 19.8 mmol/L methanol cultures. It reached a final optical density of 0.59 and was unaffected by the injection of additional air. However, this was not the case for the second replicate. Although its behaviour prior to the addition of air was similar, this culture was indeed affected by the additional air and further growth was observed, reaching a final optical density of 0.79. This resulted again in a yield increase of more than threefold the yield obtained for the cultures grown on 9.9 mmol/L of methanol.

If we only consider the 29.7 mmol/L replicate that showed further growth upon addition of air, the increase in biomass yield was proportional to the increase in carbon source concentration between the cultures grown with 19.8 mmol/L and 29.7 mmol/L This proportion was 0.027 units of optical density per mmol/L of methanol. This change in optical density is equivalent to 10.1 mg/L of cell dry weight.

Table 5-8. Oxygen-to-carbon ratios and growth multipliers for *M. trichosporium* OB3b cultures with different concentrations of methanol as carbon source.

		Final OD @ 540 nm	
Methanol	O_2:C	Value	Multiplier[(1)]
9.9 mmol/L	1.70	0.224	1.00X
19.8 mmol/L	0.85	0.542	2.42X
29.7 mmol/L			
- before air addition	0.57	0.587	2.62X
- after air addition	0.73	0.790	3.53X

[(1)]Times the observed growth is higher as compared to that of the 9.9-mmol/L of methanol condition.

5.3 PHB production under nitrogen deprivation

5.3.1 Methanol as carbon source

The effects of nitrogen deprivation on PHB accumulation in cultures growing on methanol were investigated with 25-mL liquid cultures of 60 mmol/L (1.5 mmol) with 286 mL overhead space at 103 kPa. These conditions were selected to ensure that oxygen was not limiting. In fact, the required stoichiometric ratio of oxygen to carbon is $1.5f_e$ (from Table 2-2), where f_e is the fraction of reducing

equivalents from the carbon source that are used for energy production. Since f_e can only take values between 0 and 1, the maximum value of the O_2:CH_3OH ratio is 1.5. Thus, for the 1.5 mmol of methanol supplied in the experiments, the maximum possible stoichiometric oxygen requirement would be 2.25 mmol. The 286 mL of headspace volume in these experiments contained 2.3 mmol of oxygen, slightly more than this requirement, hence suggesting oxygen was not limiting. The lowest N:C molar ratio used in preliminary experiments was 0.1. In these experiments, this molar ratio was brought to values as low as 0.01.

As can be seen in Figure 5-11, the biomass yield slightly, but significantly, increased as the N:C ratio decreased. The cell dry weight increased from 399 ± 13 mg/L to 456 ± 8 mg/L when decreasing the nitrogen-to-carbon ratio from 0.05 to 0.01. An intermediate ratio of 0.025 resulted in a cell dry weight of 421 ± 7 mg/L.

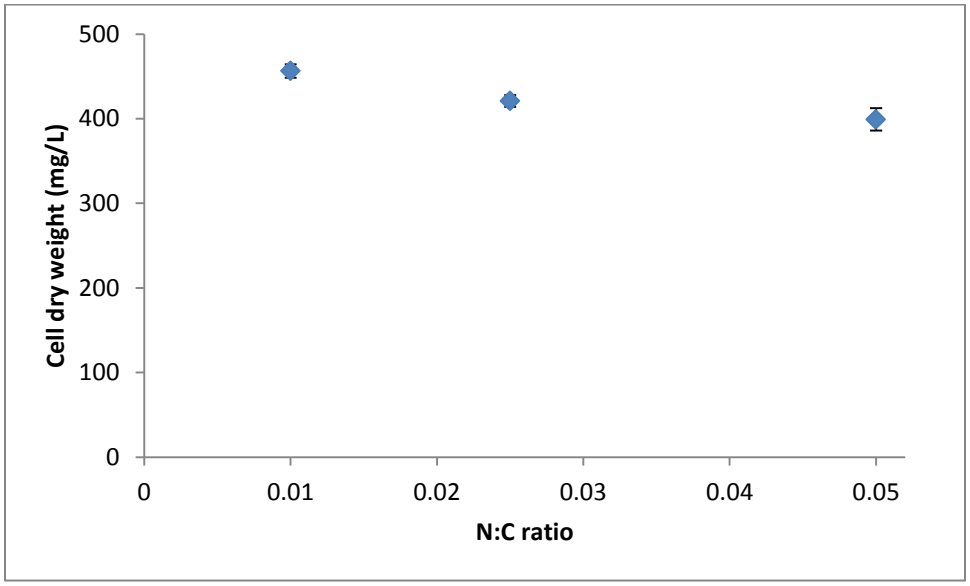

Figure 5-11. Cell dry weight for *M. trichosporium* OB3b cultures grown under different nitrogen-to-carbon ratios using methanol as carbon source. Error bars are standard deviation from two samples.

More interestingly, Figure 5-12 shows that the two lower ratios (0.01 and 0.025) resulted in an average PHB accumulation of 70 ± 14 mg/L and 65 ± 6 mg/L, respectively, while the cultures grown at the higher nitrogen-to-carbon ratio of 0.05, only reached 12 ± 6 mg/L of PHB. It should be noted that there was no significant difference between the PHB concentrations at the two lower N:C ratios.

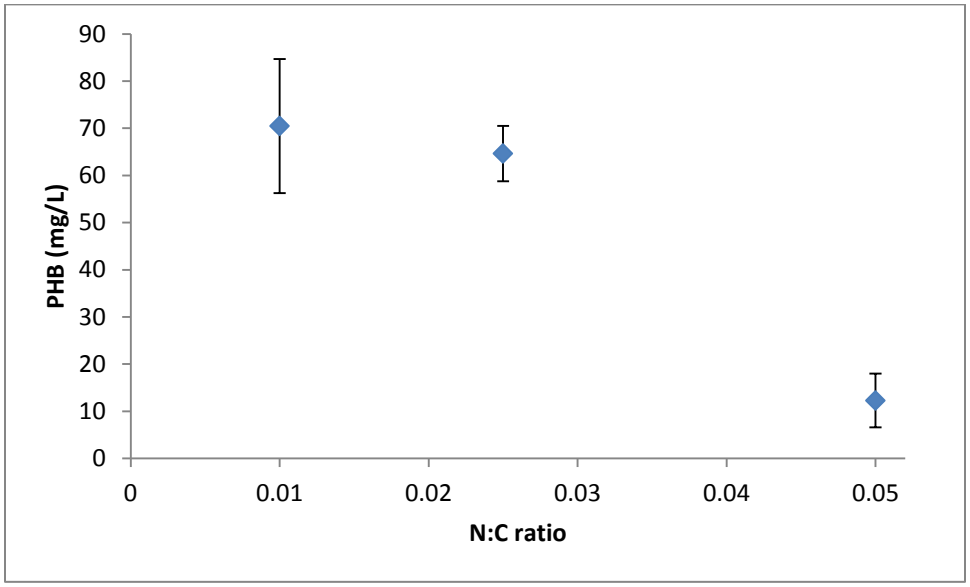

Figure 5-12. PHB concentration of *M. trichosporium* OB3b cultures under different nitrogen-to-carbon ratios using methanol as carbon source. Error bars are standard deviation from two samples.

Figure 5-13 shows the PHB content as a percentage of the cell dry weight. The difference in PHB content observed between the higher and lower ratios was somewhat tempered by the increased cell dry weights also observed at the lower nitrogen-to-carbon ratios, but given that the later were smaller than the former, a clear difference could still be observed between the 3.1% ± 1.5% PHB cell content obtained at a ratio of 0.05, and the values obtained at the lowest ratios—15.4% ± 2.8% at an N:C ratio of 0.01 and 15.3% ± 1.1% at an N:C ratio of 0.025. The range of nitrogen-to-carbon ratios used in this experiment ran from one tenth to one half that of the lowest one previously used.

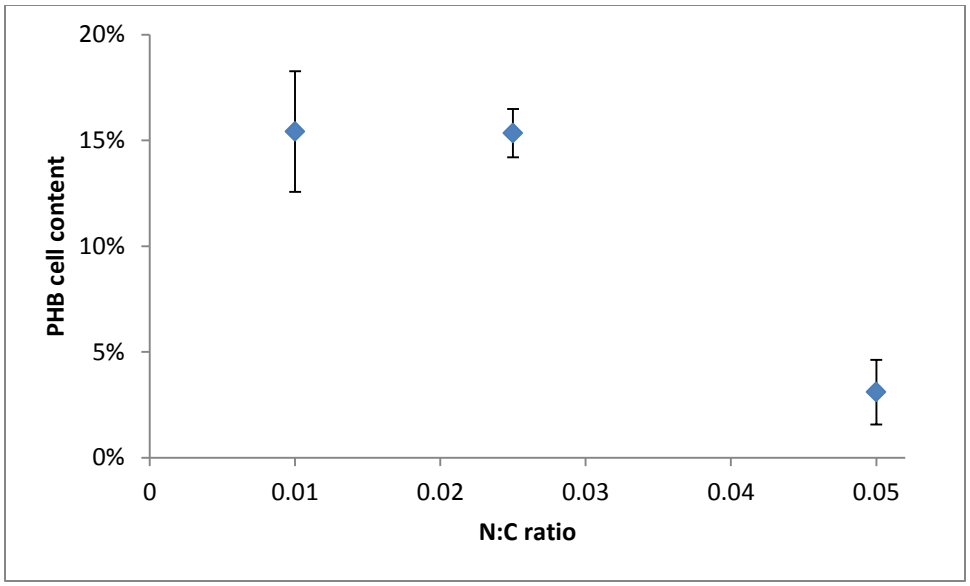

Figure 5-13. PHB cell content as a percentage of the cell dry weight for cultures of *M. trichosporium* OB3b under different nitrogen-to-carbon ratios using methanol as carbon source. Error bars are standard deviation from two samples.

5.3.2 Methane as carbon source

Similarly, to observe the production of PHB by *M. trichosporium* OB3b when methane was used as carbon source, experiments were conducted under similar conditions: 25 mL of culture volume, with a methane load of 60 mmol/L, 286 mL of overhead space, nitrate as the nitrogen source, and the same range of N:C ratios (0.01, 0.025, and 0.05).

As shown in Figure 5-14, the N:C ratio had no significant effect on the cell dry weight of the cultures. However, when looking at the PHB concentration as a function of N:C ratio (Figure 5-15) an hyperbolic trend, with a maximum at N:C ratio of 0.025, was observed, although significance was not confirmed. This lack of significance was due to the high variability observed, especially for the cultures grown using a nitrogen-to-carbon ratio of 0.025.

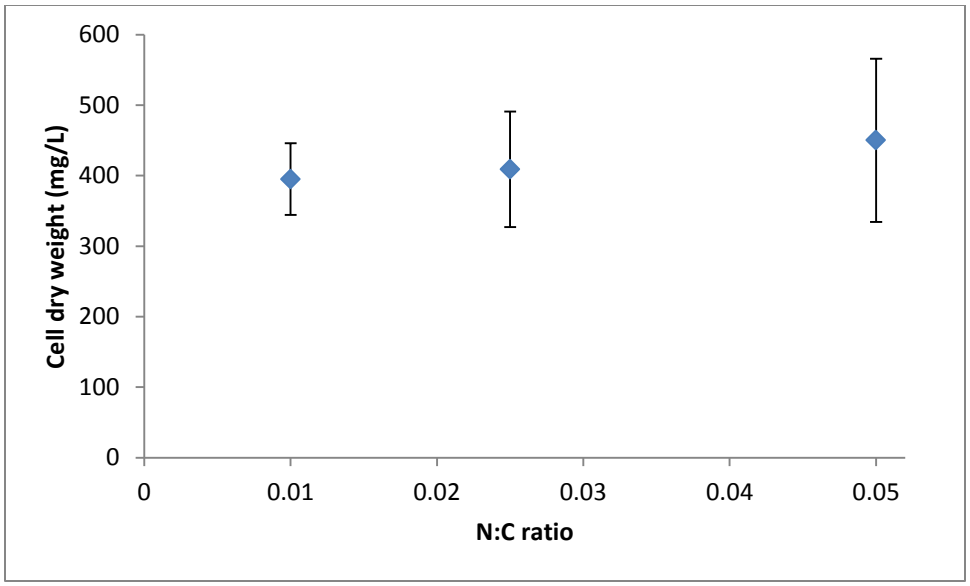

Figure 5-14. Cell dry weight for *M. trichosporium* OB3b cultures under different nitrogen-to-carbon ratios using methane as carbon source. Error bars are standard deviation from two samples.

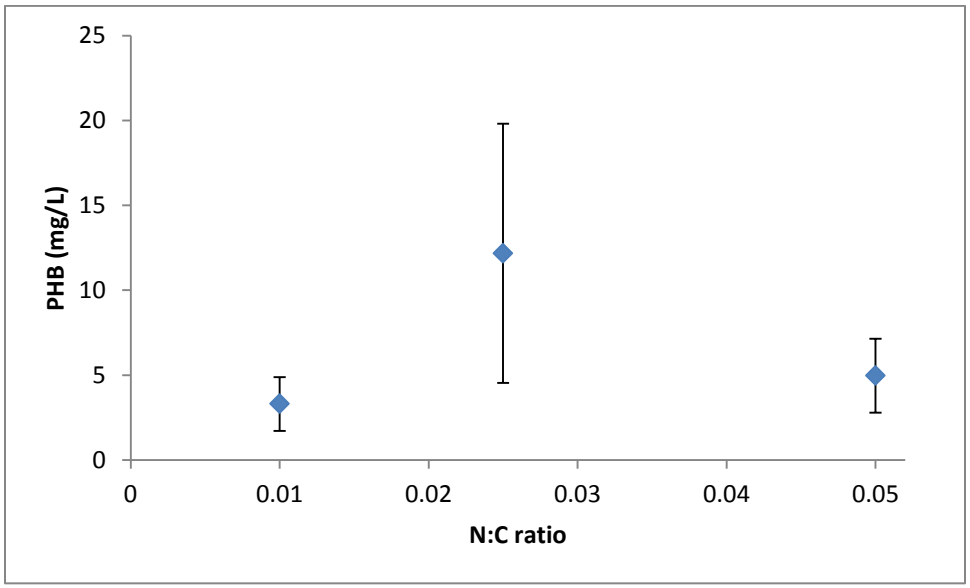

Figure 5-15. PHB concentration of *M. trichosporium* OB3b cultures under different nitrogen-to-carbon ratios using methanol as carbon source. Error bars are standard deviation from two samples.

Figure 5-16 shows the PHB cell contents as a percentage of cell dry weight. Since this data is calculated from the data found in Figure 5-14 and Figure 5-15, a hyperbolic trend is again observed and

amplified. In fact, the trend here was shown to be significant (with an $\alpha = 0.1$), with an observed maximum of 2.8% ± 1.3% PHB content when the N:C ratio was 0.025.

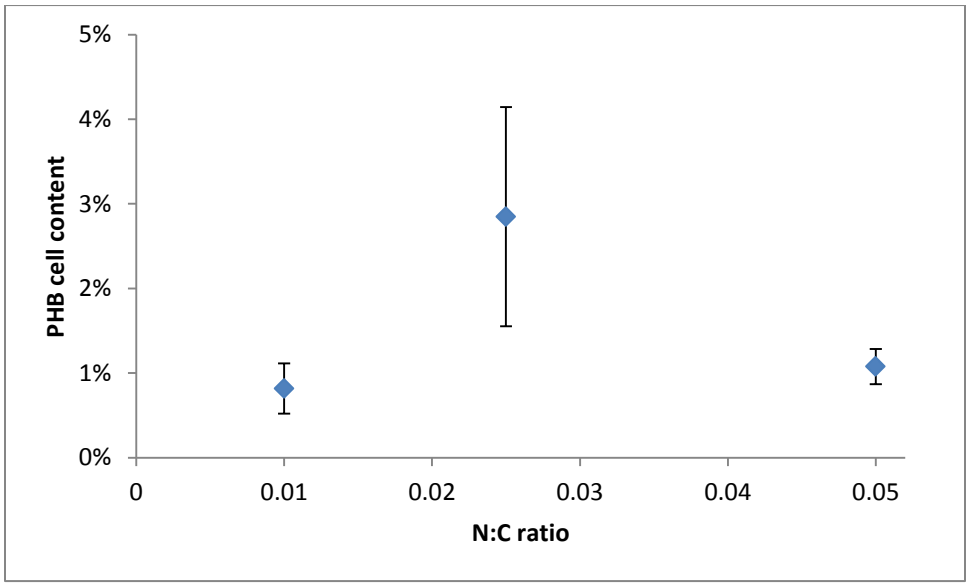

Figure 5-16. PHB cell content for cultures of *M. trichosporium* OB3b under different nitrogen-to-carbon ratios using methane as carbon source. Error bars are standard deviation from two samples.

5.4 Effect of oxygen

The effect of the total amount of available oxygen was assessed by changing the ratio of liquid to overhead volumes (using different amounts of liquid or bottles of different sizes) while keeping the other variables constant. Thus, 50-mL cultures, using methane with a carbon load of 18.8 mmol of methane per L of liquid as the carbon source, nitrate as the nitrogen source, and a nitrogen-to-carbon ratio of 0.025 were grown in 250-mL or 1-L bottles. The actual volume of the 250-mL bottles – taking into account all space available, not only the graduated portion of the volume – was 311 mL, and the actual volume of the 1-L bottles was 1.19 L. The headspace volumes were then 261 mL and 1.14 L, respectively, resulting in an oxygen content of 2.08 mmol and 9.08 mmol, respectively.

Figure 5-17 shows the growth curves obtained for the cultures grown under these two conditions. No significant effect was observed between the cultures, which reached an average final optical density of 0.349 ± 0.008 and 0.398 ± 0.049 units.

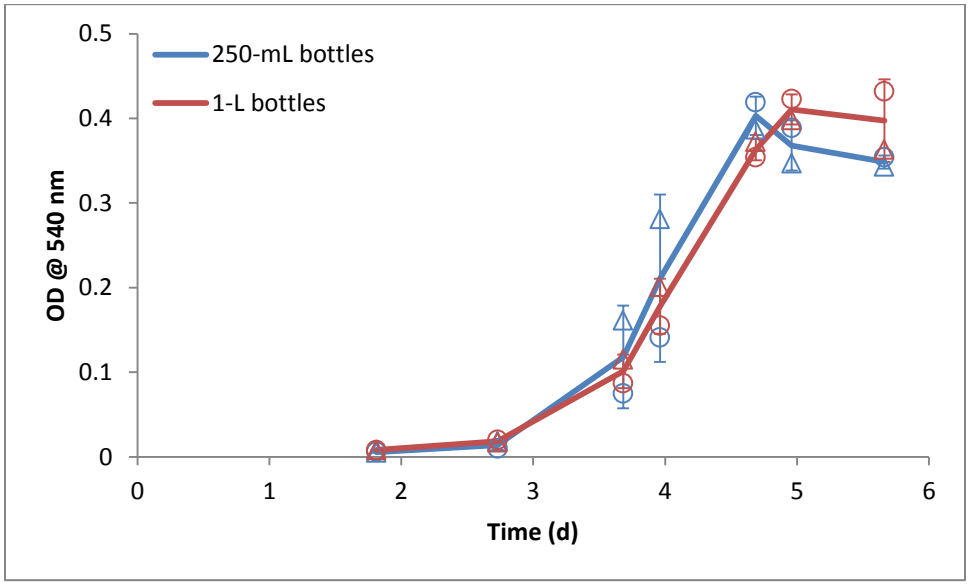

Figure 5-17. Growth curves for *M. trichosporium* OB3b cultures under different oxygen-to-carbon ratios. Error bars are standard deviation from two samples.

On the other hand, Figure 5-18 shows that the total amount of available oxygen in the headspace had a significant effect on the accumulation of PHB. Even with the high variability observed for cultures grown in 1-L bottles, the resulting PHB concentration of 28.6 ± 14.8 mg/L was significantly greater than the PHB concentration of 3.1 ± 2.0 mg/L obtained with cultures grown in the smaller 250-mL bottles

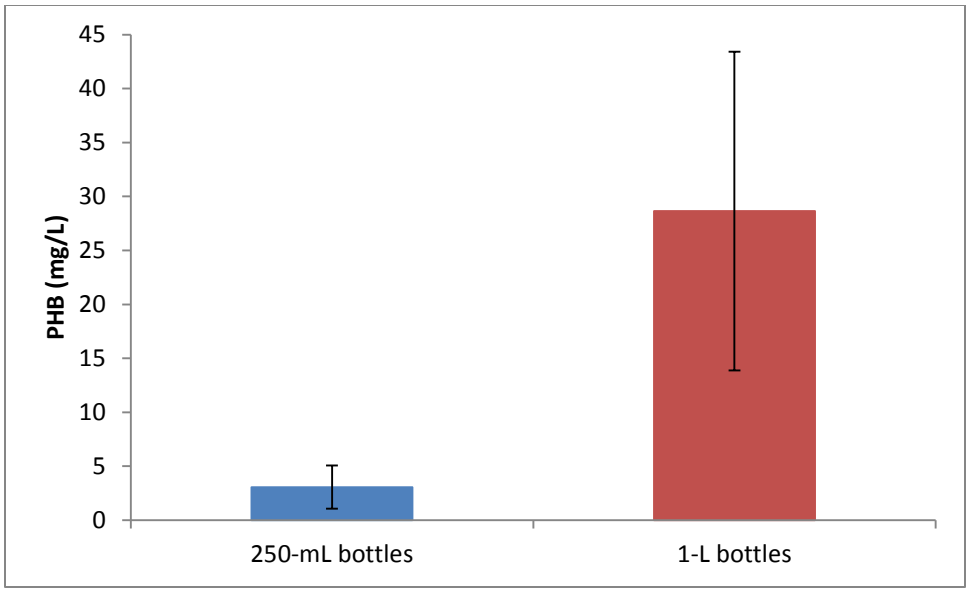

Figure 5-18. PHB concentration from *M. trichosporium* OB3b cultures under different oxygen-to-carbon ratios. Error bars are standard deviations of three samples.

5.5 Response surfaces design

The results presented in the preceding sections were used to plan the design for response surface experiments. A face-centered central composite design was selected because: 1) the region of operation was cuboidal in nature, and 2) it was desired to collect information at the corners of the experimental space (*i.e.*, the conditions at which only methane or methanol was used as carbon source and those at which only ammonium or nitrate was used as nitrogen source). The variables investigated were then the carbon source, the nitrogen source, and the nitrogen-to-carbon ratio, each one at three levels as required by the design (Table 5-9). The same design and cultures were used to gather data to fit the response surfaces for cell dry weight, PHB concentration and PHB content as percentage of cell dry weight.

Table 5-9. Factors and levels for the response surface experiments.

Studied factor	Design levels
Carbon source	100% methane, 100% methanol, and 50% methane + 50% methanol (molar basis)
Nitrogen source	100% ammonium, 100% nitrate, and 50% ammonium + 50% nitrate (molar basis)
Nitrogen-to-carbon ratio	0.005, 0.025, and 0.045

The design space forms a cubic three-dimensional region where the axes correspond to the carbon source (x_1), ranging from pure methane to pure methanol, with mixtures between them; the nitrogen source (x_2), ranging from pure ammonium to pure nitrate, with mixtures of both along the axis, and the nitrogen-to-carbon ratio (x_3), ranging from 0.005 to 0.045. The experimental space is depicted in Figure 5-19.

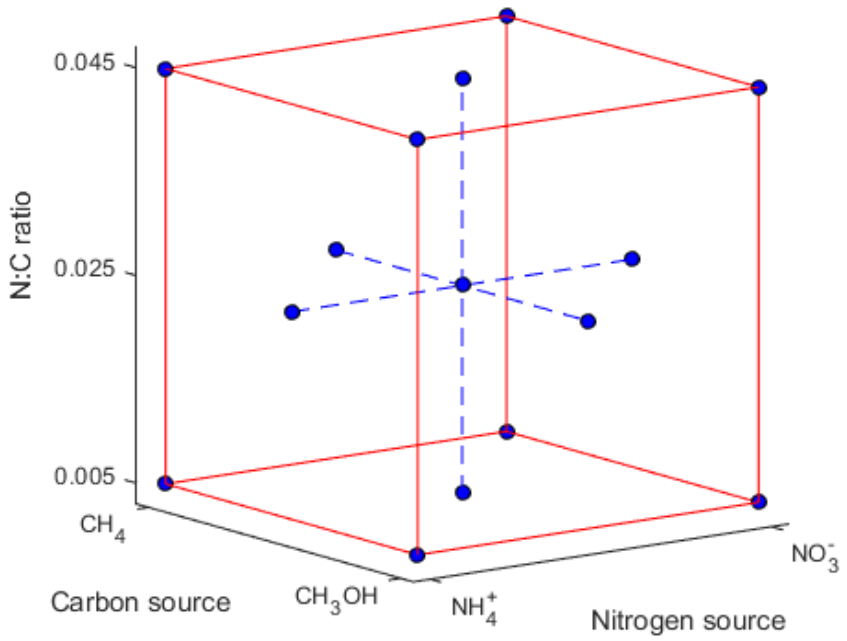

Figure 5-19. Experimental space points for the face-centered central composite design. Three levels of each variable were used in the experiment. Carbon source: pure methane, pure methanol and an equimolar mixture. Nitrogen source: pure ammonium, pure nitrate and an equimolar mixture. Nitrogen-to-carbon ratio: 0.005, 0.025, and 0.045. Four replicates were run at the center point.

To represent the carbon source, variable x_1 was used, coded as follows: let c_1 and c_2 be the molar fraction of methane and methanol in the carbon source. The coded variable for carbon source was:

$$x_1 = c_2 - c_1 \quad \text{Eq. 5-1}$$

To represent the nitrogen source, variable x_2 was used, coded as follows: let n_1 and n_2 be the molar fraction of ammonium and nitrate in the nitrogen source. The coded variable for nitrogen source was:

$$x_2 = n_2 - n_1 \quad \text{Eq. 5-2}$$

To represent the nitrogen-to-carbon ratio, variable x_3 was used, coded as follows: let r_1 and r_2 be the lower and upper limits of the nitrogen-to-carbon ratio for the experiment. If r is the nitrogen-to-carbon ratio, the coded variable for nitrogen-to-carbon ratio was:

$$x_3 = \frac{r - \frac{r_1 + r_2}{2}}{\frac{r_2 - r_1}{2}} \quad \text{Eq. 5-3}$$

As per the face-centered central composite design, coded values of -1, 0 and 1 were used for all the independent variables. These values and the corresponding values in natural units are given in Table 5-10.

This design allows the fitting of a second order polynomial of the form:

$$\hat{y} = b_0 + b_1x_1 + b_2x_2 + b_3x_3 + b_{11}x_1^2 + b_{22}x_2^2 + b_{33}x_3^2 + b_{12}x_1x_2 + b_{13}x_1x_3 + b_{23}x_2x_3 \quad \text{Eq. 5-4}$$

Two of the independent variables were found to be correlated: PHB concentration and PHB cell content. This correlation is shown in Figure 5-20.

Table 5-10. Coded and natural unit levels for the studied variables and responses from the experiments.

Coded variables			Natural units								Responses		
x_1	x_2	x_3	CH_3OH %	CH_3OH mmol	CH_4 mmol	N:C ratio	Total N mmol	NO_3^- %	NO_3^- mmol	NH_4^+ mmol	CDW mg/L	PHB mg/mL	PHB %
-1	-1	-1	0%	0.00	1.00	0.005	0.005	0%	0.0000	0.0050	175.0	29.03	16.59%
-1	-1	1	0%	0.00	1.00	0.045	0.045	0%	0.0000	0.0450	239.3	17.93	7.49%
-1	1	-1	0%	0.00	1.00	0.005	0.005	100%	0.0050	0.0000	185.7	21.32	11.48%
-1	1	1	0%	0.00	1.00	0.045	0.045	100%	0.0450	0.0000	192.9	3.97	2.06%
1	-1	-1	100%	1.00	0.00	0.005	0.005	0%	0.0000	0.0050	22.2	3.16	14.22%
1	-1	1	100%	1.00	0.00	0.045	0.045	0%	0.0000	0.0450	67.9		
1	1	-1	100%	1.00	0.00	0.005	0.005	100%	0.0050	0.0000	188.2		
1	1	1	100%	1.00	0.00	0.045	0.045	100%	0.0450	0.0000	203.6	17.60	8.65%
-1	0	0	0%	0.00	1.00	0.025	0.025	50%	0.0125	0.0125	160.7	19.12	11.90%
1	0	0	100%	1.00	0.00	0.025	0.025	50%	0.0125	0.0125	235.7	28.84	12.24%
0	-1	0	50%	0.50	0.50	0.025	0.025	0%	0.0000	0.0250	203.6	35.48	17.43%
0	1	0	50%	0.50	0.50	0.025	0.025	100%	0.0250	0.0000	267.9	31.72	11.84%
0	0	-1	50%	0.50	0.50	0.005	0.005	50%	0.0250	0.0250	164.3	34.59	21.05%
0	0	1	50%	0.50	0.50	0.045	0.045	50%	0.0225	0.0225		13.30	
0	0	0	50%	0.50	0.50	0.025	0.025	50%	0.0125	0.0125	257.1	33.46	13.01%
0	0	0	50%	0.50	0.50	0.025	0.025	50%	0.0125	0.0125	246.4	27.30	11.08%
0	0	0	50%	0.50	0.50	0.025	0.025	50%	0.0125	0.0125	192.9	41.05	21.29%
0	0	0	50%	0.50	0.50	0.025	0.025	50%	0.0125	0.0125	235.7	39.01	16.55%

CDW: Cell dry weight.

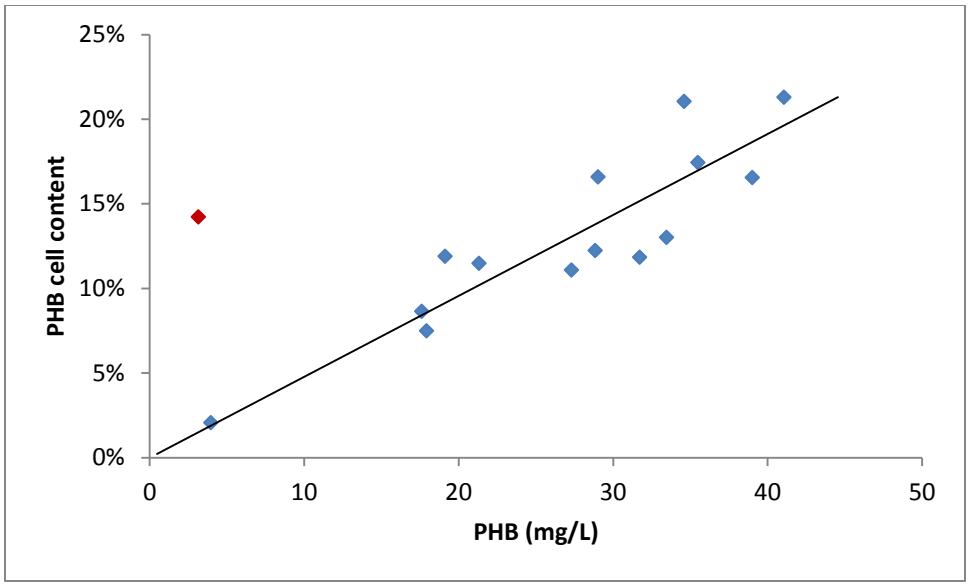

Figure 5-20. Linear correlation between PHB concentration and PHB cell content. The regression equation is $y = 0.00478x$ and the coefficient of determination is $R^2 = 0.7985$. The outlier point marked in red was not considered in the regression.

5.6 Response surface for cell dry weight

Response surface analysis was performed to determine the conditions favouring the attainment of optimal growth conditions as measured by optical density and cell dry weight. During the fitting of this response surface, two outliers were identified. Figure 5-21 shows the predicted versus observed values and residuals versus predicted values plots for the model before the elimination of these two outliers (Figure 5-21a and Figure 5-21d), after the elimination of the first outlier (Figure 5-21b and Figure 5-21e) and after the removal of both outlier points (Figure 5-21c and Figure 5-21f). It is interesting to note that the second outlier was not evident from the plots (Figure 5-21a and Figure 5-21d) until after the elimination of the first outlier (Figure 5-21b and Figure 5-21e). Moving forward, these two obvious outliers were removed from the analysis.

Figure 5-21c shows a very close fit of the model to the experimental data, with the predicted and observed values closely distributed around the $x = y$ reference line, and Figure 5-21f shows a satisfactory distribution of the residuals along the range of predicted values with no evident trend.

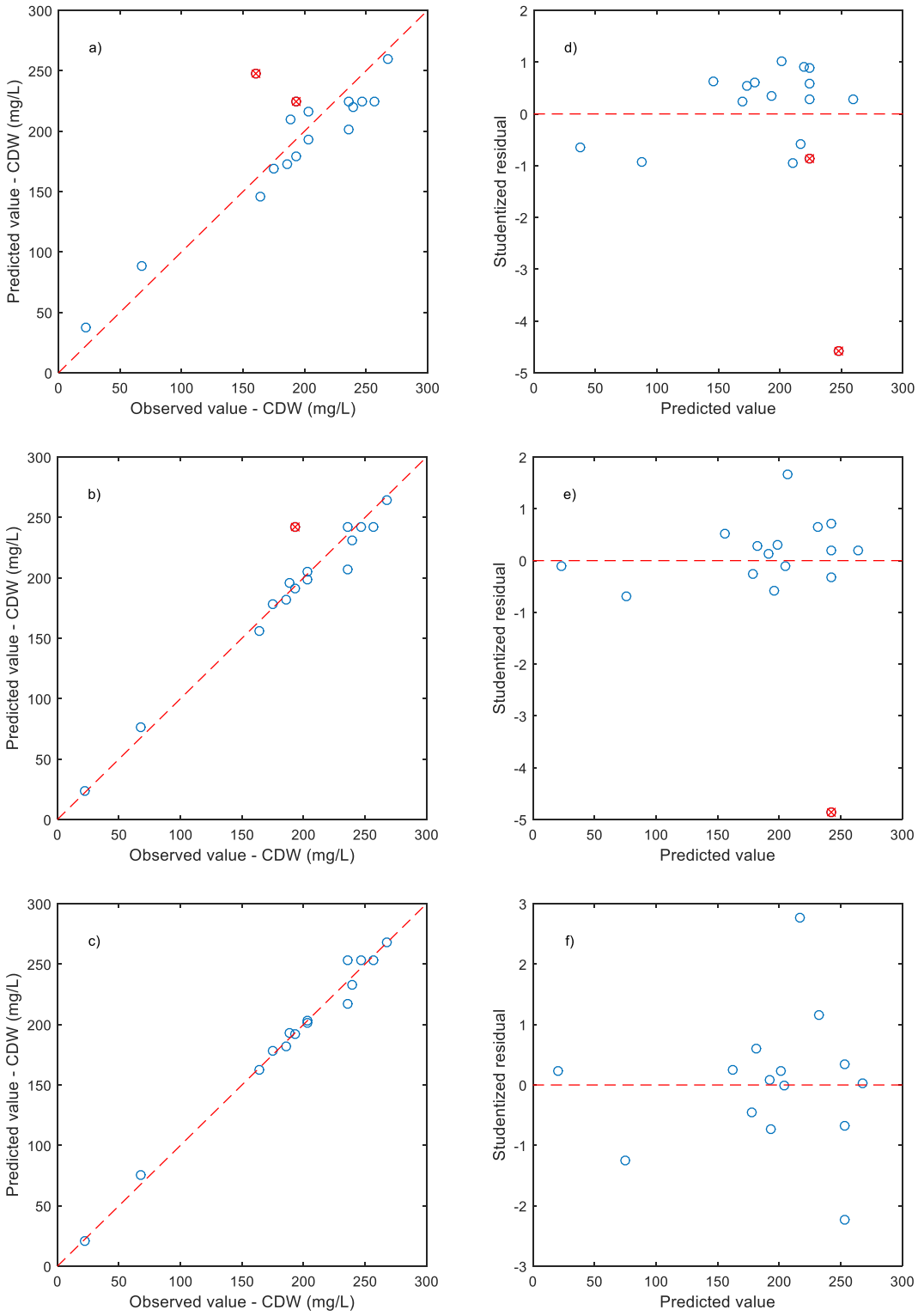

Figure 5-21. Diagnostic plots for the regression of the response surface for cell dry weight. Predicted values versus observed values (a) before taking out any of the outliers, (b) after taking out the first outlier and (c) after taking out both outliers. Studentized residuals plotted against predicted values (d) before taking out any of the outliers, (e) after taking out the first outlier and (f) after taking out both outliers. The outlier points are identified on the graphs as red crossed circles.

The ANOVA for the regression is shown on Table 5-11. The model was significant with a low *p*-value and showed no significant lack of fit. The adjusted coefficient of determination was high—0.97—as could be expected from the close agreement of the predicted and observed values for cell dry weight already shown in Figure 5-21c. (Before the outliers were eliminated from the analysis, the adjusted coefficient of determination was $R^2_{adj} = 0.62$.)

Table 5-11. Analysis of variance for the regression of cell dry weight.

	Sum of squares	Degrees of freedom	Mean square	F	*p*-Value
Total	64631.44	14	4616.53		
Model	63743.09	7	9106.16	71.75	5.5200e-06
. Linear	21882.16	3	7294.05	57.48	2.6889e-05
. Nonlinear	41860.93	4	10465.23	82.46	5.7270e-06
Residual	888.35	7	126.91		
. Lack of fit	658.76	5	131.75	1.15	0.5265
. Pure error	229.59	2	114.80		
R-squared: 0.9863, adjusted R-squared: 0.9725					

Two terms—x_1^2 and x_1x_3—were taken out of the model for lack of significance as indicated by high *p*-values (0.24 for b_{11} and 0.76 for b_{13}). The final adjusted model was thus:

$$\hat{y} = b_0 + b_1x_1 + b_2x_2 + b_3x_3 + b_{22}x_2^2 + b_{33}x_3^2 + b_{12}x_1x_2 + b_{23}x_2x_3 \quad \text{Eq. 5-5}$$

The values of the estimated coefficients are given on Table 5-12. All of the terms are significant as indicated by their *p*-values being lower than 0.05.

Table 5-12. Estimated parameters for the regression of cell dry weight and significance tests.

Parameter	Estimate	Standard error	t	*p*-Value
b_0	253.4208	5.3341	47.51	4.7876e-10
b_1	-36.5197	3.8016	-9.61	2.7860e-05
b_2	33.0299	3.5624	9.27	3.5138e-05
b_3	16.2795	3.8569	4.22	0.0039
b_{22}	-18.7883	7.7357	-2.43	0.0455
b_{33}	-75.0192	7.3904	-10.15	1.9382e-05
b_{12}	42.1802	3.9829	10.59	1.4640e-05
b_{23}	-10.9302	3.9829	-2.74	0.0287

5.6.1 Response surfaces for cell dry weight with constant carbon source

Given that the resulting response surface was tetra-dimensional, graphical representation of the response surfaces are presented holding one variable fixed and plotting the resulting three-dimensional surface against the other two variables. The first set of surfaces is reported when the carbon source is kept constant.

5.6.1.1 Methane as the carbon source

Figure 5-22 shows the response surface for cell dry weight for methane as the carbon source ($x_1 = -1$) and Figure 5-23 shows the corresponding contour plot. As can be observed, at low N:C ratios, the predicted effect of the nitrogen source had little impact—approximately the same cell dry weight was predicted irrespectively of the nitrogen source used. However, at higher N:C ratios, a greater cell dry weight was predicted for ammonium than for nitrate. In the mid-range of N:C ratio, the same phenomenon was observed, greater cell dry weight values were seen for ammonium than for nitrate, although to a lesser extent.

The response surface also showed that at a specific nitrogen-to-carbon ratio (especially in the mid-range of ratios) there was a mixture of nitrogen sources for which the predicted value of cell dry weight was maximized.

The most influential predictor was the N:C ratio. Greater values of cell dry weight were predicted at higher N:C ratios than at low ones, and the greatest were found in the medium values of the range tested.

The maximum cell dry weight, $\hat{y} = 292$ mg/L, was predicted for $x_2 = -0.28$ (64%mol NH_4^+ and 36%mol NO_3^-) and $x_3 = 0.13$ (N:C ratio of 0.028).

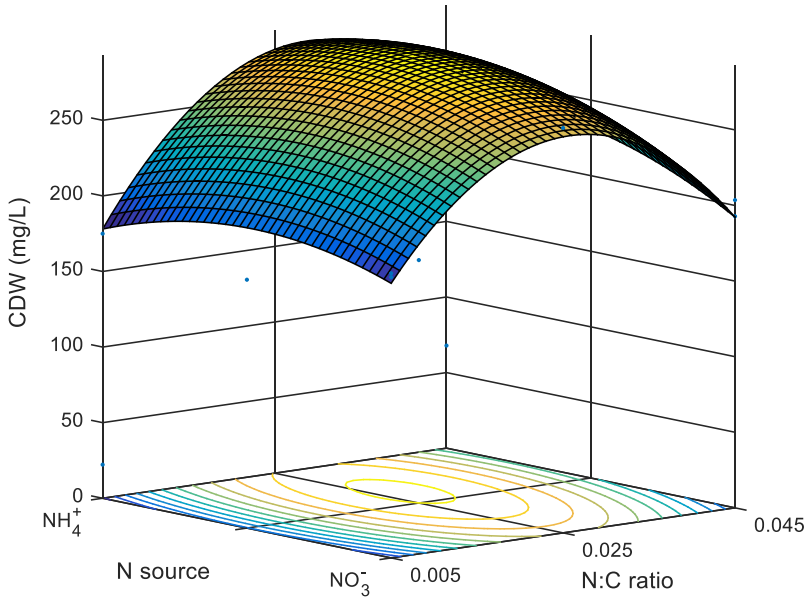

Figure 5-22. Cell dry weight response surface for methane as the carbon source ($x_1 = -1$).

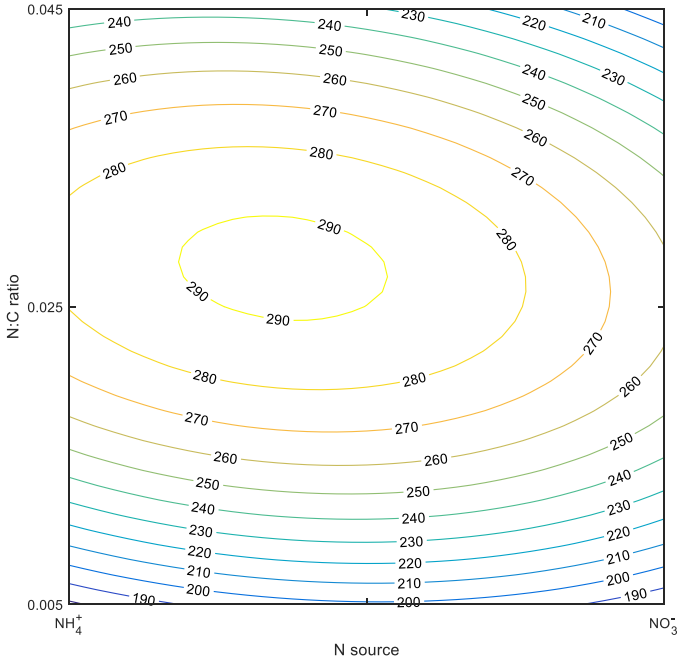

Figure 5-23. Contour plot of cell dry weight for methane as carbon source ($x_1 = -1$).

5.6.1.2 Methanol as the carbon source

Figure 5-24 shows the response surface for cell dry weight when methanol was used as the carbon source ($x_1 = 1$) and Figure 5-25 shows the corresponding contour plot. In this case, greater cell dry weights were predicted for nitrate as the nitrogen source than for ammonium, irrespective of the N:C ratio. As opposed to the previous case of methane as carbon source, mixtures of nitrogen source did not increase the predicted value above those seen with nitrate as sole nitrogen source.

The maximum cell dry weight, $\hat{y} = 273$ mg/L, lower than for methane, was observed for $x_2 = 1$ (100% NO_3^-) and $x_3 = 0.04$ (N:C ratio of 0.026).

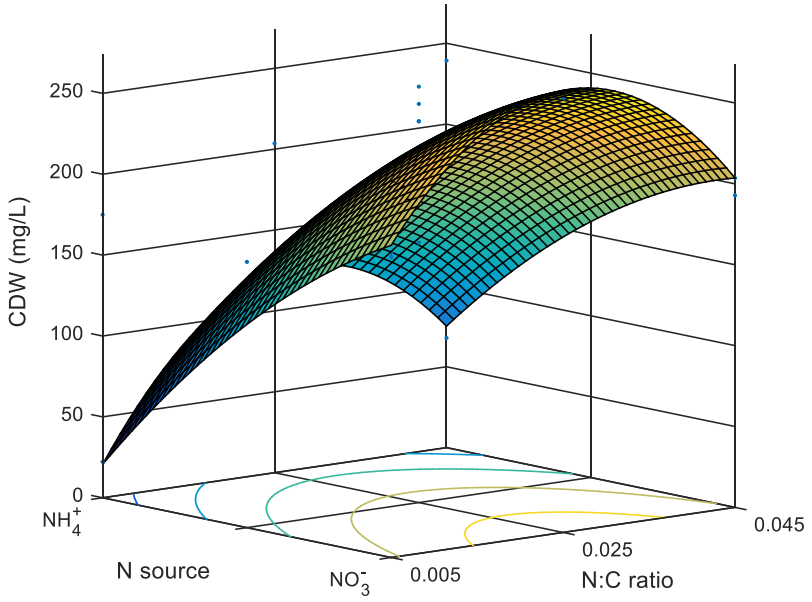

Figure 5-24. Cell dry weight response surface for methanol as the carbon source ($x_1 = 1$).

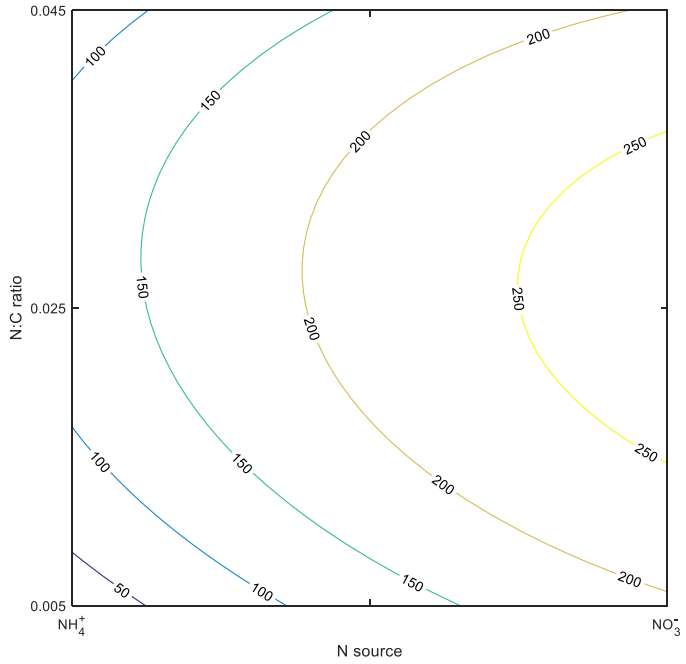

Figure 5-25. Contour plot of cell dry weight for methanol as carbon source ($x_1 = 1$).

5.6.1.3 *Equimolar mixture of carbon sources*

The response surface for an equimolar mixture of carbon sources (x_1 = 0), seen in Figure 5-26 and Figure 5-27, had a similar trend to the one observed for methanol — greater cell dry weights observed with nitrate. However, in this case, the differences in cell dry weight between the different conditions were not as large. In addition, a small region was observed in the mid-range of N:C ratios for which greater cell dry weights were predicted when mixtures of nitrate with small amounts of ammonium were used. In fact, the predicted maximum for this condition ($\hat{y} = 268$ mg/L, lower than for both methane and methanol) occurred within this region at $x_2 = 0.87$ (7%mol NH_4^+/ 93%mol NO_3^-) and $x_3 = 0.05$ (N:C ratio of 0.026).

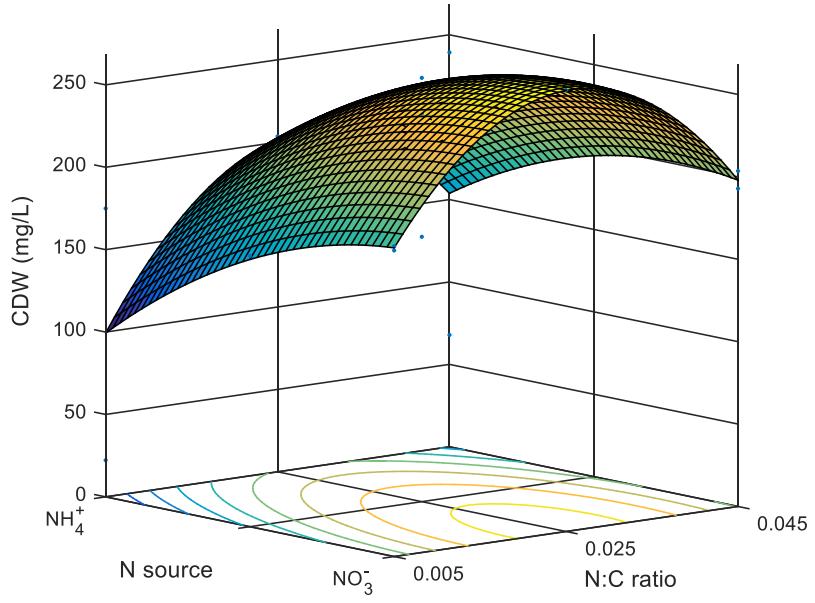

Figure 5-26. Cell dry weight response surface for an equimolar mixture of methane and methanol as carbon source ($x_1 = 0$).

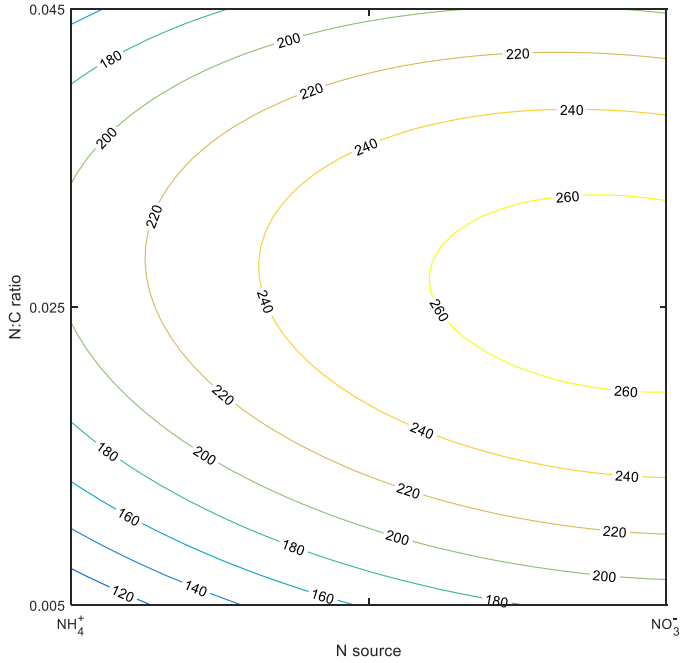

Figure 5-27. Contour plot of cell dry weight for an equimolar mixture of methane and methanol as carbon source ($x_1 = 0$).

5.6.2 Response surfaces for cell dry weight with constant nitrogen source

5.6.2.1 Ammonium as the nitrogen source

When ammonium was the nitrogen source ($x_2 = -1$), greater cell dry weights were predicted when using methane than when using methanol, and this occurred at all nitrogen-to-carbon ratios (Figure 5-28 and Figure 5-29). Also, greater cell dry weights were predicted in the mid-range of N:C ratios. The predicted maximum had a value of $\hat{y} = 283$ mg/L, and occurred at $x_1 = -1$ (100% NH_4^+) and $x_3 = 0.18$ (N:C ratio of 0.029).

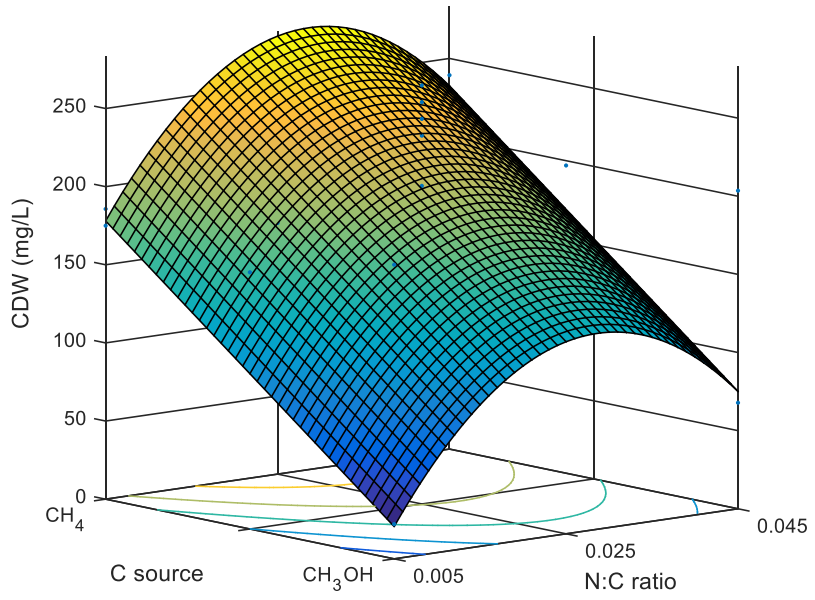

Figure 5-28. Cell dry weight response surface for ammonium as the nitrogen source ($x_2 = -1$).

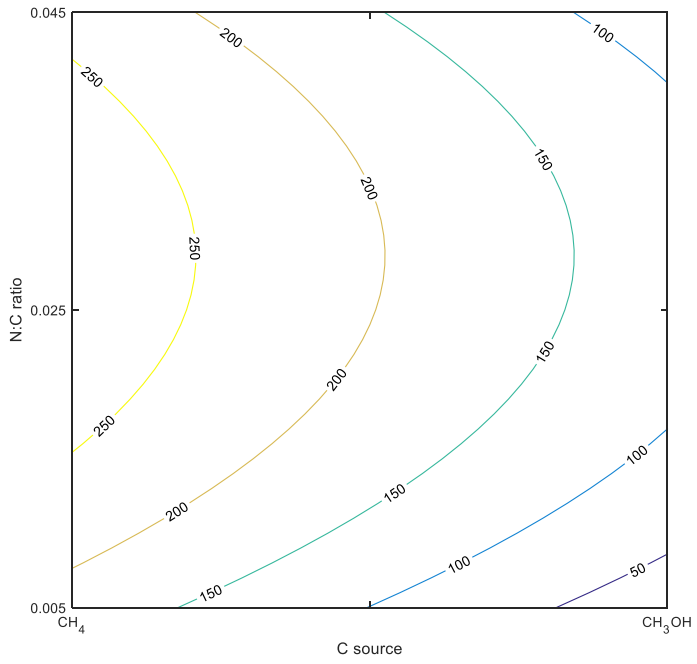

Figure 5-29. Contour plot of cell dry weight for ammonium as the nitrogen source ($x_2 = -1$).

5.6.2.2 *Nitrate as the nitrogen source*

The response surface for cell dry weight when nitrate was used as the nitrogen source ($x_2 = 1$) is shown in Figure 5-30 and the contour plot in Figure 5-31. In this case, the choice of carbon source had little effect on the predicted value of cell dry weight. Again, the use of a mid-range nitrogen-to-carbon ratio resulted in greater values of cell dry weight. The predicted maximum had a value of $\hat{y} = 273$ mg/L, and occurred at $x_1 = 1$ (100% CH_3OH) and $x_3 = 0.04$ (N:C ratio of 0.026). However, it should be noted that, for the same N:C ratio and methane (x_1 = -1), the predicted cell dry weight was only 4% lower.

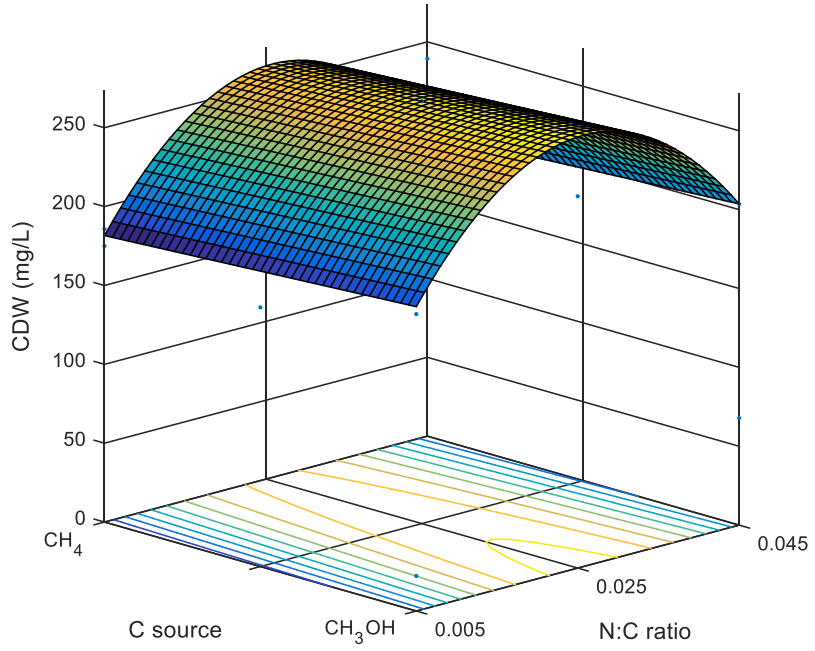

Figure 5-30. Cell dry weight response surface for nitrate as the nitrogen source ($x_2 = 1$).

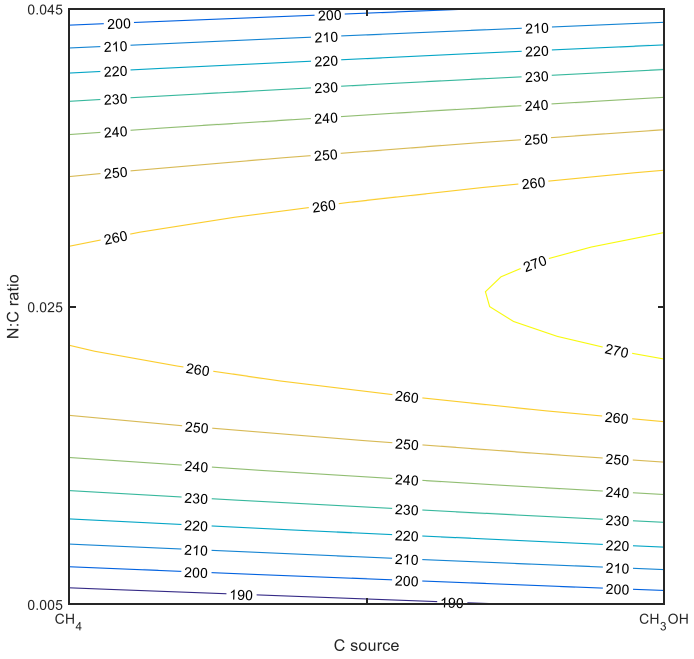

Figure 5-31. Contour plot of cell dry weight for nitrate as the nitrogen source ($x_2 = 1$).

5.6.2.3 Equimolar mixtures of nitrogen sources

The response surface for cultures grown with an equimolar mixture of nitrogen sources ($x_2 = 0$) is presented in Figure 5-32 and the contour plot in Figure 5-33. The use of an equimolar mixture of ammonium and nitrate as nitrogen source resulted in a surface similar to that observed when ammonium was used as the sole nitrogen source. Greater values of cell dry weight were observed for methane as the carbon source ($x_1 = -1$) compared to methanol ($x_1 = 1$). However, the differences in cell dry weights between these conditions were not as marked as when ammonium was used as the sole nitrogen source. As in all the previous cases, higher values of cell dry weight were predicted in the mid-range of nitrogen-to-carbon ratios. The predicted maximum had a value of $\hat{y} = 291$ mg/L, and occurred at $x_1 = -1$ (100% CH_4) and $x_3 = 0.11$ (N:C ratio of 0.027).

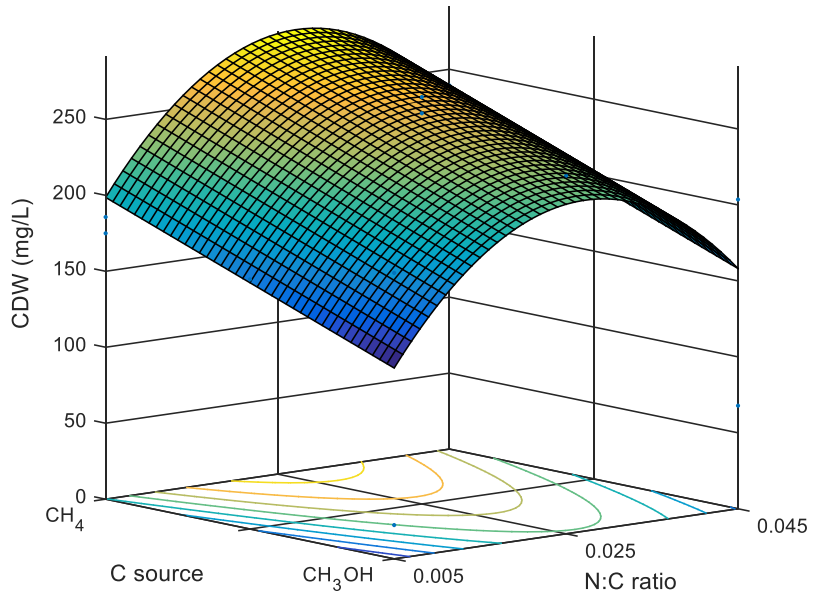

Figure 5-32. Cell dry weight response surface for an equimolar mixture of ammonium and nitrate as the nitrogen source ($x_2 = 0$).

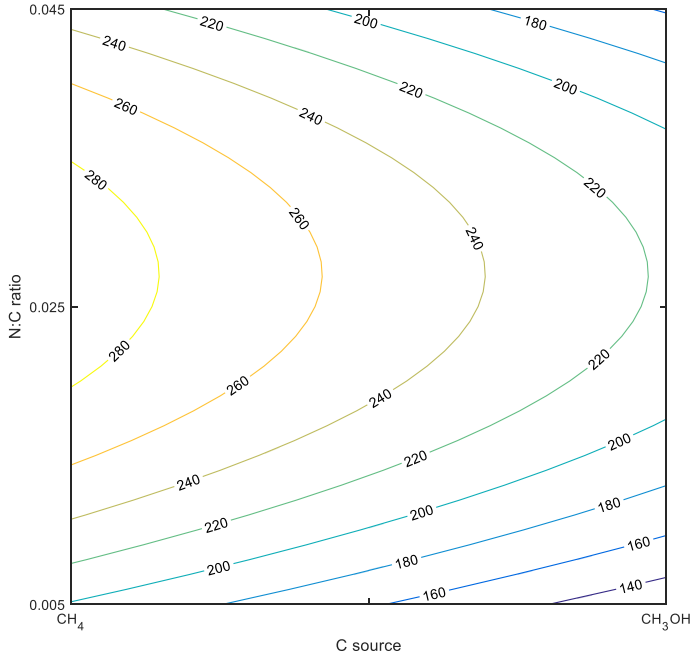

Figure 5-33. Contour plot of cell dry weight for an equimolar mixture of ammonium and nitrate as the nitrogen source ($x_2 = 0$).

5.6.3 Response surface for cell dry weight summary

In general, greater cell dry weights were predicted for methane than for methanol, and at the mid-range of nitrogen-to-carbon ratios. The choice of nitrogen source was very important when using methanol as the carbon source since concurrent use of methanol and ammonium resulted in significantly lower cell dry weights. The choice of nitrogen source was not as crucial when the carbon source was methane. Also, when using methane, some mixtures of nitrogen source resulted in higher predictions of cell dry weight when compared to the pure nitrogen sources.

The predicted maximum for the system as a whole occurred at the methane boundary of the design region, with mixed nitrogen source and medium nitrogen-to-carbon ratio. This and other fixed conditions are shown in Table 5-13.

Table 5-13. Summary of maximum cell dry weight predictions at various fixed conditions.

Fixed condition	$\hat{y}_{max}$ (mg/L)	x_1	CH_4 /CH_3OH (%mol)	x_2	NH_4^+/ NO_3^- (%mol)	x_3	N:C ratio
Carbon source							
- Methane*	292	-1	100/0	-0.28	64/36	0.13	0.028
- Methanol	273	1	0/100	1	0/100	0.04	0.026
- Equimolar	268	0	50/50	0.87	7/93	0.05	0.026
Nitrogen source							
- Ammonium	283	-1	100/0	-1	100/0	0.18	0.029
- Nitrate	273	1	0/100	1	0/100	0.04	0.026
- Equimolar	291	-1	100/0	0	50/50	0.11	0.027

*System maximum

5.7 Response surface for PHB concentration

A polynomial in the form of Eq. 5-4 was fitted to the PHB concentration data from the cultures. Three of the second order terms—x_2^2, x_1x_3, and x_2x_3—were found not to be significant and, consequently, were taken out of the model, to get a final model of the form:

$$\hat{y} = b_0 + b_1x_1 + b_2x_2 + b_3x_3 + b_{11}x_1^2 + b_{33}x_3^2 + b_{12}x_1x_2 \qquad \text{Eq. 5-6}$$

The values of the b_i parameters of Eq. 5-6 are given in Table 5-14. From this table, it can be seen that all of the parameters had a *p*-value of less than 0.05, except for those corresponding to x_1 and x_2 (b_1 and b_2). Those first-order parameters were left in the model despite their high *p*-values to support the hierarchy.

Table 5-14. Estimated parameters for the regression of PHB concentration and significance tests.

Parameter	Estimate	Standard error	t	*p*-Value
b_0	34.4532	2.2872	15.06	1.0876e-07
b_1	-1.5268	2.1975	-0.69	0.5047
b_2	2.8702	2.3724	1.21	0.2572
b_3	-7.5009	2.3724	-3.16	0.0115
b_{11}	-9.8197	3.4746	-2.83	0.0198
b_{33}	-9.8578	3.4746	-2.84	0.0195
b_{12}	9.4759	2.7703	3.42	0.0076

As can be seen from the model ANOVA table (Table 5-15), the overall *p*-value for the resulting model was 0.0035. From that table, one can also see that no significant lack of fit was found (*p*-value of 0.58) and that the value of adjusted coefficient of determination was 0.73, that is, 73% of the observed variation can be explained by the model.

Table 5-15. Analysis of variance for the regression of PHB concentration.

	Sum of squares	Degrees of freedom	Mean square	F	*p*-Value
Total	2017.49	15	134.50		
Model	1695.15	6	282.52	7.89	0.0035
. Linear	164.46	3	54.82	1.53	0.2724
. Nonlinear	1530.69	3	510.23	14.25	9.1479e-04
Residual	322.34	9	35.82		
. Lack of fit	208.16	6	34.69	0.91	0.5799
. Pure error	114.18	3	38.06		
R-squared: 0.8402, adjusted R-squared: 0.7337					

Figure 5-34 shows the values predicted by the model plotted against the values observed during the experiment. The points were distributed reasonably well around the 45° reference line ($x = y$).

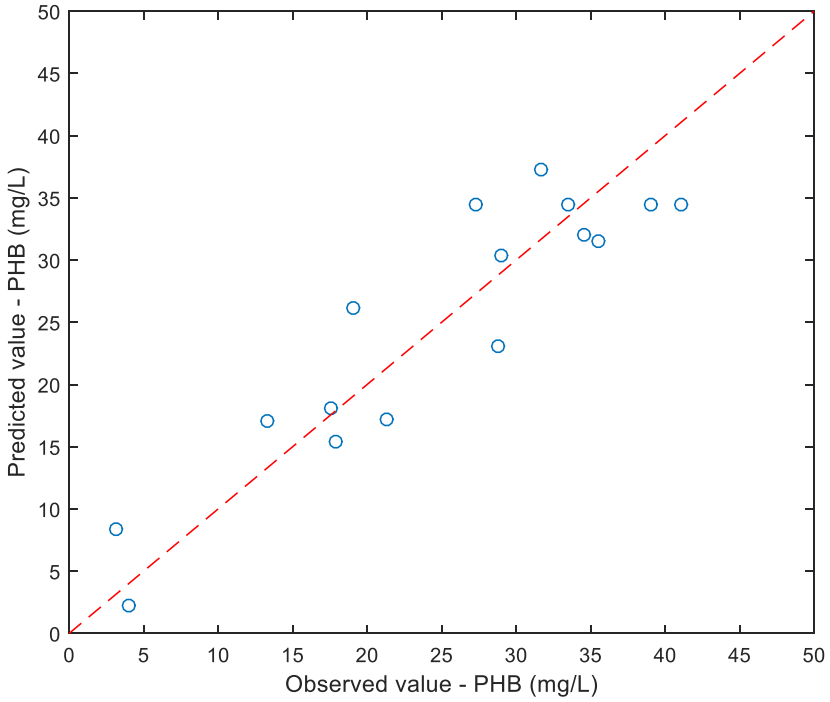

Figure 5-34. Predicted versus observed values for the PHB concentration response surface. The red diagonal is the reference line $y = x$.

The values of the residuals were further analyzed (Figure 5-35). Figure 5-35a shows the normal probability plot of the residuals. Ideally, the residuals should align approximately along the reference line and any significant deviation would indicate a non-normal distribution. No such deviation was observed. Only a slightly fat upper tail was hinted at by the upward shift of the last point on the graph. Figure 5-35b shows a plot of the residuals against the predicted value. No definite trend could be observed and the random distribution of the residuals was similar regardless of the magnitude of the predicted value.

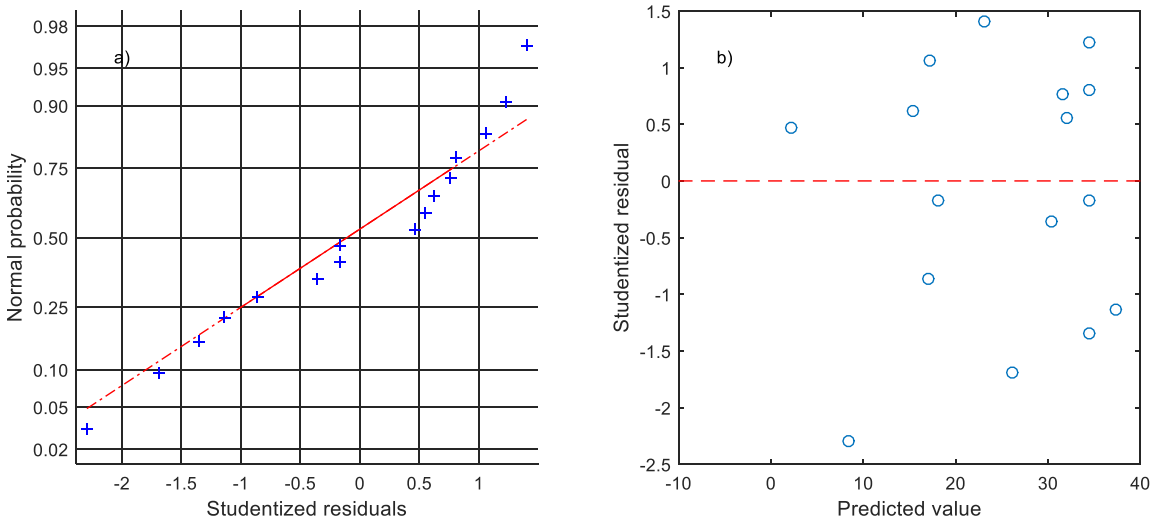

Figure 5-35. Diagnostic plots for the residuals from the regression of the response surface for PHB concentration. (a) Normal probability plot of the Studentized residuals. (b) Studentized residuals versus predicted values.

5.7.1 Response surfaces for PHB concentration with constant carbon source

As in Section 5.6, due to the tetra-dimensional nature of the response surface, graphical representation of the response surfaces are presented holding one variable fixed and plotting the resulting three-dimensional surface against the other two variables. The first set of surfaces is reported when the carbon source is kept constant.

5.7.1.1 Methane as carbon source

Fixing the value of $x_1 = -1$ is equivalent to looking at all the results for which the carbon source was methane. Figure 5-36 shows the resulting response surface and Figure 5-37 shows the corresponding contour plot. Generally, the PHB concentration was greater when ammonium was the nitrogen source. From this results, the predicted maximum, a concentration of $\hat{y} = 34$ mg/L, occurred at a boundary of the design region, at $x_2 = -1$ (100% NH_4^+), and $x_3 = -0.38$ (N:C ratio of 0.017).

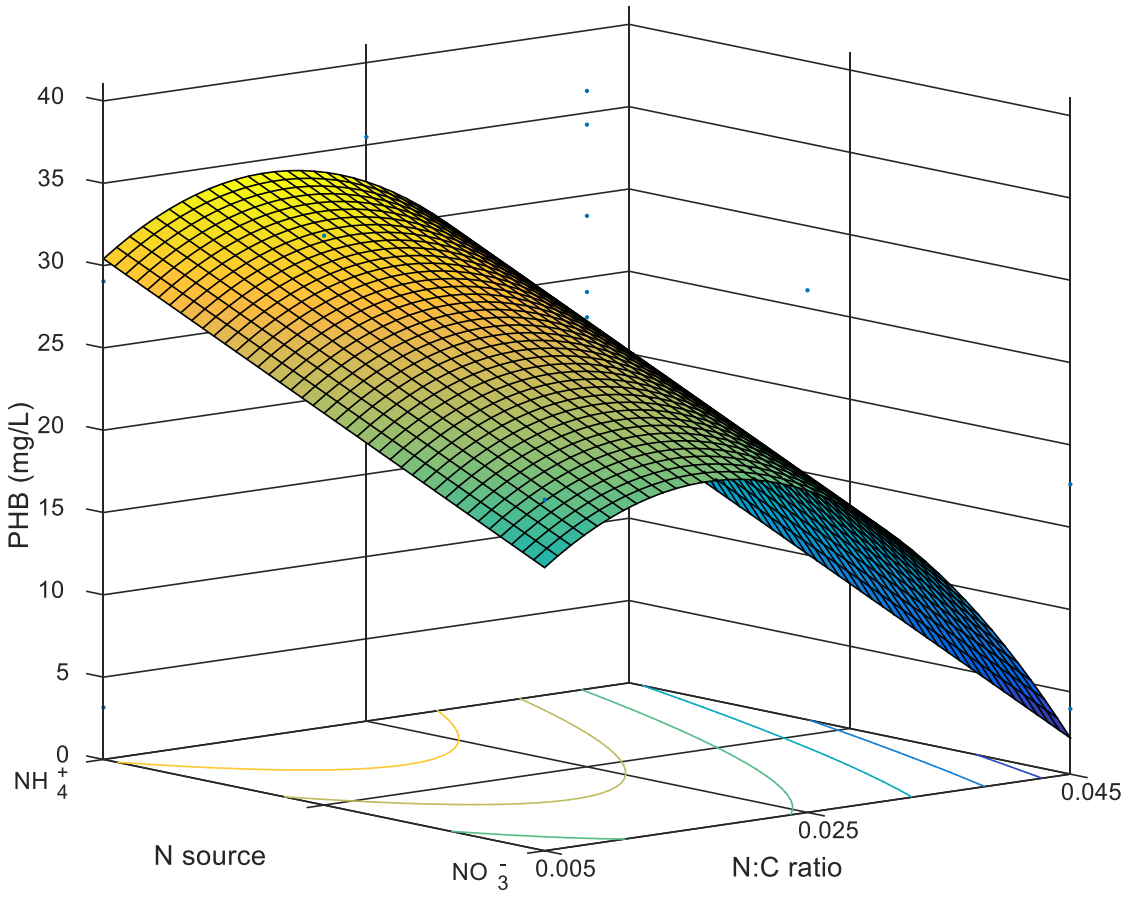

Figure 5-36. PHB concentration response surface for methane as carbon source ($x_1 = -1$).

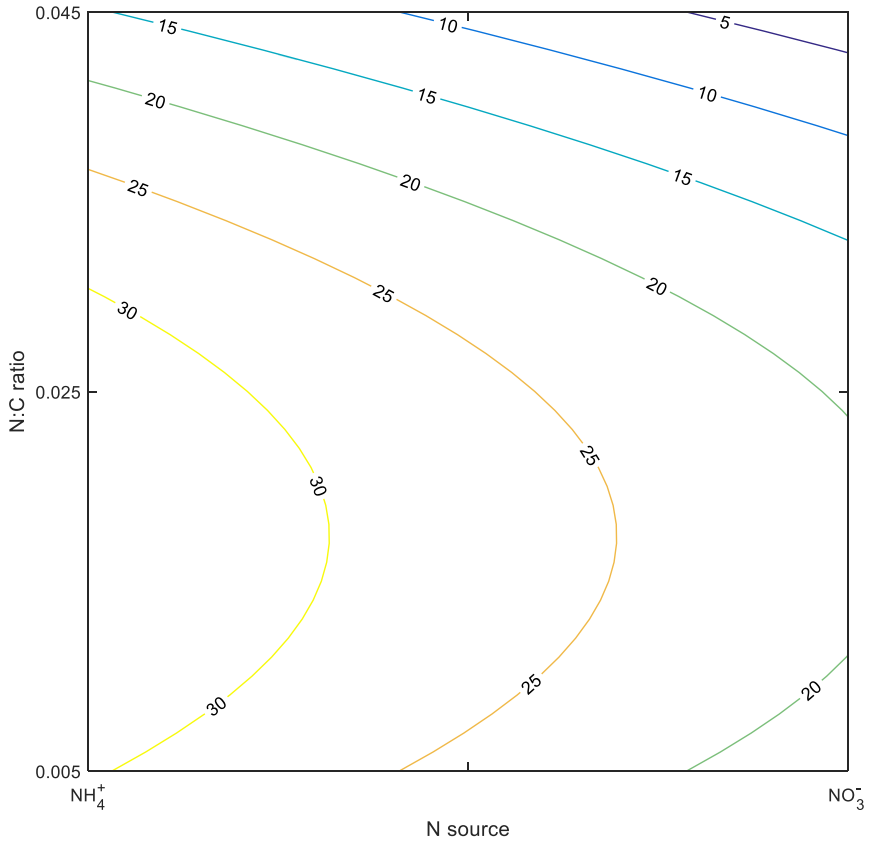

Figure 5-37. Contour plot of PHB centration for methane as carbon source ($x_1 = -1$).

5.7.1.2 Methanol as carbon source

When changing the carbon source to 100% methanol ($x_1 = 1$), the predicted behaviour changed. Figure 5-38 shows the corresponding response surface, and Figure 5-39 shows the corresponding contour plot.

The predicted maximum occurred again at a boundary of the design region, this time, at the opposite boundary where the nitrogen source was 100% nitrate ($x_2 = 1$), and an N:C ratio of 0.017 ($x_3 = -0.38$). The value of the N:C ratio at the predicted maximum was the same as in the case of methane as the carbon source, but a higher PHB concentration was predicted, $\hat{y} = 37$ mg/L.

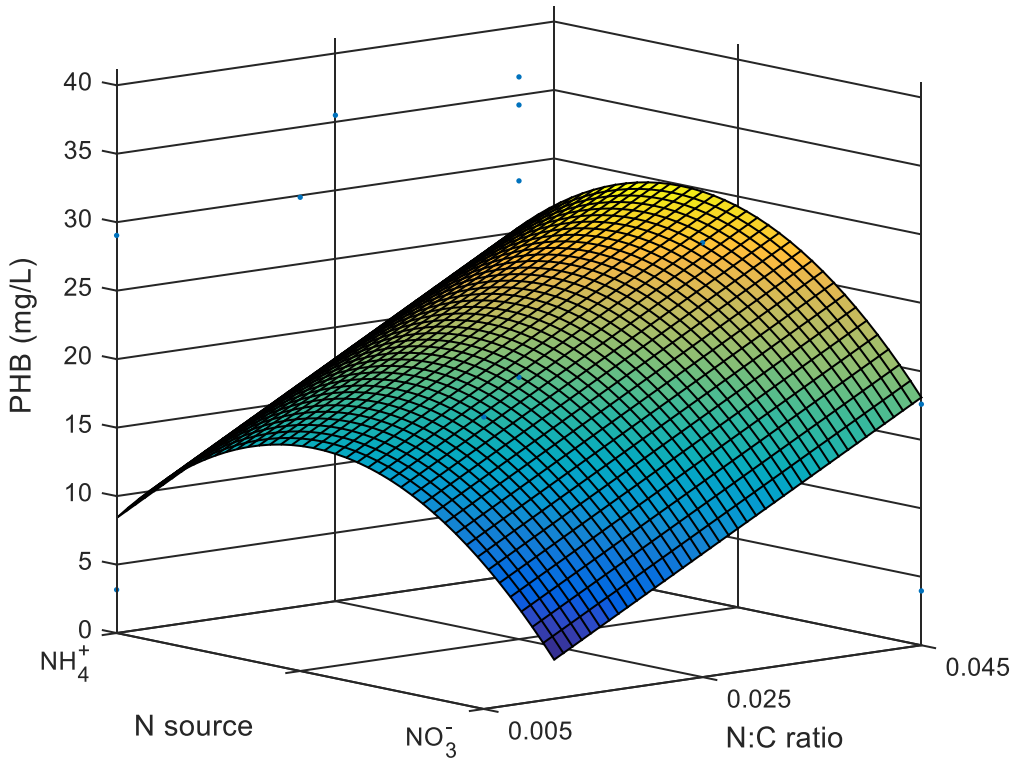

Figure 5-38. PHB concentration response surface for methanol as carbon source ($x_1 = 1$).

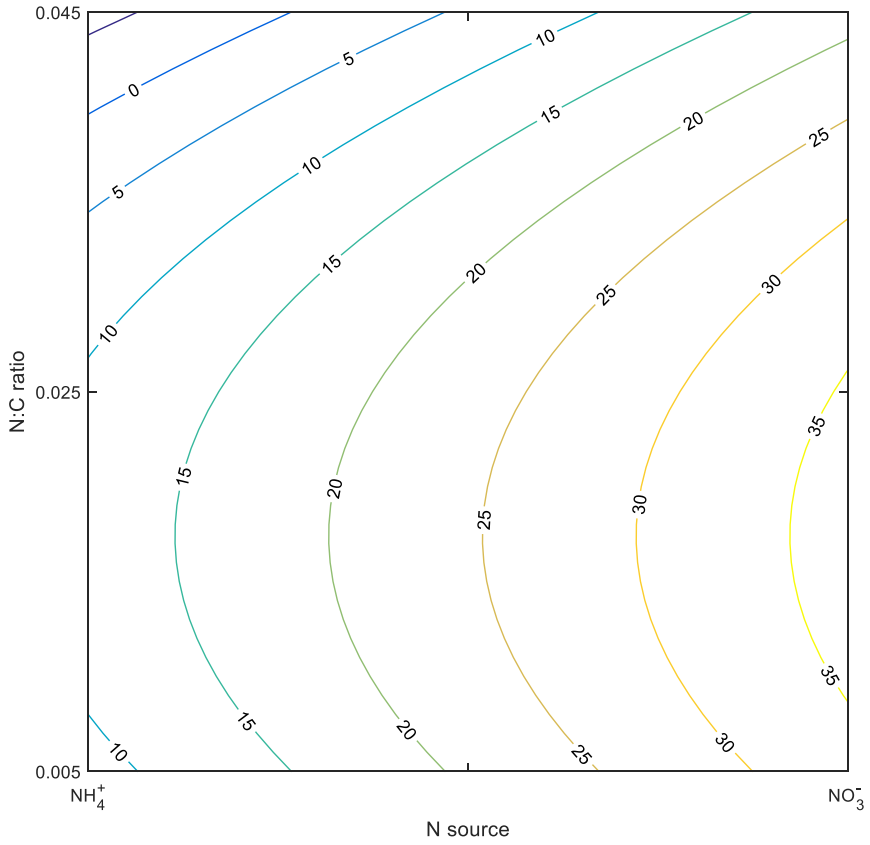

Figure 5-39. Contour plot of PHB concentration for methanol as carbon source ($x_1 = 1$).

5.7.1.3 Equimolar carbon sources

Fixing the value of $x_1 = 0$ allowed us to explore the response surface when the carbon source was an equimolar mixture of methane and methanol. Figure 5-40 shows the response surface and Figure 5-41 shows the corresponding contour plot.

The predicted maximum occurred again at the boundary of the design region corresponding to nitrate as the nitrogen source, $x_2 = 1$ (100% NO_3^-), and at the same nitrogen-to-carbon ratio as in the previous two cases, $x_3 = -0.38$ (N:C ratio of 0.017), but a synergistic effect of the mixing of methane and methanol was predicted this time, with a predicted value for the PHB concentration of $\hat{y} = 39$ mg/L.

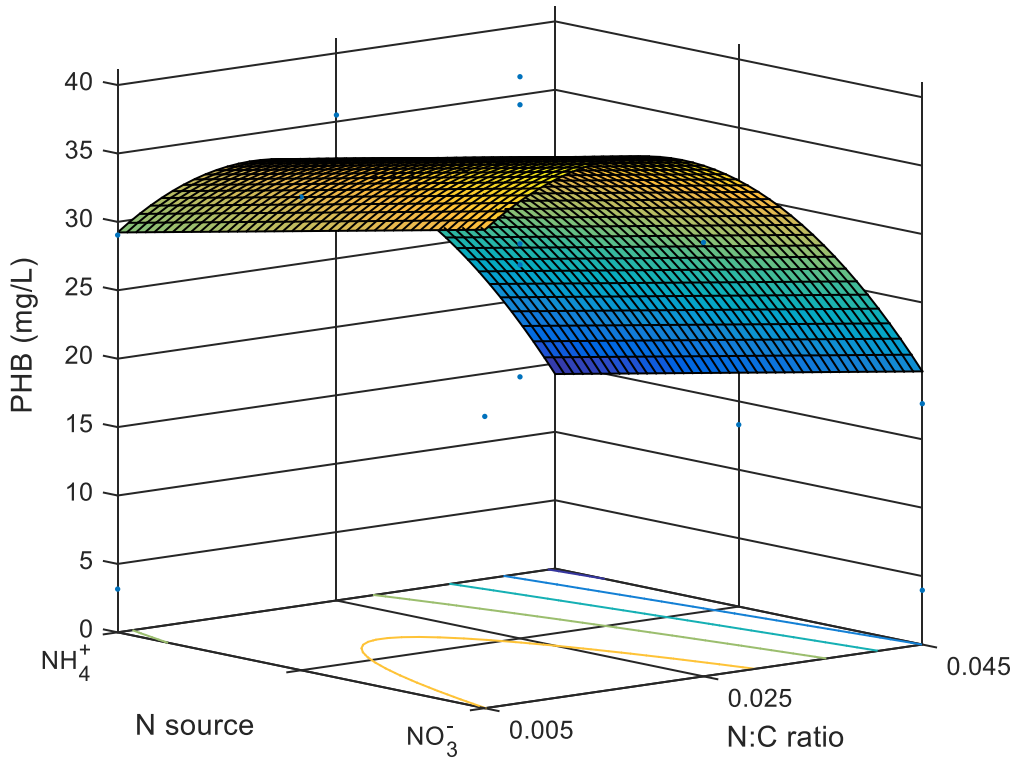

Figure 5-40. PHB concentration response surface for an equimolar mixture of methane and methanol as carbon source ($x_1 = 0$).

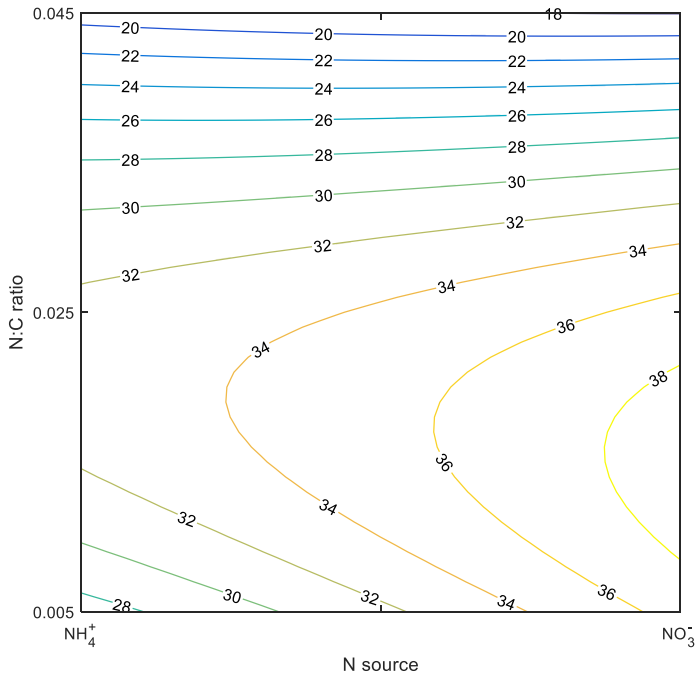

Figure 5-41. Contour plot of PHB concentration for an equimolar mixture of methane and methanol as carbon source ($x_1 = 0$).

5.7.2 Response surfaces for PHB concentration with constant nitrogen

Having explored the response surfaces while keeping the carbon source (constant values of x_1), results were analyzed when the nitrogen source was kept constant – holding the value of x_2 constant.

5.7.2.1 Ammonium as nitrogen source

Figure 5-42 shows the response surface obtained when fixing $x_2 = -1$, that is, when the nitrogen source was 100% ammonium, and Figure 5-43 shows the corresponding contour plot. In this case, the convex surface shows a predicted maximum within the experimental region, at $x_1 = -0.56$ (a mixture of 78%mol methane and 22%mol methanol) and x_3 = -0.38 (N:C ratio of 0.017). This time, the predicted PHB concentration was $\hat{y} = 36$ mg/L.

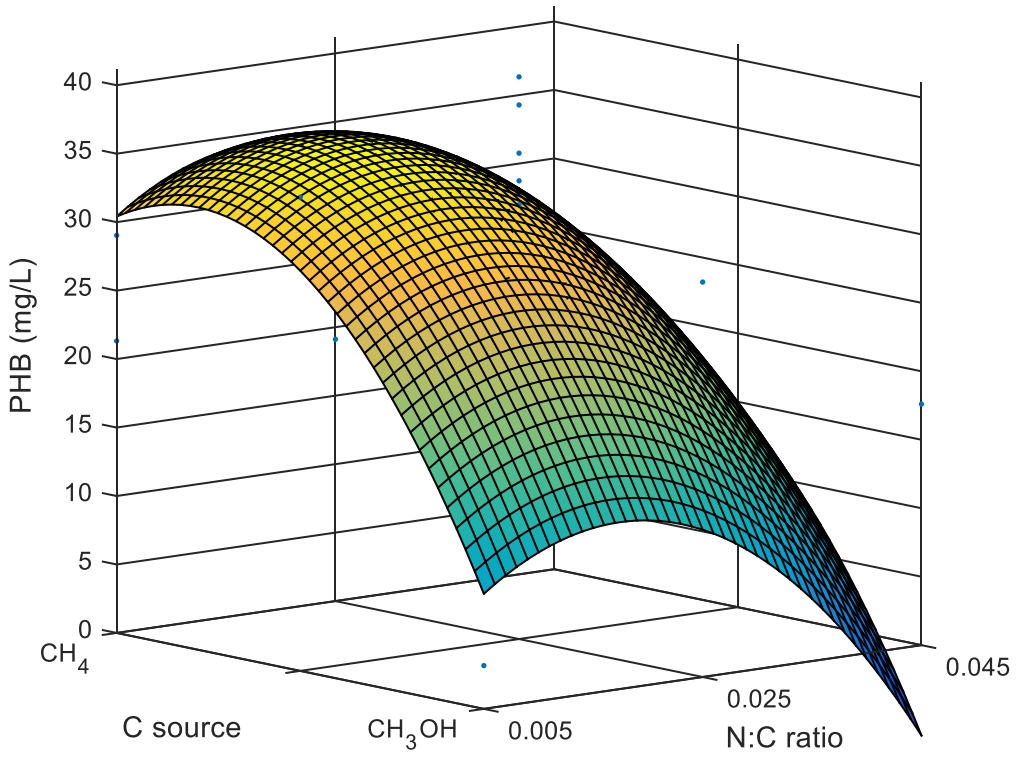

Figure 5-42. PHB concentration response surface for ammonium as nitrogen source ($x_2 = -1$).

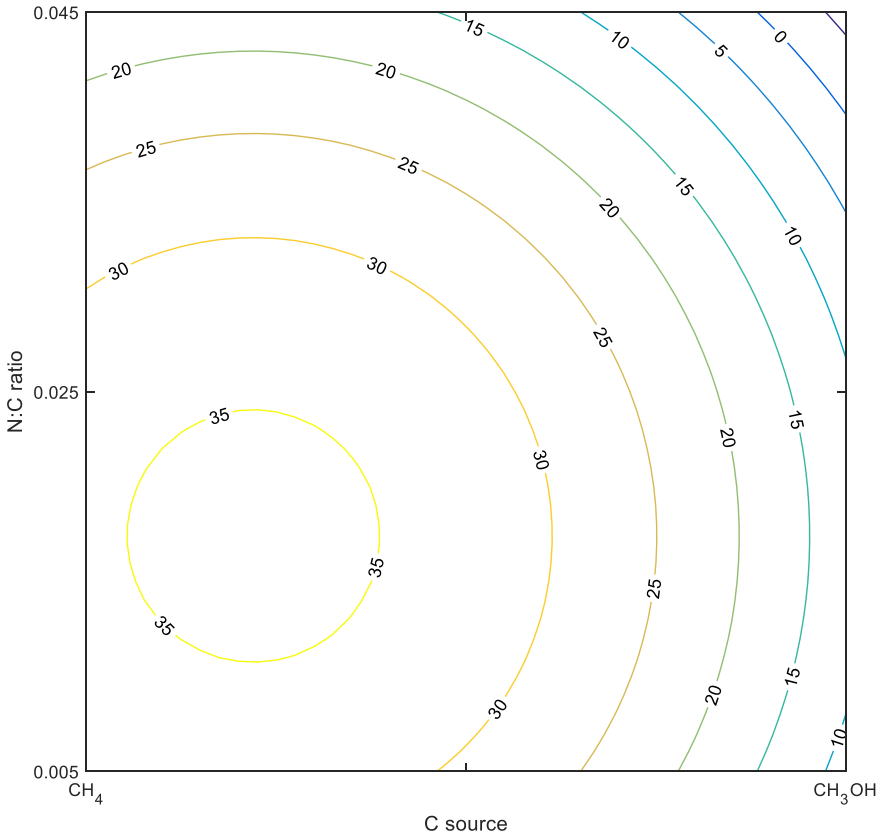

Figure 5-43. Contour plot of PHB concentration for ammonium as nitrogen source ($x_2 = -1$).

5.7.2.2 Nitrate as nitrogen source

Setting the variable $x_2 = 1$, fixed the nitrogen source at 100% nitrate. Figure 5-44 shows the response surface so obtained and Figure 5-45 shows the corresponding contour plot. The position of the predicted maximum was moved along the carbon source axis towards methanol and now occurred at $x_1 = 0.40$ (30%mol CH_4/70%mol CH_3OH) and $x_3 = -0.38$ (N:C ratio 0.017). The value of the predicted maximum in PHB concentration was greater than in all other cases encountered, reaching $\hat{y} = 40$ mg/L.

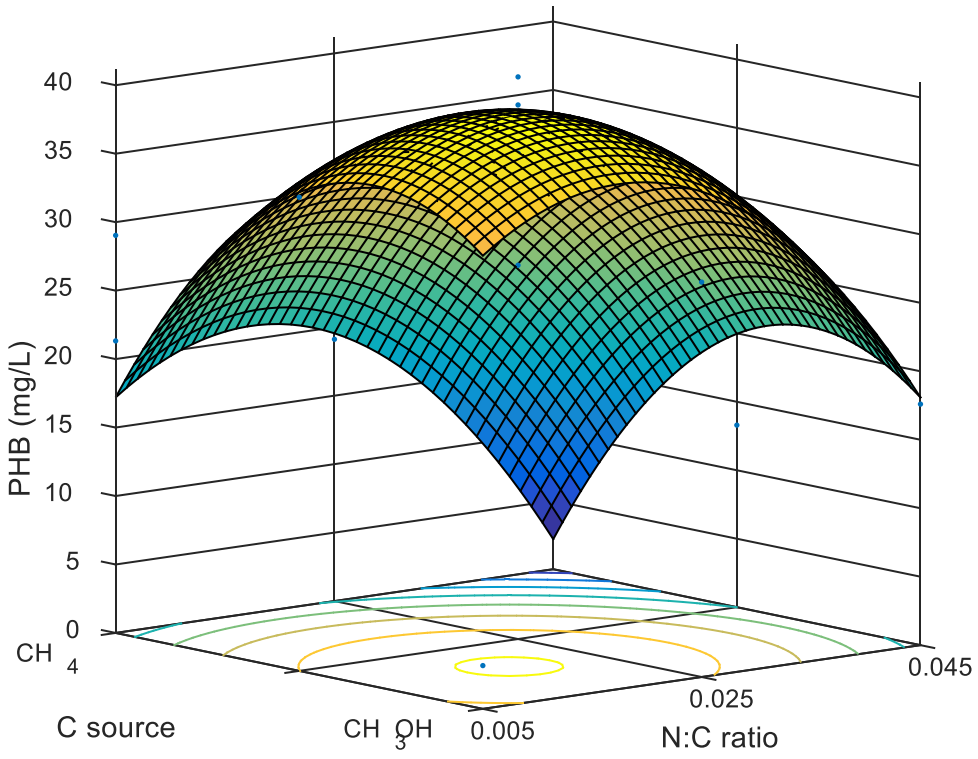

Figure 5-44. PHB concentration response surface for nitrate as nitrogen source ($x_2 = 1$).

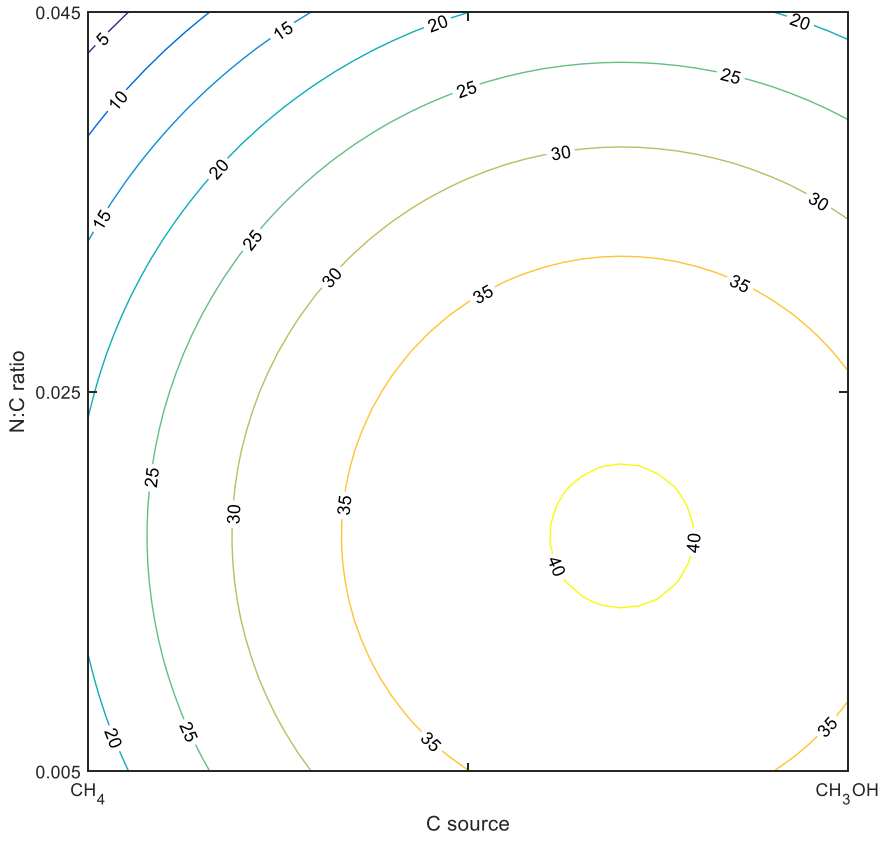

Figure 5-45. Contour plot of PHB concentration for nitrate as nitrogen source ($x_2 = 1$).

5.7.2.3 *Equimolar nitrogen sources*

Setting $x_2 = 0$, Figure 5-46 shows the response surface obtained when the nitrogen source was fixed at 50%mol ammonium and 50%mol nitrate, while Figure 5-47 shows the corresponding contour plot.

Essentially, the effect was the displacement of the position of the predicted maximum along the carbon source axis towards its centre, at $x_1 = -0.08$ (54%mol CH_4/46%mol CH_3OH) and $x_3 = -0.38$ (N:C ratio 0.017), the predicted value of the PHB concentration, $\hat{y} = 36$ mg/L, was the same as in the case of ammonium used as the sole nitrogen source ($x_2 = -1$), but the decreasing slopes around the maximum were less steep (lower rate of decrease) than in that case.

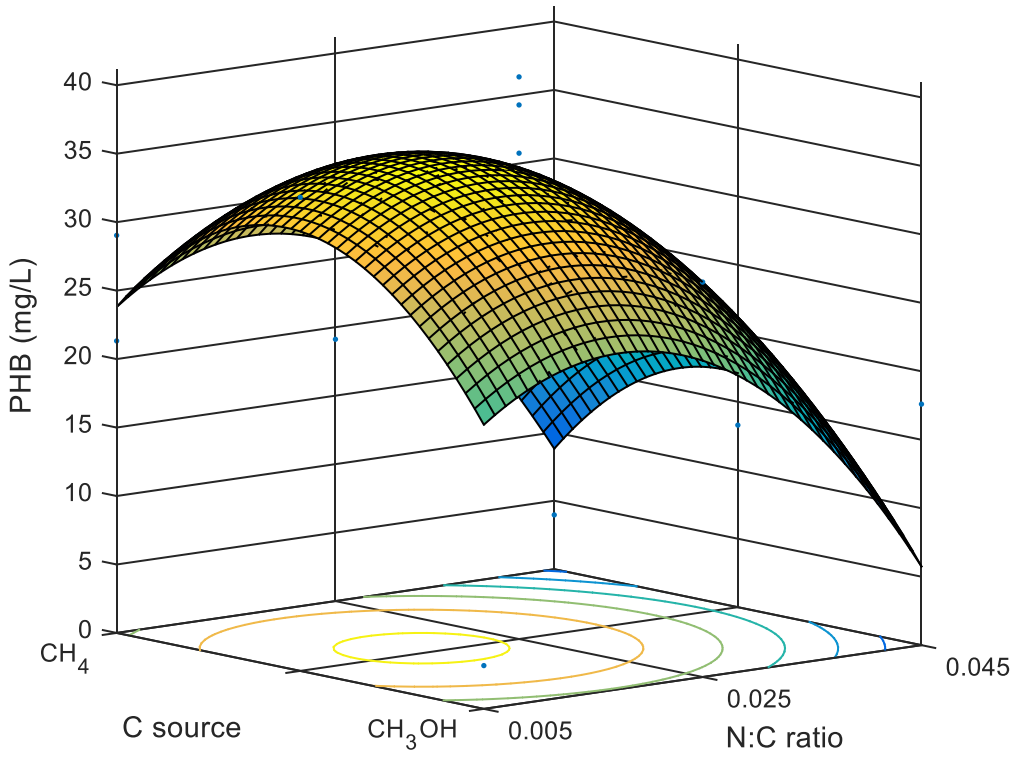

Figure 5-46. PHB concentration response surface for an equimolar mixture of ammonium and nitrate as nitrogen source ($x_2 = 0$).

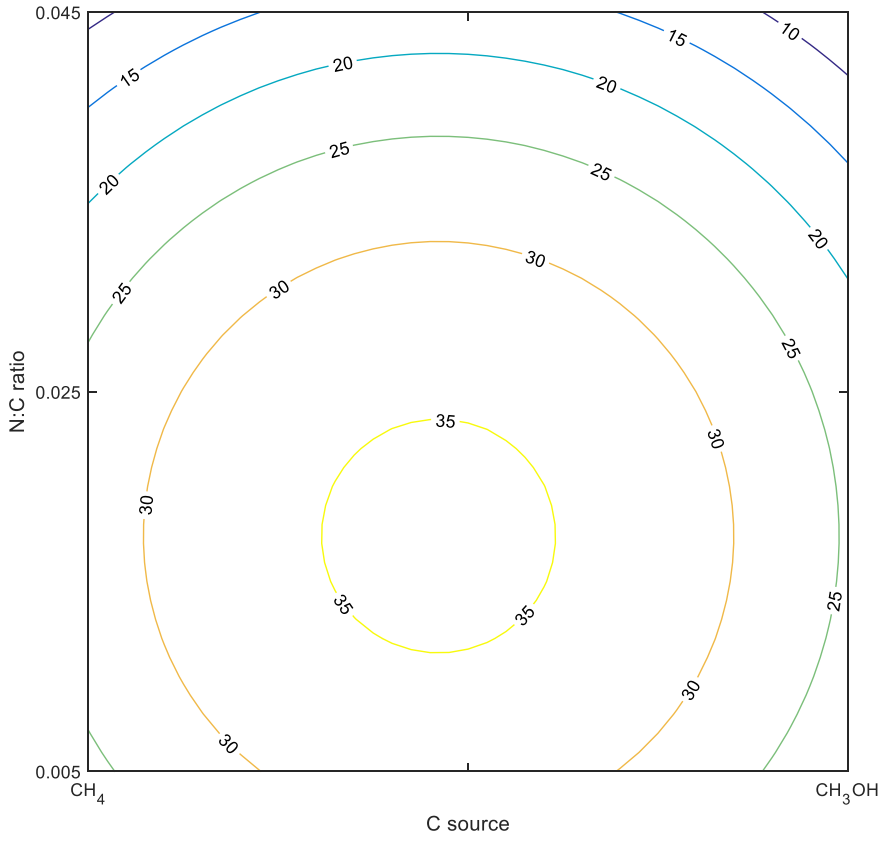

Figure 5-47. Contour plot of PHB concentration for an equimolar mixture of ammonium and nitrate as nitrogen source ($x_2 = 0$).

5.7.3 Response surfaces for PHB concentration with constant nitrogen-to-carbon ratio

The response surfaces obtained at different values of x_3 differed only by the height of the surface and the value of x_3 had no effect on the shape of the surface. All three cases led to a saddle-shaped surface. Figure 5-48 and Figure 5-49 show the response surface and corresponding contour plot, respectively, for PHB concentration at a N:C ratio value of 0.017 ($x_3 = -0.38$). This value was not tested experimentally, but was the N:C ratio for which a maximum was predicted from all carbon and nitrogen source data.

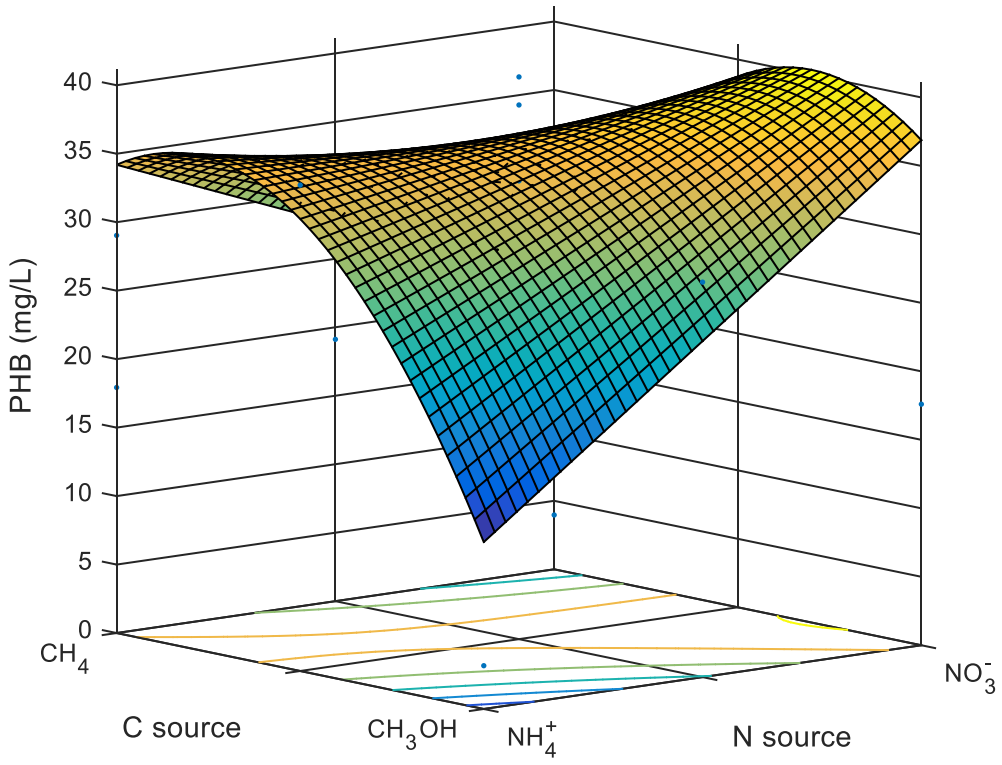

Figure 5-48. PHB concentration response surface for a fixed nitrogen-to-carbon ratio of 0.017 ($x_3 = -0.38$). This is the value at which the maximum PHB content was predicted.

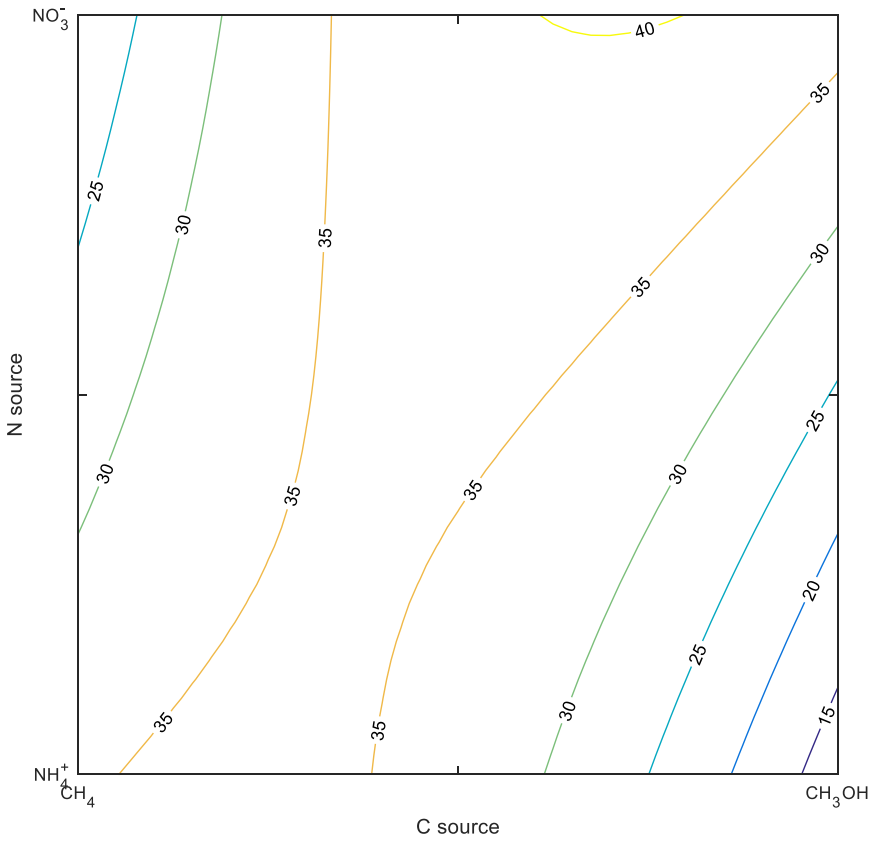

Figure 5-49. Contour plot of PHB concentration for a fixed nitrogen-to-carbon ratio of 0.017 ($x_3 = -0.38$). This is the optimum predicted ratio by the model.

5.7.4 Response surface for PHB concentration summary

The predicted maximum for the system as a whole was $\hat{y} = 40$ mg/L, and occurred at the nitrate boundary of the design region ($x_2 = 1$), with mixed carbon source, richer in methanol than in methane ($x_1 = 0.40$, or 30% methane and 70% methanol), and medium-low nitrogen-to-carbon ratio of 0.017 ($x_3 = -0.38$). This and other fixed conditions are shown in Table 5-16.

Table 5-16. Summary of maximum PHB concentration predictions at various fixed conditions.

Fixed condition	$\hat{y}_{max}$ (mg/L)	x_1	CH_4 /CH_3OH (%mol)	x_2	NH_4^+/ NO_3^- (%mol)	x_3	N:C ratio
Carbon source							
- Methane	34	-1	100/0	-1	100/0	-0.38	0.017
- Methanol	37	1	0/100	1	0/100	-0.38	0.017
- Equimolar	39	0	50/50	1	0/100	-0.38	0.017
Nitrogen source							
- Ammonium	36	-0.56	78/22	-1	100/0	-0.38	0.017
- Nitrate*	40	0.40	30/70	1	0/100	-0.38	0.017
- Equimolar	36	-0.08	54/46	0	50/50	-0.38	0.017

*System maximum

5.8 Response surface for PHB cell content

For the fitting of the response surface for PHB content as a percentage of cell dry weight (PHB cell content), four terms were dropped for lack of significance of their respective b_i parameters: x_2x_3, x_1x_2, x_3^2, and x_2^2. The coefficient b_{13} for the term x_1x_3 had also a high *p*-value but the adjusted coefficient of determination decreased when it was dropped so it was decided to keep it in the model. The final form of the model was:

$$y = b_0 + b_1x_1 + b_2x_2 + b_3x_3 + b_{11}x_1^2 + b_{13}x_1x_3 \qquad \text{Eq. 5-7}$$

The coefficient estimates and their corresponding *p*-values are listed in Table 5-17.

Table 5-17. Estimated parameters for the regression of PHB cell content and significance tests.

Parameter	Estimate	Standard error	t	*p*-Value
b_0	15.6166	1.1093	14.08	1.9554e-07
b_1	0.8986	1.0574	0.85	0.4174
b_2	-2.4803	1.1644	-2.13	0.0620
b_3	-2.9373	1.2673	-2.32	0.0457
b_{11}	-4.8145	1.5325	-3.14	0.0119
b_{13}	2.0061	1.3625	1.47	0.1750

The adjusted coefficient of determination was $R^2_{adj} = 0.67$. The model was significant and showed no significant lack of fit as can be assessed from the analysis of variance in Table 5-18.

Table 5-18. Analysis of variance for the regression of PHB cell content.

	Sum of squares	Degrees of freedom	Mean square	F	*p*-Value
Total	358.10	14	25.58		
Model	282.64	5	56.53	6.74	0.0071
. Linear	185.34	3	61.78	7.37	0.0085
. Nonlinear	97.30	2	48.65	5.80	0.0241
Residual	75.46	9	8.38		
. Lack of fit	15.14	6	2.52	0.13	0.9837
. Pure error	60.33	3	20.11		
R-squared: 0.7893, adjusted R-squared: 0.6722					

The diagnostic plots in Figure 5-50 and Figure 5-51 showed good results and the only thing to note was a small deviation from normality in the distribution of the residuals for the tail ends of the data distribution in Figure 5-51a. This can be attributed to the extreme positive and negative residuals that can be identified in Figure 5-51b. It was decided not to eliminate the two extreme values as outliers.

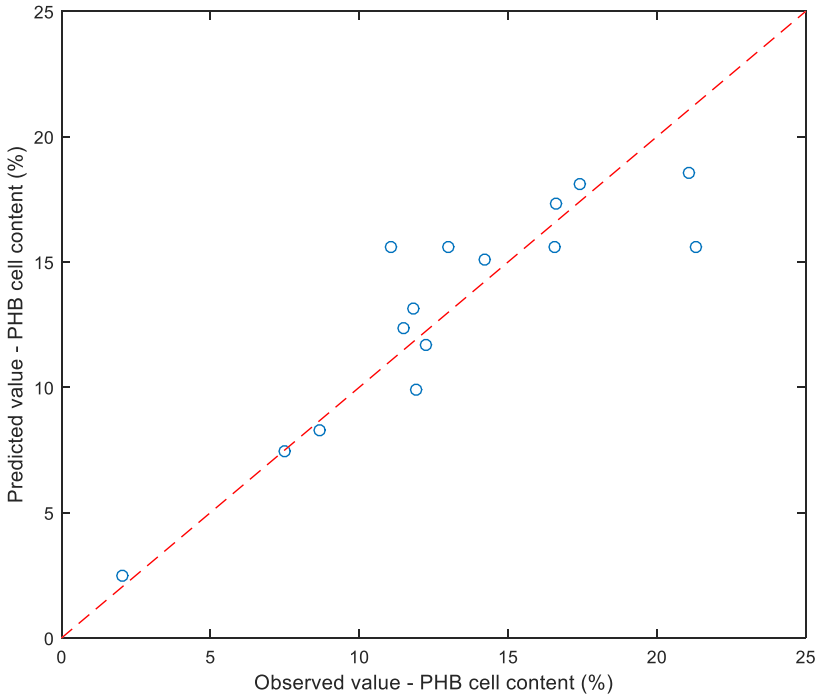

Figure 5-50. Predicted versus observed values for the PHB cell content response surface.

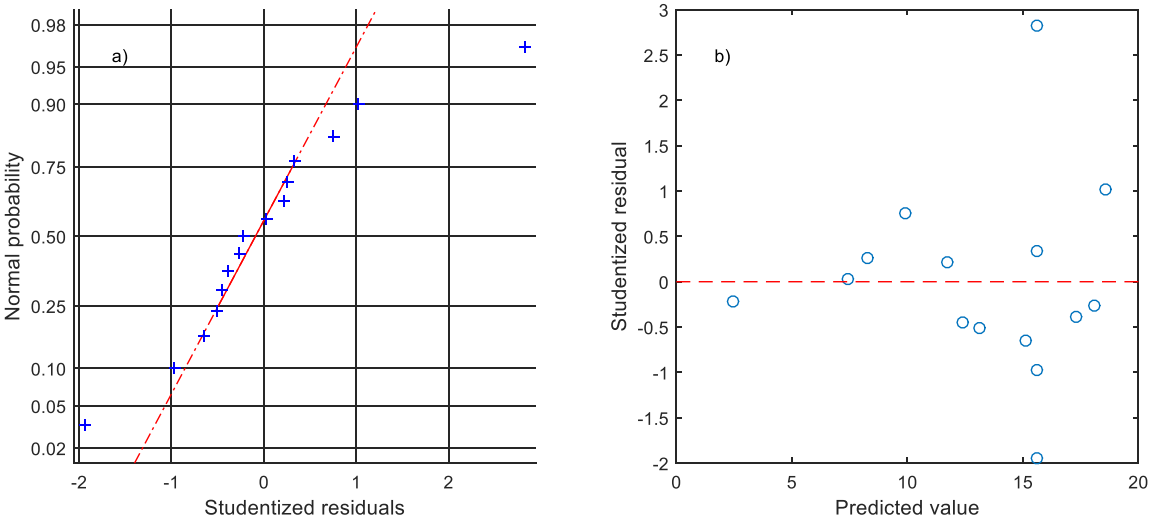

Figure 5-51. Diagnostic plots for the residuals for the PHB cell content response surface. (a) Normal probability plot of the Studentized residuals. (b) Studentized residuals versus predicted value.

5.8.1 Response surfaces for PHB cell content

Figure 5-52 shows a typical response surface, and Figure 5-53 shows the corresponding contour plot, for cases where the nitrogen source was kept as an equimolar mixture of ammonium and nitrate ($x_2 = 0$) at constant nitrogen source. Changing the value of the variable representing the nitrogen source—x_2—only displaced the surface vertically without changing its overall shape (see Figure C-2 in Appendix C for the response surfaces and contour plots for PHB cell content at different values of x_2, nitrogen source). A synergistic effect of mixing the carbon sources can be observed. Greater PHB cell contents were predicted for blends of methane and methanol compared to single carbon sources. Also, lower values of PHB cell content were predicted at higher N:C ratios. This effect was more pronounced in the case where the carbon source was methane.

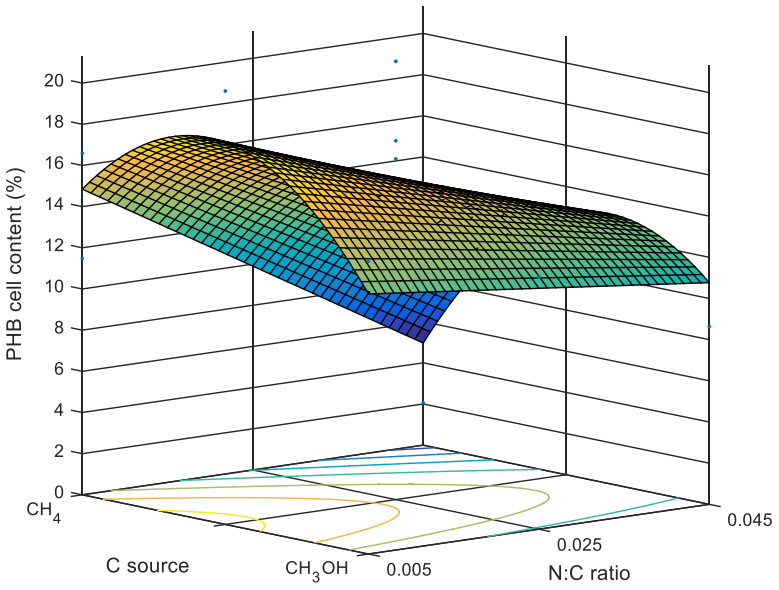

Figure 5-52. PHB cell content response surface for constant nitrogen source at $x_2 = 0$ (equimolar mixture of ammonium and nitrate).

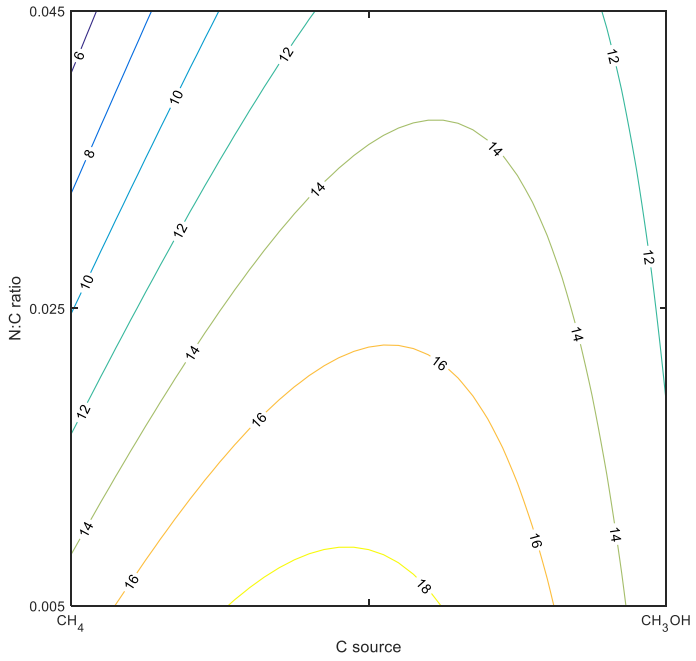

Figure 5-53. Countor plot of PHB cell content for an equimolar mixture of ammonium and nitrate as nitrogen source ($x_2 = 0$).

Figure 5-54 shows a typical response surface, and Figure 5-55 the corresponding contour plot, at constant N:C ratio (see Figure C-3 in Appendix C for additional response surfaces and contour plots for PHB cell content at different values of x_3, N:C ratio). The most important effect of changing the value of the N:C ratio on the graph was a vertical displacement of the surface with only a slight distortion of its shape. In addition to the synergy of mixed carbon sources already mentioned for the previous surface, lower values of PHB cell content were predicted when the nitrate proportion of the nitrogen source increased, that is, a decreasing linear trend was seen going from using nitrate to using ammonium. This effect was seen with both carbon sources as well as their blends.

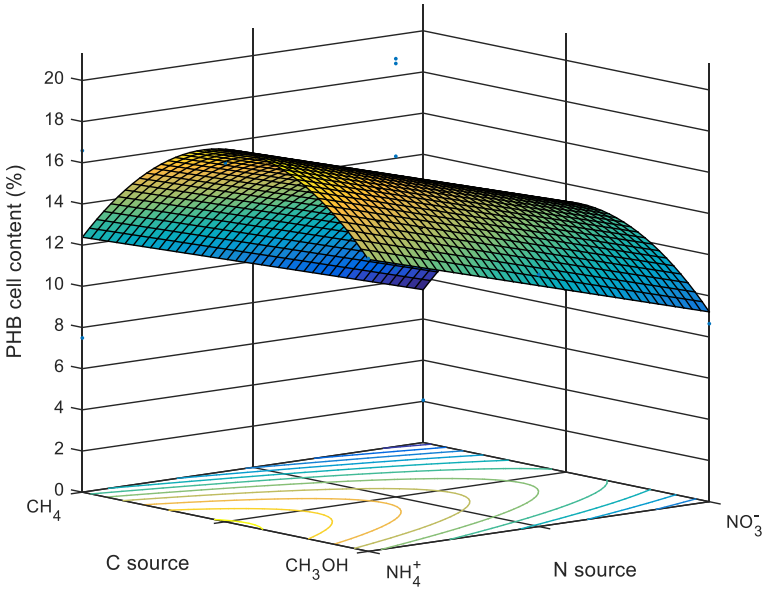

Figure 5-54. PHB cell content response surface for constant nitrogen-to-carbon of 0.025 ($x_3 = 0$).

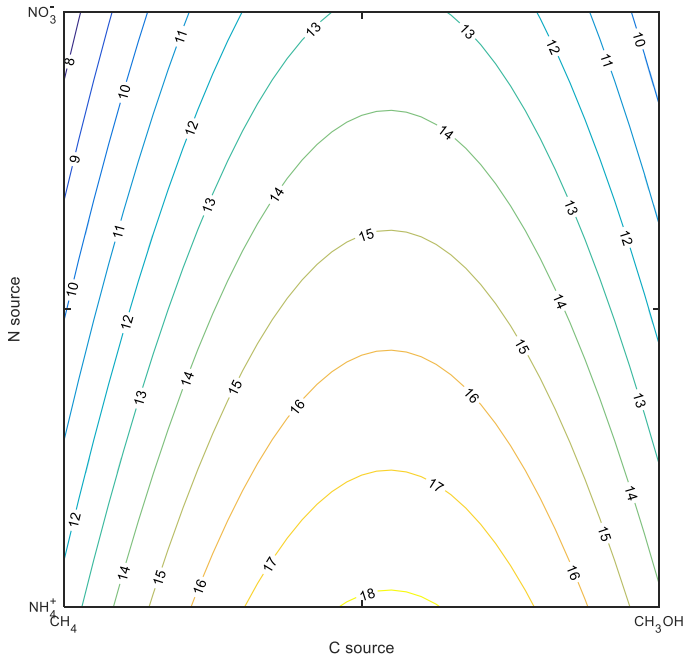

Figure 5-55. Contour plot of PHB cell content for a 0.025 N:C ratio ($x_3 = 0$).

Figure 5-56 shows the response surfaces and contour plots at constant carbon source when methane (Figure 5-56a and Figure 5-56c) or methanol (Figure 5-56b and Figure 5-56d) were used as carbon source. In both cases, the previously mentioned effects of decreasing PHB cell contents with increasing values of the N:C ratio and of the proportion of nitrate present were observed. Using different carbon sources modified the inclination of the plane in such a way that the effect of the N:C ratio was stronger (steeper surface) when the carbon source was methane. The response surface (Figure C-1e) and contour plot (Figure C-1f) for $x_1 = 0$ (equimolar mixture of carbon sources) can be consulted in Appendix C.

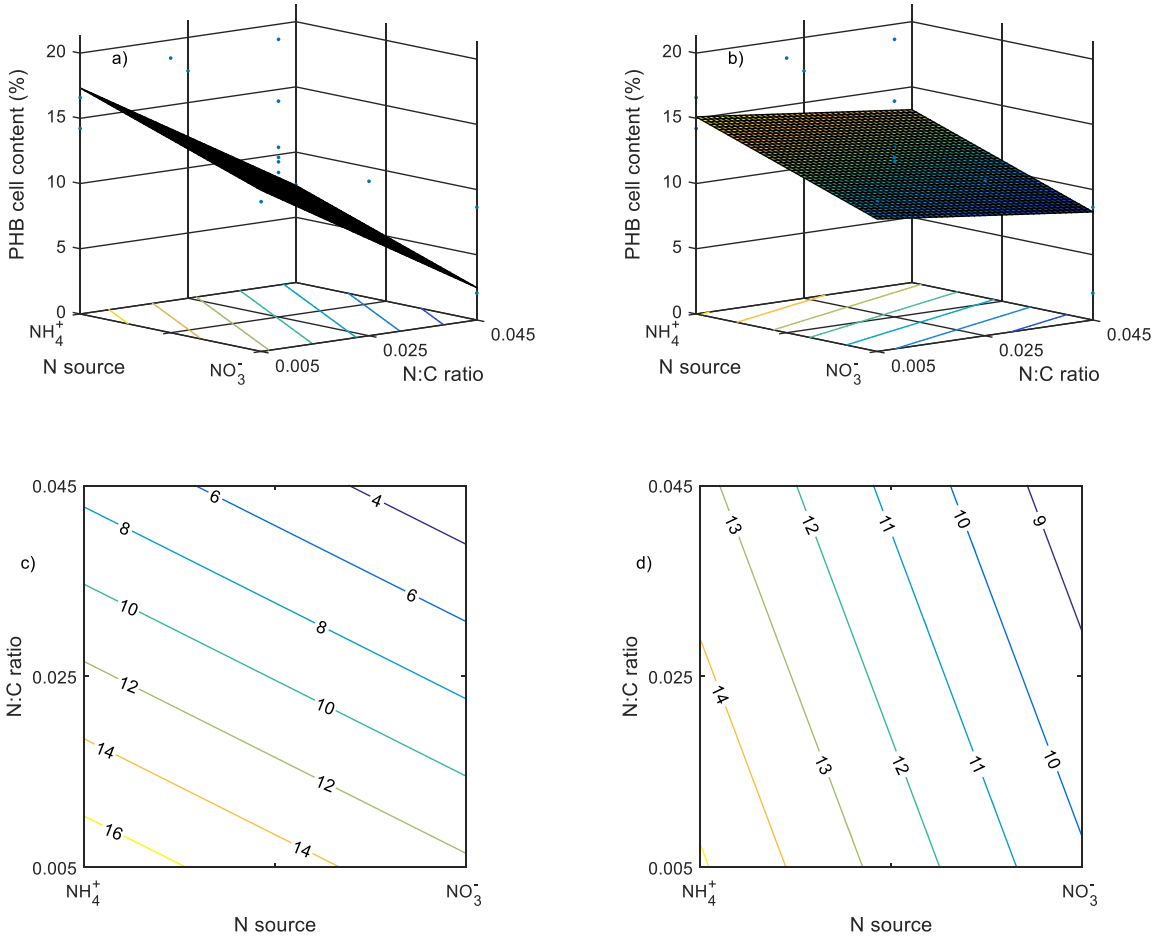

Figure 5-56. PHB cell content response surfaces for constant carbon source. (a) Methane as the carbon source ($x_1 = -1$). (b) Methanol as the carbon source ($x_1 = 1$).

5.8.2 Response surface for PHB cell content summary

The predicted maximum for the system as a whole was $\hat{y} = 21\%$, and occurred at the intersection of two boundaries of the design region: the ammonium boundary ($x_2 = -1$) and the low, *i.e.*, 0.005, N:C boundary ($x_3 = -1$). The N:C boundary is not a hard boundary, meaning that it is not a physical limit and operation at lower N:C ratios is possible. The corresponding carbon source composition for the maximum is close to equimolar ($x_1 = -0.12$, or 56% methane and 44% methanol) and, in fact, the response at equimolar carbon source ($x_1 = 0$) is only 0.3% lower. These and other fixed conditions are shown in Table 5-19.

Table 5-19. Summary of maximum PHB cell content predictions at various fixed conditions.

Fixed condition	$\hat{y}_{max}$ (%)	x_1	CH_4 /CH_3OH (%mol)	x_2	NH_4^+/ NO_3^- (%mol)	x_3	N:C ratio
Carbon source							
- Methane	17	-1	100/0	-1	100/0	-1	0.005
- Methanol	15	1	0/100	-1	100/0	-1	0.005
- Equimolar	21	0	50/50	-1	100/0	-1	0.005
Nitrogen source							
- Ammonium*	21	-0.12	56/44	-1	100/0	-1	0.005
- Nitrate	16	-0.12	56/44	1	0/100	-1	0.005
- Equimolar	19	-0.12	56/44	0	50/50	-1	0.005

*System maximum

5.9 Verification of the predictions from the response surfaces

A set of conditions was selected to verify the predictions from the model. The conditions selected were a mixture of 31% of methane with 69% of methanol as carbon source, pure nitrate as nitrogen source, and an N:C ratio of 0.016. This point was located close to the predicted maximum, which should occur at 70% methanol, 100% nitrate and N:C ratio of 0.017.

Five replicates were run in two blocks, two of the replicates, one from each block, exhibited a longer lag phase. The growth curves are shown in Figure 5-57.

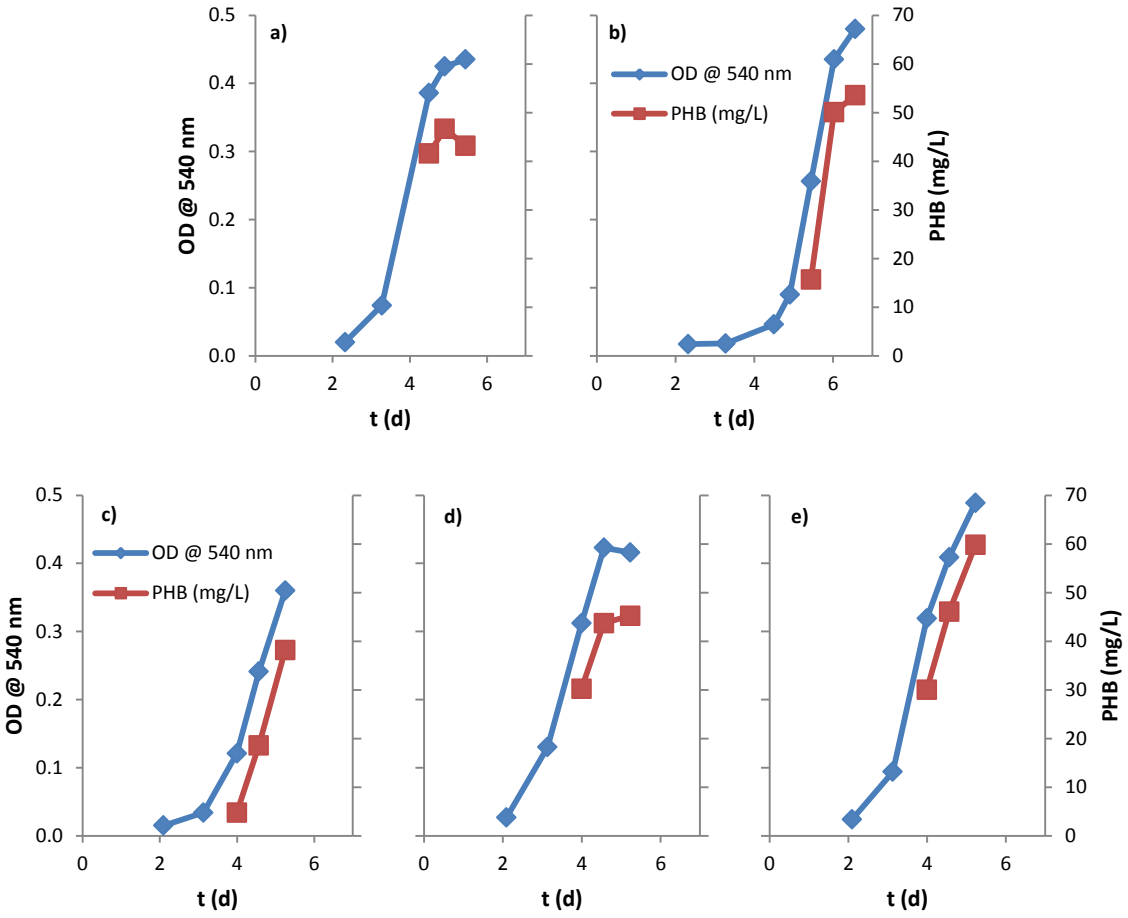

Figure 5-57. Growth curves for the five replicate cultures for the verification run. (a) and (b) First block. (c) to (e) Second block.

The results from the verification experiments are summarized in Table 5-20. Of the three predicted variables, only the PHB concentration results were within the predicted confidence region. The values obtained for cell dry weight were between one third and one half the predicted value and the observed PHB cell content was almost four times what was predicted by the model.

Table 5-20. Summary of results from the verification experiments. Observed values are reported as mean ± standard deviation from five samples.

	Predicted value	95% confidence limits	Observed value
Cell dry weight (mg/L)	250.8	232.9 — 268.7	92.7* ± 11.0
PHB concentration (mg/L)	40.28	30.91 — 49.65	48.7 ± 8.3
PHB cell content (%)	13.77	9.57 — 17.96	52.5* ± 6.3%

*Observed value is outside of the confidence region.

6 Discussion

6.1 Growth of *M. trichosporium* OB3b

6.1.1 Effect of carbon source

The effect of the carbon source on *M. trichosporium* OB3b growth was not only the most significant, with the lowest *p*-value from the experiment (9.7×10^{-34}, Table 5-4), but also the most important one in terms of its magnitude (0.12 OD units, Figure 5-2a). This was true even after the parameter was normalized by carbon source amount (*p*-value 4.0×10^{-18}, Table 5-6, Figure 5-6). This effect is actually confounding several factors.

The first factor confounded was the actual effect of the carbon source itself. Along with this effect, there was the effect due to the total amount of carbon used, since it was different for the treatments that used methane as carbon source and the ones using methanol. This effect was partially taken away when the optical density data was normalized with respect to the molar amount of carbon source supplied. However, normalization would not have eliminated any non-linearity on the response to the increased amount of available carbon. Even after normalization, the carbon source effect was the greatest and most significant (Table 5-6, Figure 5-6), but normalization reversed the carbon source that produced the highest biomass concentration, since greater normalized OD values were obtained with methanol than with methane (Figure 5-6a). However, it is important to note that this reversal of significance was due to oxygen limitation, and not solely on the parameter, as will be pointed out later.

Another factor was confounded for the methanol-grown cultures used in the initial experiments: only methane-grown inocula were initially used which led to adaptation effects of the microorganism, moving from one carbon source to the other. Methanol-grown cultures had a tendency to have longer lag phases (Table 5-3, and see, for example, Figure 5-1b, and also Figure B-1 (a, b, e, f), Figure B-2 (i, j,m, n) and Figure B-3 in Appendix B) than methane cultures (see, for example, Figure 5-1a, and also Figure B-1 (c, d, g, h) and Figure B-2 (k, l, o, p) in Appendix B). This point was later addressed with the inclusion of methanol-grown inocula, which reduced adaptation time and lag phase (Table 5-3).

Finally, the difference in mass transfer mechanisms between methane and methanol was another confounded factor. The results obtained when adding extra air to the bottles (Figure 5-7)

suggest no evident mass transfer limitation for methane, at least at the low biomass concentrations with which we worked, since growth resumed upon the addition of new oxygen, indicating the lack of dissolved oxygen, rather than the lack of dissolved methane, as the limiting factor. These results are strengthened because not only did the cultures produce additional growth upon addition of air, but the observed growth was linearly dependent on the total supplied oxygen along the studied range up to depletion of methane (Figure 5-9).

It is also important to note that, for the first experiments, the use of equal amounts of carbon in both the gas phase, in the case of methane, and in the liquid phase, in the case of methanol, was not deemed crucial, as there was no information on how much of the gaseous methane would ultimately be available to the microorganism in the aqueous phase or how limiting the transport of methane between the two phases would be.

The efforts to decouple the carbon source and carbon amount effects led us to the realisation of the importance of the oxygen limitation. On this, it is interesting to point out that oxygen limitation was more severe in the case of cultures using methane as carbon source because, first, air was extracted from the bottles in order not to increase the internal pressure significantly—resulting in a reduced amount of oxygen being present to start with—and, second, methane metabolism uses more oxygen than methanol metabolism—$(1 + f_e)$ for the former versus $1.5f_e$ for the later (Table 2-1 and Table 2-2). Even though the methane-grown cultures were more oxygen-limited, greater growth was observed than when using methane as carbon source.

Eliminating the oxygen deficiency, the final optical density reached by cultures initiated with a carbon load of 21.7 mmol of methane per L of liquid was 0.64 (from Figure 5-7), greater than the interpolated value of 0.59 for a culture containing an equivalent concentration of methanol (interpolated from Table 5-7). The biomass yield per mole of methane was thus 8% higher than that of methanol.

6.1.2 Effect of nitrogen source

On the other hand, the significance of the nitrogen source, its interaction with the carbon source, and the nitrogen-to-carbon ratio were conclusive and it was imperative to include these factors in future experiments.

6.1.3 Effect of inoculum history

There was an interest on determining whether the history of the inoculum had any effect; to verify if using solely methane-grown inocula—which are known to be indefinitely viable but for which there was no information on how the subcultured bacteria are affected as they grow older—would have an impact on the experiments at hand. Fresh methane-grown inocula were between four and eight weeks old at the time of inoculation, and grown with ammonium as nitrogen source. Aged methane-grown inocula were between 5.5 and 6.3 months old at the time of inoculation, and grown with nitrate as nitrogen source.

Since interaction effects involving inoculum history and carbon source were found (Table 5-4, Figure 5-4), and the lag time of the cultures under methanol were very long (Table 5-3), the design was augmented to use also fresh and aged methanol-grown inocula. Fresh methanol-grown inoculum was 2.1 to 2.3 weeks old (3 to 4 days into stationary phase) and grown with ammonium as nitrogen source. Aged methanol-grown inocula were between 3.1 and 3.3 weeks old and grown also with ammonium as nitrogen source.

The dependence or independence of the final biomass concentration on the methane-grown inoculum history could not be proven conclusively, since the results varied when analyzing the normalized (*p*-value of 0.015 from Table 5-6) and unnormalized data (*p*-value of 0.15 from Table 5-4). However, the lag phases were considered prohibitively long from a practical point of view (Table 5-3), and the decision was made to use carbon-source-specific-grown inocula. Furthermore, since the single most important factor for biomass yield for methanol-grown cultures obtained from methanol-grown inocula was the history of the inoculum (Table 5-5, Figure 5-5c), it was decided that fresh methanol-grown inocula would be used in the case of cultures grown on methanol, this also had the effect of a shorter lag phase (Table 5-3).

It is also interesting to note that the distinction on how to characterise an inoculum as fresh or aged is quite different depending on the carbon source used. In the case of methanol, a single week difference in age produced noticeable changes in the lag phase, roughly doubling its duration on the cultures inoculated with aged inoculum as compared to those inoculated with a fresh one. On the other hand, a difference of five months between the ages of methane-grown inocula failed to produce such

dramatic effects (Table 5-3). In fact, the methanol cultures inoculated with fresh methane-grown inoculum usually showed longer lag phases than the corresponding treatment inoculated with aged inoculum (Table 5-3).

6.2 Growth with increased amounts of carbon

The important effect of carbon source on biomass yield generated an interest on decoupling the effect of carbon load from the pure effect of carbon source, but there was also an interest in exploring higher carbon loads to obtain higher cell densities, at the same time verifying whether a linear response of the biomass with respect to carbon load was observed at the levels tested.

6.2.1 Methane

Greater growth had been observed when using methane (Figure 5-2, Figure 5-3, Figure 5-4). 100-mL cultures with carbon loads of 21.7, 32.5, 43.4, or 65.0 mmol of methane per L of liquid were used. Initially, lower growth was obtained with higher amounts of methane used. Since air was being extracted from the bottles not to increase the internal pressure when adding methane to the headspace, this effect was attributed to the reducing in oxygen present at greater methane loads.

When 60-mL portions of air were repeatedly injected to bottles until the overhead pressure made both the addition of more air and the sampling from the bottle difficult, every injection of air resulted in additional growth (Figure 5-7, Figure 5-9). However, the growth curves for the higher loads of methane always remained below those of the lower loads (Figure 5-7). The only exception being the curve for the 21.7-mmol of methane per L of liquid culture, in which the final two additions of air produced no additional growth. This lack of additional growth was attributed to the depletion of methane in the gas phase to a level low enough to make it unavailable to the bacteria in the liquid phase. It could be determined that the oxygen-to-methane ratio up to which additional growth was recorded was 1.5 (from Figure 5-7). This value is in agreement with (Asenjo and Suk 1986). Moreover, the final growth was 1.9 times that obtained before under oxygen-limited conditions, as measured by the OD of 0.643 (from Figure 5-7) versus one of 0.334 (treatments 3 and 4 from Table 5-2, second cluster on Figure 5-3).

Furthermore, a linear relationship was observed between total oxygen and total growth (Figure 5-9), independent of the methane load or the initial ratio of the two gases. Each additional millimole of oxygen resulted in an increase of 0.18 OD units (Figure 5-9), equivalent to 6.8 mg of biomass. This was also observed in the experiments in which all the air was added at the beginning of the culture (Figure 5-8, Figure 5-9), so this relationship held whether the increased amount of oxygen was present at the start of the experiment or added afterwards, even repeatedly.

The stoichiometric relationships between oxygen and methane; oxygen and cellular material, and oxygen and PHB are (from Table 2-1, (Rostkowski et al. 2013))

$$\frac{O_2}{CH_4} = 1 + f_e \qquad \text{Eq. 6-1}$$

$$\frac{O_2}{C_5H_7O_2N} = \frac{\frac{1}{4} + \frac{f_e}{4}}{\frac{f_s}{23}} \qquad \text{Eq. 6-2}$$

$$\frac{O_2}{C_4H_6O_2} = \frac{\frac{1}{4} + \frac{f_e}{4}}{\frac{f_s}{18}} \qquad \text{Eq. 6-3}$$

The observed relationship of 1.5 mmol O_2 per 1 mmol CH_4 corresponds to an f_e value of 0.50; and the observed relationship of 6.8 mg CDW per 1 mmol O_2 corresponds to an f_e value between 0.49—for cellular material production—and 0.48—for PHB production. These values are in close agreement.

Also, the growth observed in the experiments with carbon loads of 21.7 mmol of methane per L of liquid before the addition of extra air (Figure 5-7), and that observed for the experiments with carbon loads of 65.0 mmol of methane per L of liquid and no air additions (Figure 5-8), were in agreement with the results from the initial growth experiments (treatments 3 and 4 from Table 5-2, second cluster on Figure 5-3, Figure B-1 in Appendix B). All contained the same amount of oxygen.

6.2.2 Methanol

The results for the methanol cultures with 19.8 mmol/L showed higher growth compared to the 9.9-mmol/L cultures, over twofold greater. Maximum OD reached a value 3.0 times greater and final OD

was 2.4 times greater (Figure 5-10, Table 5-7). The behaviour of the 29.7-mmol/L cultures before the addition of air matched with that of the 19.8-mmol/L cultures, achieving similar ODs. After the addition of air, a difference was observed (Figure 5-10, Table 5-7). Neither the 9.9-mmol/L nor the 19.8-mmol/L cultures showed any additional growth upon the addition of air. On the other hand, one of the 29.7-mmol/L cultures reached higher OD values with the extra supply of oxygen (Figure 5-10, Table 5-7).

The lack of additional growth in the 9.9-mmol/L and 19.8-mmol/L cultures can be attributed to the amount of oxygen initially present within the bottles being sufficient to metabolize the supplied methanol. In contrast to the case of methane, it can be pointed out that methanol metabolism requires less oxygen than methane at a given f_e—the ratio being $(f_e + 1)$ for methane (Table 2-1) versus $(1.5f_e)$ for methanol (Table 2-2). On the other hand, methanol cultures had a greater amount of oxygen to start with, since no air had been withdrawn from them to equilibrate any addition of gaseous material. This difference in operating procedure resulted in the presence of 1.68 mmol O_2 in the headspace of the methanol cultures but only 1.36 mmol O_2 for the methane ones, a 24% difference.

The observation of similar levels of growth between the 19.8-mmol/L and 29.7-mmol/L cultures before the addition of air is evidence that the latter were oxygen limited. The fact that those levels reached very similar values suggests that the former may had been at the border of oxygen sufficiency, *i.e.*, that the oxygen contained within the bottles was just enough to metabolize the 1.98 mmol of methanol supplied. The oxygen-to-carbon ratio being 0.85 (Table 5-8) would imply an $f_e = 0.57$ from the stoichiometric relationship.

As for the difference in the observed behaviour between the two replicates at 29.7-mmol/L methanol (Figure 5-10, Table 5-7), it can be attributed to the timing of the air additions. While the additions occurred at approximately the same time after inoculation (one day earlier, in fact, for the first replicate, which did not show additional growth), the lag phases for the second replicate were longer (attributable to an aged inoculum—41 days elapsed between the two replicates and the same inoculum was used). This resulted in air being added to the first replicate (no additional growth observed) after the OD had been decreasing for a little over two days, while the addition of air to the second replicate (additional growth) took place just as it was experiencing its maximum OD, *i.e.*, just out of exponential growth phase. Perhaps if more time had been given to the first replicate, additional growth would have been observed.

Both the 19.8-mmol/L and the 29.7-mmol/L conditions (after additional oxygen was supplied) showed greater growths than could be attributed just to the increased carbon administered—21% and 18% higher, respectively (Table 5-8). It can also be seen (Table 5-8) that the 29.7-mmol/L cultures' oxygen-to-carbon ratio after air addition was still 14% lower than that of the 19.8-mmol/L cultures before air addition. Since this ratio (0.85) appeared to be a borderline condition for minimum oxygen, additional growth could be expected with the supply of more oxygen.

Another possibility exists: the similitude in the behaviour of the 19.8-mmol/L and 29.7-mmol/L cultures before the injection of additional air could have been merely incidental and not indicative that the 0.85 oxygen-to-carbon ratio of the 19.8-mmol/L cultures is the necessary ratio for the oxygen not to be limiting. Given that the OD was proportional to the methanol amount at these two levels, an effect of methanol concentration on biomass yield per mole of methanol was observed at the lowest concentration. When 9.9 mmol/L of methanol were used (corresponding to 0.99 mmol per 100 mL of culture), a yield of only 0.226 OD units per mmol of methanol—as opposed to the average of 0.270 OD units/mmol—was observed (Table 5-7, Table 5-8). These values are equivalent to 8.46 mg CDW/mmol CH_3OH and 10.10 mg CDW/mmol CH_3OH, respectively; or, in units of mass, 0.264 g CDW/g CH_3OH and 0.315 g CDW/g CH_3OH.

If the oxygen-to-carbon ratio necessary to overcome the oxygen limitation was, effectively, 0.85, the 2.97-mmol cultures would have been able to grow to higher optical densities. That would mean that the effect of methanol concentration on cell dry weight yield per amount of methanol (lower yields at lower concentrations) was not restricted to the 10 mmol/L range but extended at least to the 30 mmol/L concentration.

6.3 Effect of nitrogen on PHB production

When using lower N:C ratios to increase the accumulation of PHB in the cell, the oxygen supply had to permit metabolism of all the carbon source. This would ensure that the observed effects were due to nitrogen limitation without interference from any potential oxygen limitation. It had already been demonstrated experimentally (Figure 5-10, Table 5-7, Table 5-8) that the oxygen present in the headspace of a 100-mL culture in a 250-mL bottle was sufficient to support the growth of *M. trichosporium* OB3b when up to approximately 2 mmol of methanol were supplied as carbon source

(Section 5.2.2). To guarantee that the cultures were not deprived of oxygen, a lower amount of methanol, 1.5 mmol, was used in the nitrogen limitation experiments, as well as a lower culture volume, 25 mL, to increase the headspace ratio and thus the available oxygen per culture volume. The concentration was 60 mmol/L.

When working with N:C ratios in the range from 0.1 to 1, no appreciable quantities of PHB were accumulated by the cells. It was not until the N:C ratio was lowered to half the minimum value previously tested—to 0.05—that PHB accumulation could be measured in methanol-grown cultures (Figure 5-12, Figure 5-13). An additional twofold decrease—to 0.025—further increased the accumulation of PHB. When the ratio was approximately halved again—to 0.01—no significant increase in PHB production was observed.

A somewhat similar trend was observed in the methane-grown cultures with three key differences. The first was that the concentration of PHB in the methane cultures—with a maximum of 12.2 ± 7.6 mg/L (Figure 5-15)—was significantly lower than that of the methanol-grown ones—which reached a maximum of 70.5 ± 14.2 mg/L (Figure 5-12). Since the cell dry weight between the two set of cultures was not significantly different— from 395 ± 51 mg/L to 450 ± 116 mg/L for methane (Figure 5-14) and from 399 ± 13 mg/L to 457 ± 8 mg/L for methanol (Figure 5-11)—this also had the effect of a much lower PHB content of cells—with a maximum of 2.8% ± 1.3% for methane (Figure 5-16) and 15.4% ± 2.9% for methanol (Figure 5-13). These results are in accordance with our response surface model that predicted that the preferred nitrogen source for PHB accumulation was ammonium—rather than nitrate, as was used here—when methane is used as the carbon source (Figure 5-36, Figure 5-37).

The second difference was the increased variability observed in the methane cultures. In the case of the PHB concentration results, the absolute size of the variations was similar (Figure 5-12, Figure 5-15), it was the smaller mean value that made the variation look relatively large. However, that rationalization cannot be made for the cell dry weight values; even though the mean values were similar (Figure 5-11, Figure 5-14), the variability of the results for the methane-grown cultures (Figure 5-14) was significantly greater.

The third difference was that the PHB concentration of the methane-grown cultures reached a maximum at the mid N:C ratio—0.025 (Figure 5-15)—while, when the carbon source was methanol, the PHB concentration reached a plateau at the lower N:C ratio of 0.01 (Figure 5-12). This behaviour was not

predicted by our model, which predicted similar PHB concentrations at those ratios, with a maximum between them (Figure 5-36, Figure 5-37). Since no significant interaction was found for the N:C ratio with any of the other variables, the predicted PHB concentration maximum was located at the same N:C ratio irrespective of the carbon source or nitrogen source used (Eq. 5-6, Figure 5-36, Figure 5-37, Figure 5-38, Figure 5-39, Figure 5-40, Figure 5-41). It should be noted that our model was developed for carbon loads of 20 mmol/L of liquid culture and these experiments were run at three times that carbon load. The effect of methane loads greater than 20 mmol/L was not assessed because we could not surpass the oxygen limitation at such loads (Figure 5-7) in the experimental setups used. However, we did find a significant effect of the methanol concentration on cell dry weight yield (Table 5-8). We could not assess whether this effect extended to PHB production because the N:C ratios were too high for significant PHB accumulation in those experiments. It is not discarded that increased methanol concentrations affect PHB production, and that these effects could extend to growth and PHB production under increased loads of methane.

Finally, the model predicted no great variation in cell dry weight between both carbon sources when nitrate was the nitrogen source (Figure 5-30, Figure 5-31), as was observed (Figure 5-11, Figure 5-14). But it did predict a maximum in cell dry weight around the 0.025 N:C ratio (Figure 5-30, Figure 5-31), which was not observed (Figure 5-11, Figure 5-14).

6.4 Effect of oxygen on PHB production

Since excess of oxygen had no appreciable effect on cell dry weight (Figure 5-17), it was surprising to discover the magnitude of the effect it had on PHB accumulation. This was consistent with increases in the percent PHB content from 2.5% ± 1.6% to 21.3% ± 12.4% when increasing the oxygen-to-methane ratio from 2.2 to 9.7 (Figure 5-18). As a comparison, increasing the O_2:CH_4 ratio over 1.5 up to 2.0 did not result in any further carbon metabolism (Figure 5-7, first series) – attributed to the depletion of methane in the gas phase, at least to a level at which the concentration of methane in the liquid phase was too low for the bacteria to continue growing on it. That level of methane was expected to be essentially zero, since, as dissolved methane is consumed, more is dissolved. It is unlikely that the effect of the increased availability of oxygen was due to any shift in the solubility of methane. Moreover, no significant changes in pressure were involved, only volume changes and, in fact, the initial pressure of

the cultures with increased oxygen were slightly lower since the same volume of methane was added to a larger volume, resulting in a smaller pressure change.

6.5 Experimental design

The selection of a face-centered design over a rotatable central composite design or a Box-Behnken design was in accordance with the nature of the operative space at hand. This space was cuboidal in nature, not spherical, in two of the three dimensions studied, *i.e.*, the carbon source composition (x_1) and the nitrogen source composition (x_2). This plane is shown in Figure 6-1. The operative region is delimited by the red square; within it are all possible combinations of carbon and nitrogen sources compositions, and any combination outside this square is physically impossible, as it would imply compositions of more than 100% of one of the components. A rotatable design implies a spherical region (blue circles in Figure 6-1). Such a region that includes the vertices would imply predictions in those areas of inoperability (Figure 6-1a). If the radius of the spherical design were adjusted to fit within the operative region (Figure 6-1b), the experimental region would exclude the vertices of the operative region, the extreme values of the compositions. The inclusion of the vertices, which represent combinations of the pure carbon and nitrogen sources, in the experimental design, to provide stability of the predictions at those vertices, was deemed more important than rotatability.

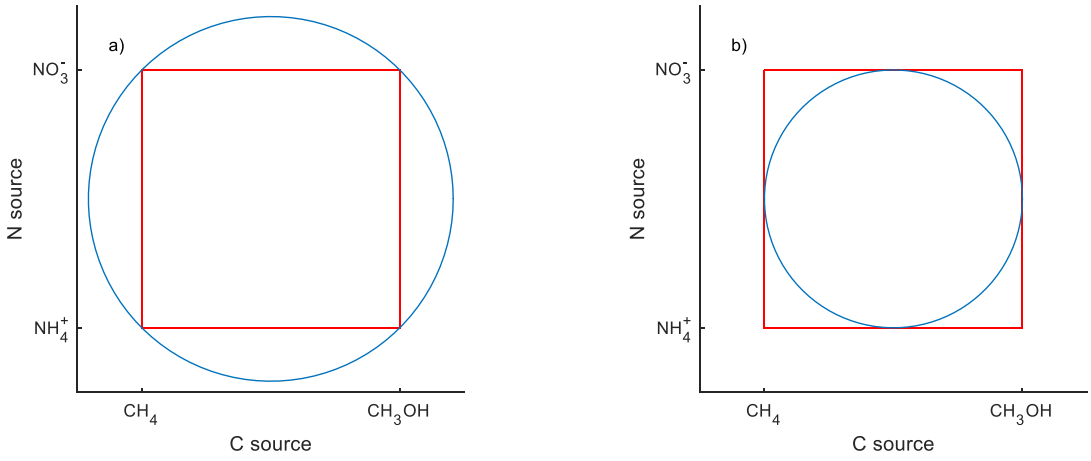

Figure 6-1. Comparison of cuboidal and spherical design spaces for carbon and nitrogen sources. (a) Circumscribed spherical design. (b) Inscribed spherical design.

6.6 Response surfaces

Table 6-1 shows a summary of the results of the fits of the response surfaces. All three of the response surface models were significant, with no significant lack of fit. The adjusted determination coefficients indicated a reasonable amount of the observed variability was explained by the model—from 67% to 97%, depending on the specific model. The distributions of the residuals from the models were satisfactory as well (Figure 5-21, Figure 5-34, Figure 5-35, Figure 5-50, Figure 5-51).

Table 6-1. Summary of the regression parameters for the response surface models (compiled from Table 5-11, Table 5-15, Table 5-18).

Model	Model *p*-value	Lack of fit *p*-value	Model R^2_{adj}
Cell dry weight	5.52e-6	0.5265	0.9725
PHB concentration	0.0035	0.5799	0.7337
PHB content	0.0071	0.9837	0.6722

It is interesting to note that both interaction terms involving the x_3 variable (N:C ratio) were removed from the PHB concentration model (Eq. 5-6) due to the lack of significance of their respective coefficients. This had the effect that the predicted value of the nitrogen-to-carbon ratio for maximum PHB concentration did not vary between the combination of carbon and nitrogen sources. In other words, the absence of interaction effects permitted the independent optimization of this factor.

It was deceptively surprising that the predictive power of the cell dry weight model, which performed the best in the regressions (Table 5-11, Table 6-1), with the highest significance ($p = 5.5 \times 10^{-6}$) and greater adjusted coefficient of determination ($R^2_{adj} = 0.97$), could not be proven. The observed value was about one third of the predicted value (Table 5-20) and lower than all but two of the cell dry weights obtained for the samples used to fit the model (Table 5-10).

With respect to cell dry weight determinations, it must be said that the low cell densities encountered throughout the experiments, coupled with the limited amount of culture available for sampling, resulted in very small amounts of cell material to weigh and relatively high errors. The weight of the cellular material was between 1.9 and 7.5 mg, while the precision of the balance used was 0.1 mg. The error resulting from the weighing alone could then be as high as 5%, leading to a low signal-to-noise ratio.

This low signal-to-noise ratio was not restricted to the cell dry weight but was more evident there because the GC method used for the PHB determination had greater precision.

The low cell densities were the result of physiological and logistics factors. Methanotrophs typically grow to low cell densities in batch systems. Moreover, to avoid oxygen limitations which would limit PHB production, limitations existed on the volume of the cultures and the total amount of carbon source present. Even halving the oxygen-to-carbon ratio resulted in decreased accumulation of PHB (data not shown). The increase of culture volume would have provided us with a bigger sample, but it would have been more diluted, so there would not have been any advantage.

Although not readily apparent, there are some indications that there is a lack of range in the values of cell dry weight (Figure 5-20). One way to increase this range would have been to increase carbon loads (total carbon supplied per litre of culture), but again, increased carbon loads were limited by the oxygen restrictions outlined above.

The regression equation for the two independent variables that were found to be correlated with a coefficient of determination of 0.80 is (Figure 5-20):

$$[\text{PHB cell content}] = 0.00478 \times [\text{PHB concentration}] \qquad \text{Eq. 6-4}$$

Since the PHB cell content is defined as:

$$[\text{PHB cell content}] = \frac{[\text{PHB concentration}]}{[\text{Cell dry weight}]} \qquad \text{Eq. 6-5}$$

This would imply:

$$[\text{Cell dry weight}] = \frac{1}{0.00478} \qquad \text{Eq. 6-6}$$

In other words, 80% of the variability observed in the PHB cell content can be explained by the variability of the PHB concentration assuming a constant cell dry weight of 209 mg/L, and hence the implied lack of range in cell dry weight.

However, interesting predicted trends were in line with what was observed in previous experiments. For example, higher cell dry weight was predicted when using ammonium as the nitrogen source at high N:C ratios, when methane was the carbon source (Figure 5-22, Figure 5-23). This was

confirmed experimentally (Figure 5-2b). Also, the predicted independence of the cell dry weight on the carbon source when nitrate was used as the nitrogen source (Figure 5-30, Figure 5-31) was observed (Figure 5-11, Figure 5-14).

Since the PHB cell content is a calculated value obtained by dividing the PHB concentration by the cell dry weight and expressing the result as a percentage, it is natural that a lack of predictive power for the cell dry weight model would result in weak predictions from the PHB cell content model.

On the other hand, the values of PHB concentration predicted by the model were confirmed in the verification experiment (Table 5-20). The terms included in the model (Eq. 5-6) resulted in a prediction of synergistic effects between the carbon sources. This prediction was confirmed as well, and the 48.7 ± 8.3 mg/L PHB concentration obtained (Table 5-20) was higher than in any of the previous attempts (Figure 5-15, Figure 5-18, Table 5-10) except for one. Nevertheless, that higher PHB concentration of 70.5 ± 14.2 mg/L (Figure 5-12) was obtained on methanol concentrations of 60 mmol/L as opposed to the carbon load of 20 mmol/L used for the verification experiment. Normalizing the PHB concentration by the carbon load, results in a yield of 1.18 mg PHB/mmol C for the previous experiment versus 2.44 mg PHB/mmol C for the optimized run—a 107% improvement.

From an industrial point of view, the attainment of high cell densities is desirable to maximize bioreactor volume utilization and decrease energy costs in pumping, agitation, heating, and so on. At the same time, high concentrations of PHB can facilitate separation and purification of the product. A high PHB content of the cells is also desirable because it means that more of the raw materials are used in the synthesis of the product and not diverted to the production of cellular biomass that would have to be eventually disposed of. Ideally, the greatest possible concentration of biomass producing the greatest possible amount of PHB is desired. For the process developer, understanding how the changes in operating conditions affect these parameters, especially in the presence of interactions, is crucial. Having information on the sensitivity of the process to the variations in those conditions, especially on the existence of regions of high sensitivity or of relative stability can help in the development of a more robust process and on the design and selection of better process control strategies.

Such are the improvements gained from the exploration of the experimental space through the response surface models. Not only was it possible to identify the set of conditions within the design space that would optimize the desired response for PHB concentration (Table 5-16): A mixed carbon

source consisting in 30% of methane and 70% of methanol, nitrate as the sole nitrogen source, and a nitrogen-to-carbon ratio of 0.017; but the model also provided useful information on trends, such as the preferred nitrogen source for increased PHB accumulation depending on the carbon source used or vice versa, and the existence of a synergistic mixing effect of the carbon sources on PHB production; and information on the sensitivity or lack thereof against changes in the operating conditions, such as the insensibility of cell dry weight to changes in the carbon source when nitrate is used as the nitrogen source at any nitrogen-to-carbon ratio. Efforts should be made to expand the model and incorporate increased carbon loads, not only to stabilize the predictions for cell dry weight and PHB cell content, but to increase the usefulness and applicability of the models. As it is, it provides valuable information for continuing the investigation for the development of a viable industrial production process.

7 Conclusion

The present work provided insight on the response in growth and PHB production of *M. trichosporium* OB3b due to changes in the carbon source, the nitrogen source and the nitrogen-to-carbon ratio.

Several important trends were identified: the independence of the biomass yield on the carbon source when the nitrogen source was nitrate; the preferred nitrogen source for greater PHB accumulation for each of the carbon sources—ammonium for methane and nitrate for methanol—; the optimum restriction levels of nitrogen availability for PHB accumulation.

A synergistic effect of the blend of methane and methanol on PHB accumulation was identified and verified experimentally. The predicted optimization was attained; the initial experiments showed an almost nonexistent accumulation that was increased by the restriction of nitrogen. Those levels of PHB concentration were further increased as the results of exploring the experimental space, as suggested by the response surface model. Greater concentration of PHB and PHB cell content were observed in the verification experiments than had been obtained in previous experiments.

Other important parameters were identified. Oxygen was shown to have minimal impact on the total biomass, as long as it was not limiting, but a significant impact on the accumulation of PHB. In fact, it was shown that excess oxygen increased accumulation of PHB compared to oxygen conditions at stoichiometric ratios.

It was initially believed that the PHB accumulation would occur as a distinct phase after growth could no longer continue due to lack of a specific nutrient — nitrogen; this turned out not to be the case. PHB production was concurrent with growth and accumulated PHB would be consumed after the exogenous carbon source supplied was depleted.

This knowledge and understanding can inform the design of future experiments towards the development on a viable industrial production process of PHB from C1 substrates utilizing *M. trichosporium* OB3b.

8 Future work and recommendations

The expansion of the current model to incorporate the effect of increased carbon loads up to operational limits would be definitively beneficial. It would be expected that new interactions would be uncovered, and effects that were not significant under the conditions tested in this work could become relevant. These could be methanol toxicity or mass transfer limitations as the cell density, and thus methane and oxygen demand, increases.

The inclusion of the oxygen supply among the regressors of the model, to assess quantitatively its effects, would also be desirable. A numerical model that could predict the increase in accumulation of PHB depending on oxygen availability would provide important information in the design of the aeration systems of processes through, for example, enabling the cost-benefit analysis of increasing aeration.

Not only the addition of independent variables, but also of additional responses, should be considered. The use of variable amounts of supplied carbon would indeed require including specific carbon yield as a modeled response. Other not so obvious responses, such as average molecular weight and molecular weight distribution of the polymer, could also be explored.

Additional investigations to elucidate the mechanism for the increased accumulation of PHB under excess oxygen could also prove productive. Understanding the mechanisms involved can help make informed decisions – which could influence the costs involved in supplying huge amounts of aeration.

Help in elucidating these mechanisms, from an engineering point of view, can come from monitoring the nutrients during experiments. Obvious candidates are methanol, methane, ammonium, nitrate, oxygen and PHB concentrations. In the cases of methane and oxygen, both dissolved and headspace concentrations would be valuable monitored parameters.

Finally, moving forward and scaling up the experiments is in order. Given that the maximum PHB concentration is transient, it will pay off to identify the relevant point of maximum accumulation during the growth cycle, before depletion starts, and how it depends on the operating conditions. Steady-state operation under those conditions, even if there is no manifest nitrogen limitation is an alternative to

identifying the conditions for optimal accumulation of PHB. Fed-batch and continuous experiments would help gather important data in this respect.

References

Adegbola, O. (2008). "High cell density methanol cultivation of *Methylosinus trichosporium* OB3b". Master of Science (Engineering). Queen's University, 2008, .

Anderson, A. J., and Dawes, E. A. (1990). "Occurrence, metabolism, metabolic role, and industrial uses of bacterial polyhydroxyalkanoates." *Microbiol. Rev.,* 54(4), 450-472.

Asenjo, J. A., and Suk, J. S. (1986). "Microbial conversion of methane into poly-β-hydroxybutyrate (PHB): Growth and intracellular product accumulation in a type II methanotroph." *Journal of Fermentation Technology,* 64(4), 271-278.

Bodelier, P. L. E., and Laanbroek, H. J. (2004). "Nitrogen as a regulatory factor of methane oxidation in soils and sediments." *FEMS Microbiol. Ecol.,* 47(3), 265-277.

Bowman, J. P. (2005). "Family V. **Methylocystaceae** *fam. nov.*." *Bergey's Manual of Systematic Bacteriology,* D. J. Brenner, and J. T. Staley, eds., Springer, New York, 411-422.

Bowman, J. P., and Sayler, G. S. (1994). "Optimization and maintenance of soluble methane monoxygenase activity in *Methylosinus trichosporium* OB3b." *Biodegradation,* 5(1), 1-11.

Braunegg, G., Sonnleitner, B., and Lafferty, R. M. (1978). "A rapid gas chromatographic method for the determination of poly-β-hydroxybutyric acid in microbial biomass." *Eur. J. Appl. Microbiol. Biotechnol.,* 6(1), 29-37.

Byrom, D. (1987). "Polymer synthesis by microorganisms: technology and economics." *Trends Biotechnol.,* 5(9), 246-250.

Campbell, R. (2010). "notBoxPlot - alternative to box plots." .

Choi, J., and Lee, S. Y. (1997). "Process analysis and economic evaluation for poly(3-hydroxybutyrate) production by fermentation." *Bioprocess Eng.,* 17(6), 335-342.

Cornell, J. (2002). *Experiments with mixtures : Designs, models, and the analysis of mixture data.* Wiley, New York.

Dedysh, S. N., Ricke, P., and Liesack, W. (2004). "NifH and NifD phylogenies: an evolutionary basis for understanding nitrogen fixation capabilities of methanotrophic bacteria." *Microbiology,* 150 1301-1313.

Doronina, N. V., Ezhov, V. A., and Trotsenko, Y. A. (2008). "Growth of *Methylosinus trichosporium* OB3b on methane and poly-β-hydroxybutyrate biosynthesis." *Appl. Biochem. Microbiol.,* 44(2), 202-206.

Duan, C., Luo, M., and Xing, X. (2011). "High-rate conversion of methane to methanol by Methylosinus trichosporium OB3b." *Bioresour. Technol.,* 102(15), 7349-7353.

Dunfield, P., and Knowles, R. (1995). "Kinetics of inhibition of methane oxidation by nitrate, nitrite, and ammonium in a humisol." *Appl. Environ. Microbiol.,* 61(8), 3129-3135.

EPA. (2014). "Methane emissions." http://epa.gov/climatechange/ghgemissions/gases/ch4.html (October 1, 2014).

Holmes, P. A. (1988). "Biologically produced (R)-3-hydroxyalkanoate polymers and copolymers." *Developments in crystalline polymers,* D. C. Bassett, ed., Springer Netherlands, 1-65.

Hou, C. T. (1984). "Microbiology and biochemistry of methylotrophic bacteria." *Methylotrophs : microbiology, biochemistry, and genetics,* CRC Press, Boca Raton, Fla., 1-53.

Institute for Bioplastics and Biocomposites. (2014). "Material share of biopolymer production capacity sorted by material grade 2013." http://ifbb.wp.hs-hannover.de/downloads/content/Statistics/Market%20statistics/Production%20capacities/By%20material%20type/2013/Material%20share%20of%20biopolymer%20production%20capacity%20sorted%20by%20material%20grade%202013.png (August 26, 2015).

Kelly, D. P., and Wood, A. P. (2010). "Isolation and characterization of methanotrophs and methylotrophs: Diversity of methylotrophic organisms and of one-carbon substrates." *Handbook of Hydrocarbon and Lipid Microbiology,* Springer, Berlin, 3827-3845.

Khanna, S., and Srivastava, A. K. (2005). "Recent advances in microbial polyhydroxyalkanoates." *Process Biochemistry,* 40(2), 607-619.

Khosravi-Darani, K., Mokhtari, Z., Amai, T., and Tanaka, K. (2013). "Microbial production of poly(hydroxybutyrate) from C_1 carbon sources." *Appl. Microbiol. Biotechnol.,* 97(4), 1407-1424.

Kim, P., Kim, J., and Oh, D. (2003). "Improvement in cell yield of *Methylobacterium* sp. by reducing the inhibition of medium components for poly-β-hydroxybutyrate production." *World J. Microb. Biot.,* 19(4), 357-361.

Lee, S. Y. (1996). "Bacterial polyhydroxyalkanoates." *Biotechnol. Bioeng.,* 49(1), 1-14.

Lemoigne, M. (1926). "Produit de déshydratation et de polymérisation de l'acide β-oxybutyrique." *Bull. Soc. Chim. Biol.,* 8 770-782.

Lenz, R. W., and Marchessault, R. H. (2005). "Bacterial polyesters: Biosynthesis, biodegradable plastics and biotechnology." *Biomacromolecules,* 6(1), 1-8.

Lichtenthaler, F. W. (2000). "Carbohydrates as organic raw materials." *Ullmann's Encyclopedia of Industrial Chemistry,* Wiley, 583-616.

Lontoh, S., and Semrau, J. D. (1998). "Methane and trichloroethylene degradation by *Methylosinus trichosporium* OB3b expressing particulate methane monooxygenase." *Appl. Environ. Microbiol.,* 64(3), 1106-1114.

Luengo, J. M., García, B., Sandoval, A., Naharro, G., and Olivera, E. R. (2003). "Bioplastics from microorganisms." *Curr. Opin. Microbiol.,* 6(3), 251-260.

Madison, L. L., and Huisman, G. W. (1999). "Metabolic engineering of poly(3-hydroxyalkanoates): From DNA to plastic." *Microbiol. Mol. Biol. Rev.,* 63(1), 21-53.

Marvi, S. P. M., and Mahdi, M. (2011). "Thermoplastic biopolymer production (PHB, poly 3-hydroxybutyric acid) using secondary carbon source bioreactor based on nitrogen fixation biotechnology." *Bioresearch Bulletin,* 2(1), 20-34.

Mason, R. L., Gunst, R. F., and Hess, J. L. (2003). *Statistical design and analysis of experiments : With applications to engineering and science.* Wiley, Hoboken, New Jersey.

McCarty, P. L. (1975). "Stoichiometry of biological reactions." *Progress in Water Technology,* 7 157-172.

Murrell, J. C. (2010). "The aerobic methane oxidizing bacteria (methanotrophs)." *Handbook of Hydrocarbon and Lipid Microbiology,* K. N. Timmis, ed., Springer, Berlin, 1953-1966.

Myers, R. H., Montgomery, D. C., and Anderson-Cook, C. (2009). *Response surface methodology : process and product optimization using designed experiments.* Wiley, Hoboken, New Jersey.

NIST/SEMATECH. (2013). "NIST/SEMATECH e-handbook of statistical methods." http://www.itl.nist.gov/div898/handbook/ (May 1, 2015).

nova Institute for Ecology and Innovation. (2013). "Bio-based polymers – Production capacity will triple from 3.5 million tonnes in 2011 to nearly 12 million tonnes in 2020." http://news.bio-based.eu/bio-based-polymers-production-capacity-will-triple-from-3-5-million-tonnes-in-2011-to-nearly-12-million-tonnes-in-2020/ (August 27, 2015).

Oehmen, A., Keller-Lehmann, B., Zeng, R. J., Yuan, Z., and Keller, J. (2005). "Optimisation of poly-β-hydroxyalkanoate analysis using gas chromatography for enhanced biological phosphorus removal systems." *J. Chromatogr. A,* 1070(1-2), 131-136.

Park, S., Hanna, M. L., Taylor, R. T., and Droege, M. W. (1991). "Batch cultivation of *Methylosinus trichosporium* OB3b. I. Production of soluble methane monooxygenase." *Biotechnol. Bioeng.,* 38(4), 423-433.

Pieja, A. J., Sundstrom, E. R., and Criddle, C. S. (2012). "Cyclic, alternating methane and nitrogen limitation increases PHB production in a methanotrophic community." *Bioresour. Technol.,* 107 385-392.

Pieja, A. J., Sundstrom, E. R., and Criddle, C. S. (2011). "Poly-3-hydroxybutyrate metabolism in the type II methanotroph *Methylocystis parvus* OBBP." *Appl. Environ. Microbiol.,* 77(17), 6012-6019.

Rostkowski, K. H., Pfluger, A. R., and Criddle, C. S. (2013). "Stoichiometry and kinetics of the PHB-producing type II methanotrophs *Methylosinus trichosporium* OB3b and *Methylocystis parvus* OBBP." *Bioresour. Technol.,* 132 71-77.

Serafim, L. S., Lemos, P. C., Oliveira, R., and Reis, M. A. M. (2004). "Optimization of polyhydroxybutyrate production by mixed cultures submitted to aerobic dynamic feeding conditions." *Biotechnol. Bioeng.,* 87(2), 145-160.

Shah, N. N., Hanna, M. L., and Taylor, R. T. (1996). "Batch cultivation of *Methylosinus trichosporium* OB3b: V. Characterization of poly-β-hydroxybutyrate production under methane-dependent growth conditions." *Biotechnol. Bioeng.,* 49(2), 161-171.

Statista. (2014). "Global production of plastics 1990-2013." http://www.statista.com/statistics/282732/global-production-of-plastics-since-1950/ (September 6, 2015).

Stein, L. Y., Yoon, S., Semrau, J. D., DiSpirito, A. A., Crombie, A., Murrell, J. C., Vuilleumier, S., Kalyuzhnaya, M. G., Op den Camp, Huub J.M., Bringel, F., Bruce, D., Cheng, J. -., Copeland, A., Goodwin, L., Han, S., Hauser, L., Jetten, M. S. M., Lajus, A., Land, M. L., Lapidus, A., Lucas, S., Médigue, C., Pitluck, S., Woyke, T., Zeytun, A., and Klotz, M. G. (2010). "Genome sequence of the obligate methanotroph *Methylosinus trichosporium* strain OB3b." *J. Bacteriol.,* 192(24), 6497-6498.

Veillette, M., Viens, P., Avalos Ramirez, A., Brzezinski, R., and Heitz, M. (2011). "Effect of ammonium concentration on microbial population and performance of a biofilter treating air polluted with methane." *Chem. Eng. J.,* 171(3), 1114-1123.

Volova, T. G. (2004). *Polyhydroxyalkanoates - Plastic materials of the 21st century: Production, properties and application.* Nova Science Publishers, New York.

Vorob'ev, A., and Dedysh, S. (2008). "Inadequacy of enrichment culture technique for assessing the structure of methanotrophic communities in peat soil." *Microbiology,* 77(4), 504-507.

Wendlandt, K. -., Jechorek, M., Helm, J., and Stottmeister, U. (2001). "Producing poly-3-hydroxybutyrate with a high molecular mass from methane." *J.Biotechnol.,* 86(2), 127-133.

Whitman, W. B., Coleman, D. C., and Wiebe, W. J. (1998). "Prokaryotes: The unseen majority." *Proc. Natl. Acad. Sci. U.S.A.,* 95(12), 6578-6583.

Whittenbury, R., Phillips, K. C., and Wilkinson, J. F. (1970). "Enrichment, isolation and some properties of methane-utilizing bacteria." *J.Gen.Microbiol.,* 61(2), 205-218.

Yu, Y., Ramsay, J. A., and Ramsay, B. A. (2009). "Production of soluble methane monooxygenase during growth of *Methylosinus trichosporium* on methanol." *J. Biotechnol.,* 139(1), 78-83.

Appendix A. License for copyrighted material

Table 2-1 was reprinted from *Bioresource Technology*, 132 (2013), Rostkowski, K. H., Pfluger, A. R., and Criddle, C. S., "Stoichiometry and kinetics of the PHB-producing type II methanotrophs *Methylosinus trichosporium* OB3b and *Methylocystis parvus* OBBP.", 71-77, Copyright (2013), with permission from Elsevier.

ELSEVIER LICENSE
TERMS AND CONDITIONS

Sep 12, 2015

This is a License Agreement between Jorge Zaldivar ("You") and Elsevier ("Elsevier") provided by Copyright Clearance Center ("CCC"). The license consists of your order details, the terms and conditions provided by Elsevier, and the payment terms and conditions.

All payments must be made in full to CCC. For payment instructions, please see information listed at the bottom of this form.

Supplier	Elsevier Limited The Boulevard,Langford Lane Kidlington,Oxford,OX5 1GB,UK
Registered Company Number	1982084
Customer name	Jorge Zaldivar
Customer address	7th Floor, ECERF Edmonton, AB T6G 2V4
License number	3704650384512
License date	Sep 08, 2015
Licensed content publisher	Elsevier
Licensed content publication	Bioresource Technology
Licensed content title	Stoichiometry and kinetics of the PHB-producing Type II methanotrophs Methylosinus trichosporium OB3b and Methylocystis parvus OBBP
Licensed content author	Katherine H. Rostkowski,Andrew R. Pfluger,Craig S. Criddle
Licensed content date	March 2013
Licensed content volume number	132
Licensed content issue number	n/a
Number of pages	7
Start Page	71
End Page	77
Type of Use	reuse in a thesis/dissertation
Portion	figures/tables/illustrations
Number of figures/tables/illustrations	1
Format	electronic
Are you the author of this Elsevier article?	No
Will you be translating?	No
Original figure numbers	Table 1
Title of your thesis/dissertation	Optimization of PHB production in Methylosinus trichosporium OB3b

Expected completion date	Sep 2015
Estimated size (number of pages)	
Elsevier VAT number	GB 494 6272 12
Permissions price	0.00 CAD
VAT/Local Sales Tax	0.00 CAD / 0.00 GBP
Total	0.00 CAD
Terms and Conditions	

INTRODUCTION

1. The publisher for this copyrighted material is Elsevier. By clicking "accept" in connection with completing this licensing transaction, you agree that the following terms and conditions apply to this transaction (along with the Billing and Payment terms and conditions established by Copyright Clearance Center, Inc. ("CCC"), at the time that you opened your Rightslink account and that are available at any time at http://myaccount.copyright.com).

GENERAL TERMS

2. Elsevier hereby grants you permission to reproduce the aforementioned material subject to the terms and conditions indicated.

3. Acknowledgement: If any part of the material to be used (for example, figures) has appeared in our publication with credit or acknowledgement to another source, permission must also be sought from that source. If such permission is not obtained then that material may not be included in your publication/copies. Suitable acknowledgement to the source must be made, either as a footnote or in a reference list at the end of your publication, as follows:

"Reprinted from Publication title, Vol /edition number, Author(s), Title of article / title of chapter, Pages No., Copyright (Year), with permission from Elsevier [OR APPLICABLE SOCIETY COPYRIGHT OWNER]." Also Lancet special credit - "Reprinted from The Lancet, Vol. number, Author(s), Title of article, Pages No., Copyright (Year), with permission from Elsevier."

4. Reproduction of this material is confined to the purpose and/or media for which permission is hereby given.

5. Altering/Modifying Material: Not Permitted. However figures and illustrations may be altered/adapted minimally to serve your work. Any other abbreviations, additions, deletions and/or any other alterations shall be made only with prior written authorization of Elsevier Ltd. (Please contact Elsevier at permissions@elsevier.com)

6. If the permission fee for the requested use of our material is waived in this instance, please be advised that your future requests for Elsevier materials may attract a fee.

7. Reservation of Rights: Publisher reserves all rights not specifically granted in the combination of (i) the license details provided by you and accepted in the course of this licensing transaction, (ii) these terms and conditions and (iii) CCC's Billing and Payment terms and conditions.

8. License Contingent Upon Payment: While you may exercise the rights licensed immediately upon issuance of the license at the end of the licensing process for the transaction, provided that you have disclosed complete and accurate details of your proposed use, no license is finally effective unless and until full payment is received from you (either by publisher or by CCC) as provided in CCC's Billing and Payment terms and conditions. If full payment is not received on a timely basis, then any license preliminarily granted shall be deemed automatically revoked and shall be void as if never granted. Further, in the event that you breach any of these terms and conditions or any of CCC's Billing and Payment terms and conditions, the license is automatically revoked and shall be void as if never granted. Use of materials as described in a revoked license, as well as any use of the materials beyond the scope of an unrevoked license, may constitute copyright infringement and publisher reserves the right to take any and all action to protect its copyright in the materials.

9. Warranties: Publisher makes no representations or warranties with respect to the licensed material.

10. Indemnity: You hereby indemnify and agree to hold harmless publisher and CCC, and their respective officers, directors, employees and agents, from and against any and all claims arising out of your use of the licensed material other than as specifically authorized pursuant to this license.

11. No Transfer of License: This license is personal to you and may not be sublicensed, assigned, or transferred by you to any other person without publisher's written permission.

12. No Amendment Except in Writing: This license may not be amended except in a writing signed by both parties (or, in the case of publisher, by CCC on publisher's behalf).

13. Objection to Contrary Terms: Publisher hereby objects to any terms contained in any purchase order, acknowledgment, check endorsement or other writing prepared by you, which terms are inconsistent with these terms and conditions or CCC's Billing and Payment terms and conditions. These terms and conditions, together with CCC's Billing and Payment terms and conditions (which are incorporated herein), comprise the entire agreement between you and publisher (and CCC) concerning this licensing transaction. In the event of any conflict between your obligations established by these terms and conditions and those established by CCC's Billing and Payment terms and conditions, these terms and conditions shall control.

14. Revocation: Elsevier or Copyright Clearance Center may deny the permissions described in this License at their sole discretion, for any reason or no reason, with a full refund payable to you. Notice of such denial will be made using the contact information provided by you. Failure to receive such notice will not alter or invalidate the denial. In no event will Elsevier or Copyright Clearance Center be responsible or liable for any costs, expenses or damage incurred by you as a result of a denial of your permission request, other than a refund of the amount(s) paid by you to Elsevier and/or Copyright Clearance Center for denied permissions.

LIMITED LICENSE

The following terms and conditions apply only to specific license types:

15. **Translation**: This permission is granted for non-exclusive world **English** rights only unless your license was granted for translation rights. If you licensed translation rights you may only translate this content into the languages you requested. A professional translator

must perform all translations and reproduce the content word for word preserving the integrity of the article. If this license is to re-use 1 or 2 figures then permission is granted for non-exclusive world rights in all languages.

16. **Posting licensed content on any Website**: The following terms and conditions apply as follows: Licensing material from an Elsevier journal: All content posted to the web site must maintain the copyright information line on the bottom of each image; A hyper-text must be included to the Homepage of the journal from which you are licensing at http://www.sciencedirect.com/science/journal/xxxxx or the Elsevier homepage for books at http://www.elsevier.com; Central Storage: This license does not include permission for a scanned version of the material to be stored in a central repository such as that provided by Heron/XanEdu.

Licensing material from an Elsevier book: A hyper-text link must be included to the Elsevier homepage at http://www.elsevier.com . All content posted to the web site must maintain the copyright information line on the bottom of each image.

Posting licensed content on Electronic reserve: In addition to the above the following clauses are applicable: The web site must be password-protected and made available only to bona fide students registered on a relevant course. This permission is granted for 1 year only. You may obtain a new license for future website posting.

17. **For journal authors:** the following clauses are applicable in addition to the above:

Preprints:

A preprint is an author's own write-up of research results and analysis, it has not been peer-reviewed, nor has it had any other value added to it by a publisher (such as formatting, copyright, technical enhancement etc.).

Authors can share their preprints anywhere at any time. Preprints should not be added to or enhanced in any way in order to appear more like, or to substitute for, the final versions of articles however authors can update their preprints on arXiv or RePEc with their Accepted Author Manuscript (see below).

If accepted for publication, we encourage authors to link from the preprint to their formal publication via its DOI. Millions of researchers have access to the formal publications on ScienceDirect, and so links will help users to find, access, cite and use the best available version. Please note that Cell Press, The Lancet and some society-owned have different preprint policies. Information on these policies is available on the journal homepage.

Accepted Author Manuscripts: An accepted author manuscript is the manuscript of an article that has been accepted for publication and which typically includes author-incorporated changes suggested during submission, peer review and editor-author communications.

Authors can share their accepted author manuscript:

- immediately
    - via their non-commercial person homepage or blog
    - by updating a preprint in arXiv or RePEc with the accepted manuscript

- via their research institute or institutional repository for internal institutional uses or as part of an invitation-only research collaboration work-group
- directly by providing copies to their students or to research collaborators for their personal use
- for private scholarly sharing as part of an invitation-only work group on commercial sites with which Elsevier has an agreement

– after the embargo period

- via non-commercial hosting platforms such as their institutional repository
- via commercial sites with which Elsevier has an agreement

In all cases accepted manuscripts should:

– link to the formal publication via its DOI

– bear a CC-BY-NC-ND license - this is easy to do

– if aggregated with other manuscripts, for example in a repository or other site, be shared in alignment with our hosting policy not be added to or enhanced in any way to appear more like, or to substitute for, the published journal article.

Published journal article (JPA): A published journal article (PJA) is the definitive final record of published research that appears or will appear in the journal and embodies all value-adding publishing activities including peer review co-ordination, copy-editing, formatting, (if relevant) pagination and online enrichment.

Policies for sharing publishing journal articles differ for subscription and gold open access articles:

Subscription Articles: If you are an author, please share a link to your article rather than the full-text. Millions of researchers have access to the formal publications on ScienceDirect, and so links will help your users to find, access, cite, and use the best available version.

Theses and dissertations which contain embedded PJAs as part of the formal submission can be posted publicly by the awarding institution with DOI links back to the formal publications on ScienceDirect.

If you are affiliated with a library that subscribes to ScienceDirect you have additional private sharing rights for others' research accessed under that agreement. This includes use for classroom teaching and internal training at the institution (including use in course packs and courseware programs), and inclusion of the article for grant funding purposes.

Gold Open Access Articles: May be shared according to the author-selected end-user license and should contain a CrossMark logo, the end user license, and a DOI link to the formal publication on ScienceDirect.

Please refer to Elsevier's posting policy for further information.

18. **For book authors** the following clauses are applicable in addition to the above: Authors are permitted to place a brief summary of their work online only. You are not allowed to download and post the published electronic version of your chapter, nor may you

scan the printed edition to create an electronic version. **Posting to a repository:** Authors are permitted to post a summary of their chapter only in their institution's repository.

19. **Thesis/Dissertation**: If your license is for use in a thesis/dissertation your thesis may be submitted to your institution in either print or electronic form. Should your thesis be published commercially, please reapply for permission. These requirements include permission for the Library and Archives of Canada to supply single copies, on demand, of the complete thesis and include permission for Proquest/UMI to supply single copies, on demand, of the complete thesis. Should your thesis be published commercially, please reapply for permission. Theses and dissertations which contain embedded PJAs as part of the formal submission can be posted publicly by the awarding institution with DOI links back to the formal publications on ScienceDirect.

Elsevier Open Access Terms and Conditions

You can publish open access with Elsevier in hundreds of open access journals or in nearly 2000 established subscription journals that support open access publishing. Permitted third party re-use of these open access articles is defined by the author's choice of Creative Commons user license. See our open access license policy for more information.

Terms & Conditions applicable to all Open Access articles published with Elsevier:

Any reuse of the article must not represent the author as endorsing the adaptation of the article nor should the article be modified in such a way as to damage the author's honour or reputation. If any changes have been made, such changes must be clearly indicated.

The author(s) must be appropriately credited and we ask that you include the end user license and a DOI link to the formal publication on ScienceDirect.

If any part of the material to be used (for example, figures) has appeared in our publication with credit or acknowledgement to another source it is the responsibility of the user to ensure their reuse complies with the terms and conditions determined by the rights holder.

Additional Terms & Conditions applicable to each Creative Commons user license:

CC BY: The CC-BY license allows users to copy, to create extracts, abstracts and new works from the Article, to alter and revise the Article and to make commercial use of the Article (including reuse and/or resale of the Article by commercial entities), provided the user gives appropriate credit (with a link to the formal publication through the relevant DOI), provides a link to the license, indicates if changes were made and the licensor is not represented as endorsing the use made of the work. The full details of the license are available at http://creativecommons.org/licenses/by/4.0.

CC BY NC SA: The CC BY-NC-SA license allows users to copy, to create extracts, abstracts and new works from the Article, to alter and revise the Article, provided this is not done for commercial purposes, and that the user gives appropriate credit (with a link to the formal publication through the relevant DOI), provides a link to the license, indicates if changes were made and the licensor is not represented as endorsing the use made of the work. Further, any new works must be made available on the same conditions. The full details of the license are available at http://creativecommons.org/licenses/by-nc-sa/4.0.

CC BY NC ND: The CC BY-NC-ND license allows users to copy and distribute the Article, provided this is not done for commercial purposes and further does not permit distribution of the Article if it is changed or edited in any way, and provided the user gives appropriate credit (with a link to the formal publication through the relevant DOI), provides a link to the license, and that the licensor is not represented as endorsing the use made of the work. The full details of the license are available at http://creativecommons.org/licenses/by-nc-nd/4.0. Any commercial reuse of Open Access articles published with a CC BY NC SA or CC BY NC ND license requires permission from Elsevier and will be subject to a fee.

Commercial reuse includes:

- Associating advertising with the full text of the Article
- Charging fees for document delivery or access
- Article aggregation
- Systematic distribution via e-mail lists or share buttons

Posting or linking by commercial companies for use by customers of those companies.

20. **Other Conditions**:

v1.7

Questions? customercare@copyright.com or +1-855-239-3415 (toll free in the US) or +1-978-646-2777.

Appendix B. Growth experiment of *M. trichosporium* OB3b

Table B-1 show the conditions under which each of the 24 treatments for the M. trichosporium OB3b growth experiment were run and the results obtained for each of the replicates, and Figure B-1 to Figure B-3 show the corresponding growth curves.

Table B-1. Conditions and results from the growth experiment of *M. trichosporium* OB3b.

Treatment	C source	N source	N:C ratio	Inoculum	Final ODs		
1	CH_3OH	NH_4^+	high	aged	0.204	0.197	0.177
2	CH_3OH	NH_4^+	high	fresh	0.190	0.187	0.171
3	CH_4	NH_4^+	high	aged	0.350	0.310	0.334
4	CH_4	NH_4^+	high	fresh	0.339	0.348	0.322
5	CH_3OH	NH_4^+	low	aged	0.191	0.201	0.187
6	CH_3OH	NH_4^+	low	fresh	0.231	0.211	0.232
7	CH_4	NH_4^+	low	aged	0.360	0.352	0.350
8	CH_4	NH_4^+	low	fresh	0.344	0.338	0.356
9	CH_3OH	NO_3^-	high	aged	0.153	0.167	0.160
10	CH_3OH	NO_3^-	high	fresh	0.135	0.156	0.176
11	CH_4	NO_3^-	high	aged	0.284	0.289	0.300
12	CH_4	NO_3^-	high	fresh	0.256	0.292	0.276
13	CH_3OH	NO_3^-	low	aged	0.168	0.191	0.161
14	CH_3OH	NO_3^-	low	fresh	0.185	0.217	0.190
15	CH_4	NO_3^-	low	aged	0.290	0.284	0.299
16	CH_4	NO_3^-	low	fresh	0.236	0.291	0.285
17	CH_3OH	NH_4^+	high	aged	0.184	0.164	
18	CH_3OH	NH_4^+	low	aged	0.180	0.199	
19	CH_3OH	NO_3^-	high	aged	0.158	0.168	
20	CH_3OH	NO_3^-	low	aged	0.174	0.167	
21	CH_3OH	NH_4^+	high	fresh	0.229	0.217	
22	CH_3OH	NH_4^+	low	fresh	0.228	0.251	
23	CH_3OH	NO_3^-	high	fresh	0.192	0.172	
24	CH_3OH	NO_3^-	low	fresh	0.208	0.208	

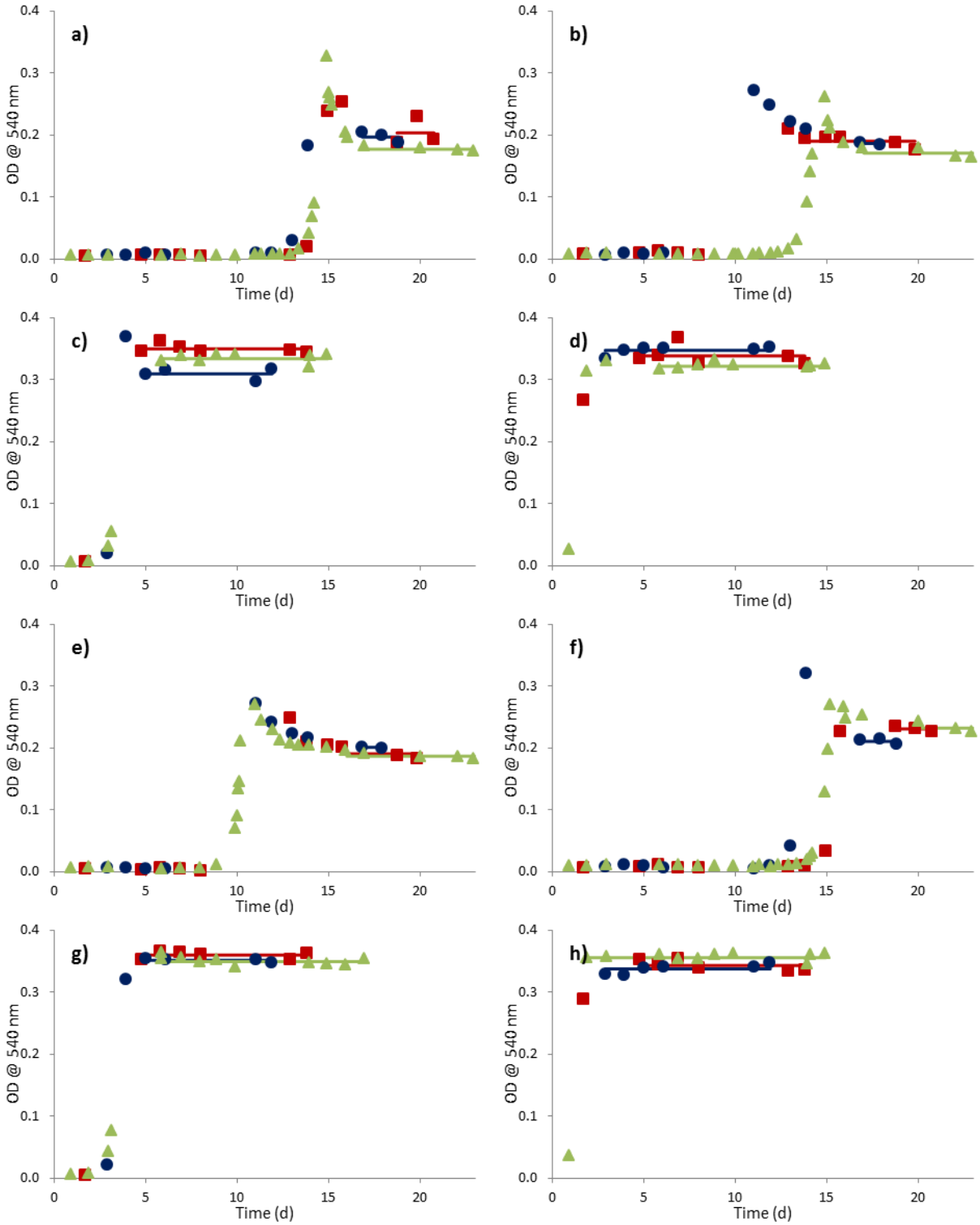

Figure B-1. Growth curves for cultures of *M. trichosporium* OB3b under different conditions. Each symbol and color represents a different replicate. The horizontal lines in matching colors represent the average final optical density calculated from the corresponding data points. The treatment numbers correspond to those listed in Table B-1. (a) Treatment 1. (b) Treatment 2. (c) Treatment 3. (d) Treatment 4. (e) Treatment 5. (f) Treatment 6. (g) Treatment 7. (h) Treatment 8.

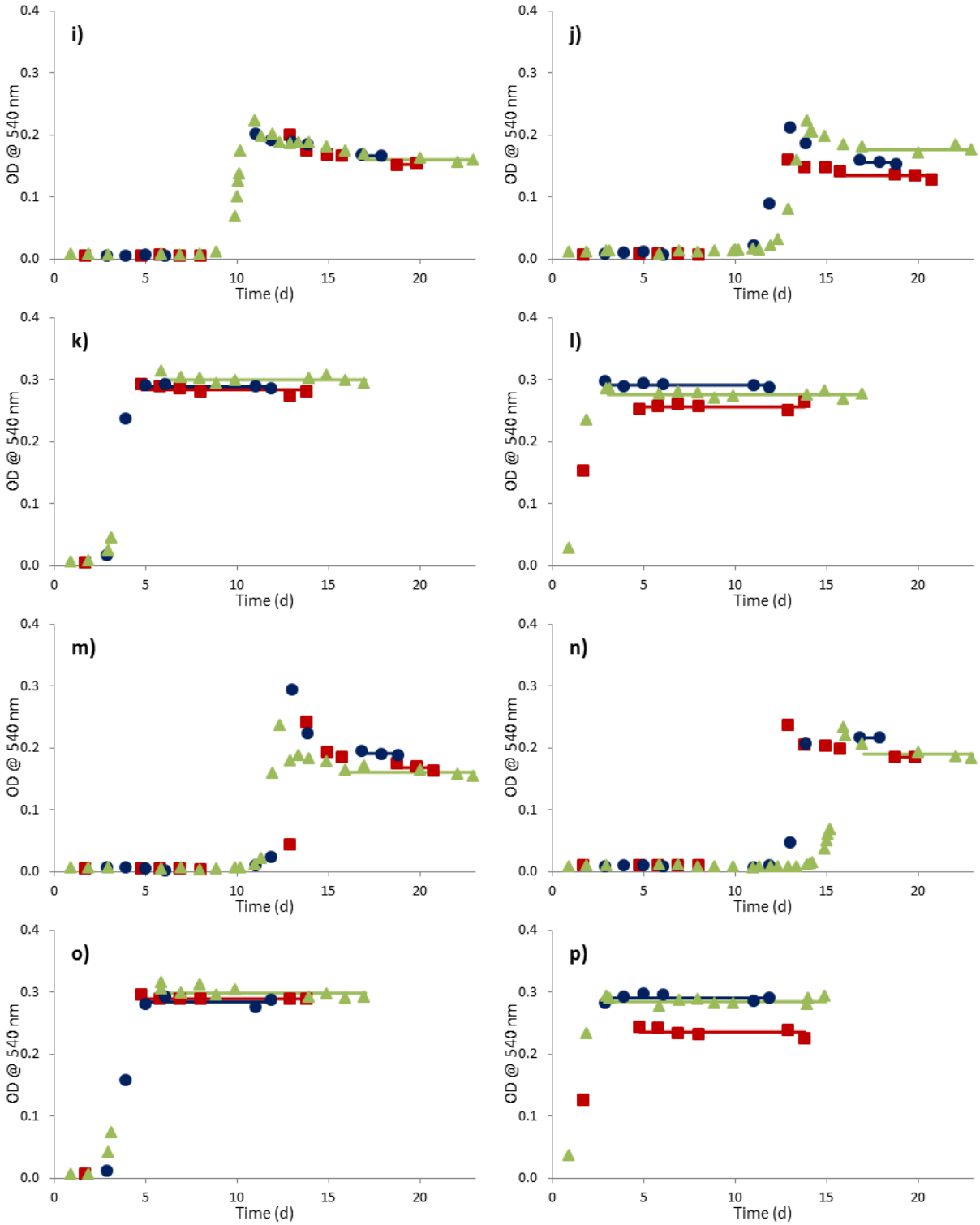

Figure B-2. Growth curves for cultures of *M. trichosporium* OB3b under different conditions (continued). Each symbol and color represents a different replicate. The horizontal lines in matching colors represent the average final optical density calculated from the corresponding data points. The treatment numbers correspond to those listed in Table B-1. (i) Treatment 9. (j) Treatment 10. (k) Treatment 11. (l) Treatment 12. (m) Treatment 13. (n) Treatment 14. (o) Treatment 15. (p) Treatment 16.

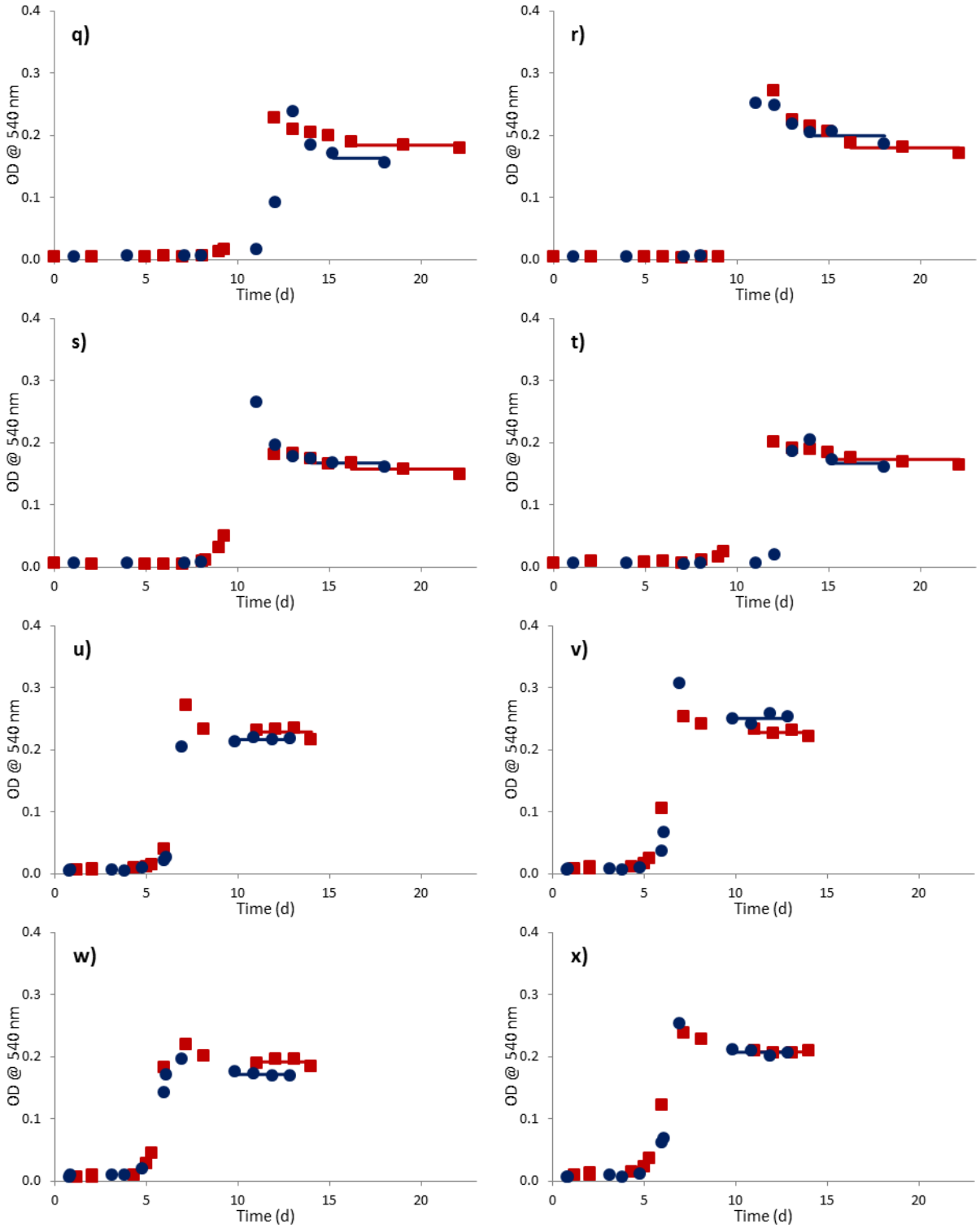

Figure B-3. Growth curves for cultures of *M. trichosporium* OB3b under different conditions (continued). Each symbol and color represents a different replicate. The horizontal lines in matching colors represent the average final optical density calculated from the corresponding data points. The treatment numbers correspond to those listed in Table B-1.
(q) Treatment 17. (r) Treatment 18. (s) Treatment 19. (t) Treatment 20. (u) Treatment 21. (v) Treatment 22. (w) Treatment 23. (x) Treatment 24.

Appendix C. Response surfaces for PHB cell content

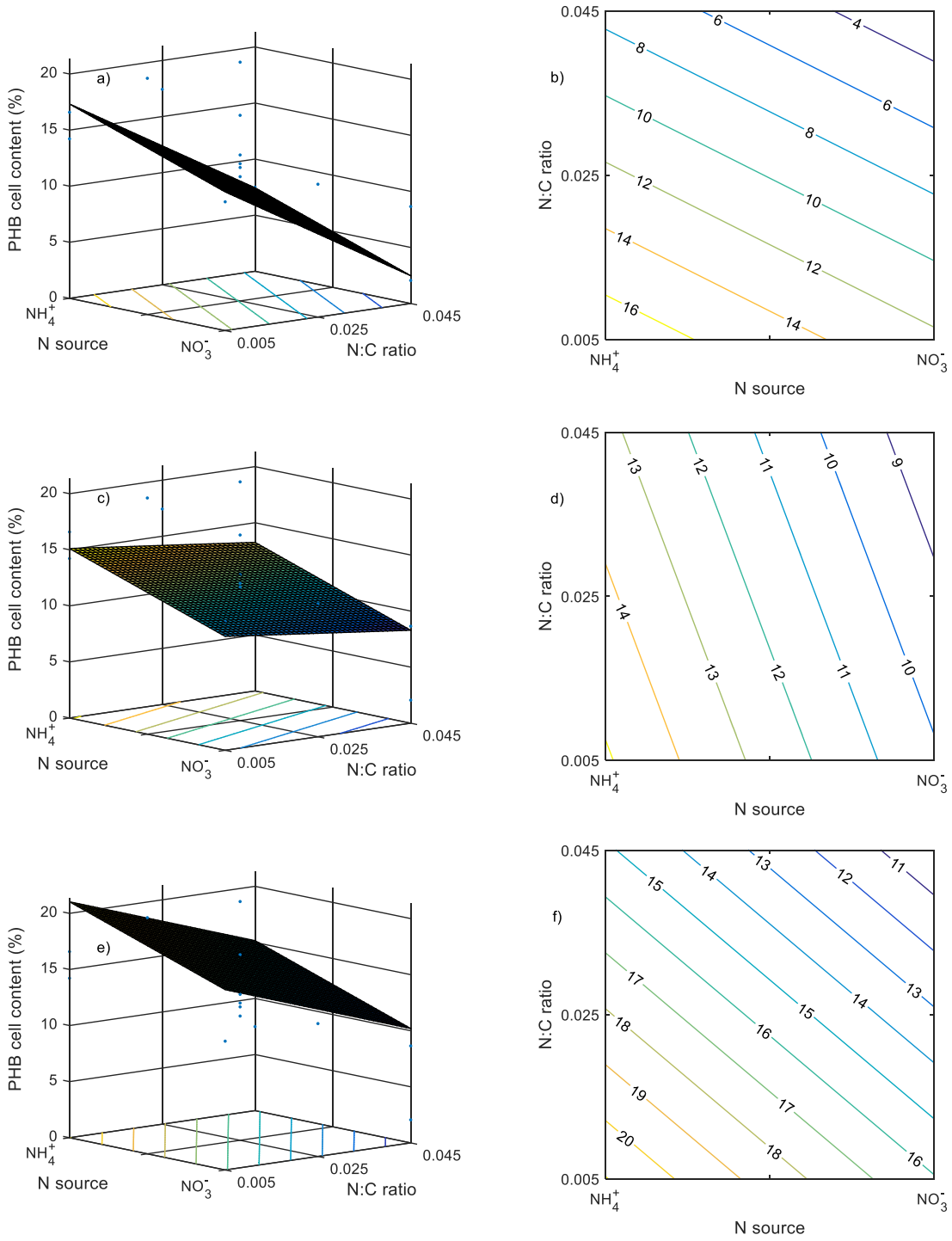

Figure C-1. Response surfaces (a, c, e) and contour plots (b, d, f) for PHB cell content for different values of x_1 (carbon source): Methane, $x_1 = -1$ (a, b); methanol, $x_1 = 1$ (c, d), and equimolar mixture of methane and methanol, $x_1 = 0$ (e, f).

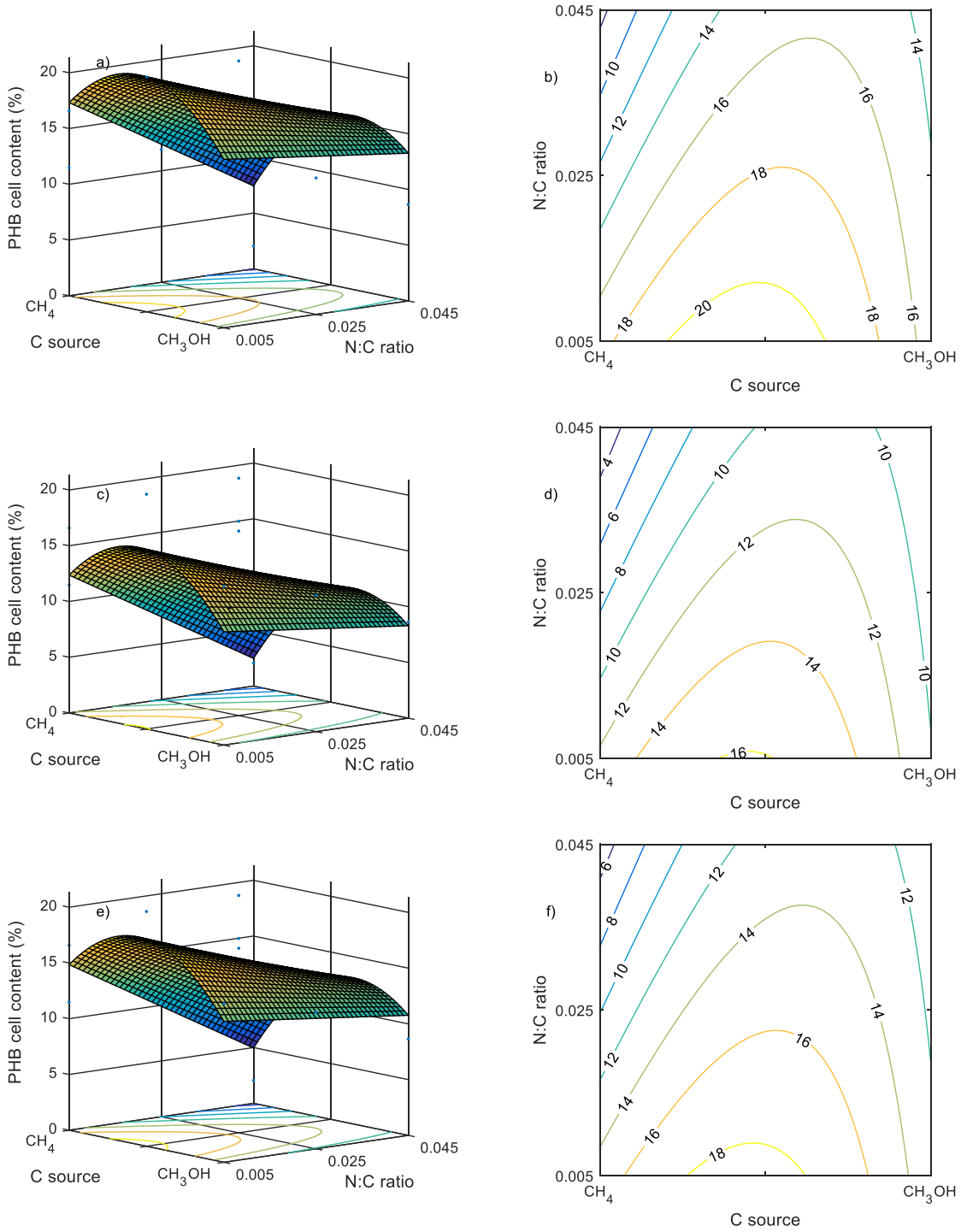

Figure C-2. Response surfaces (a, c, e) and contour plots (b, d, f) for PHB cell content for different values of x_2 (nitrogen source): Ammonium, $x_2 = -1$ (a, b); nitrate, $x_2 = 1$ (c, d), and equimolar mixture of ammonium and nitrate, $x_2 = 0$ (e, f).

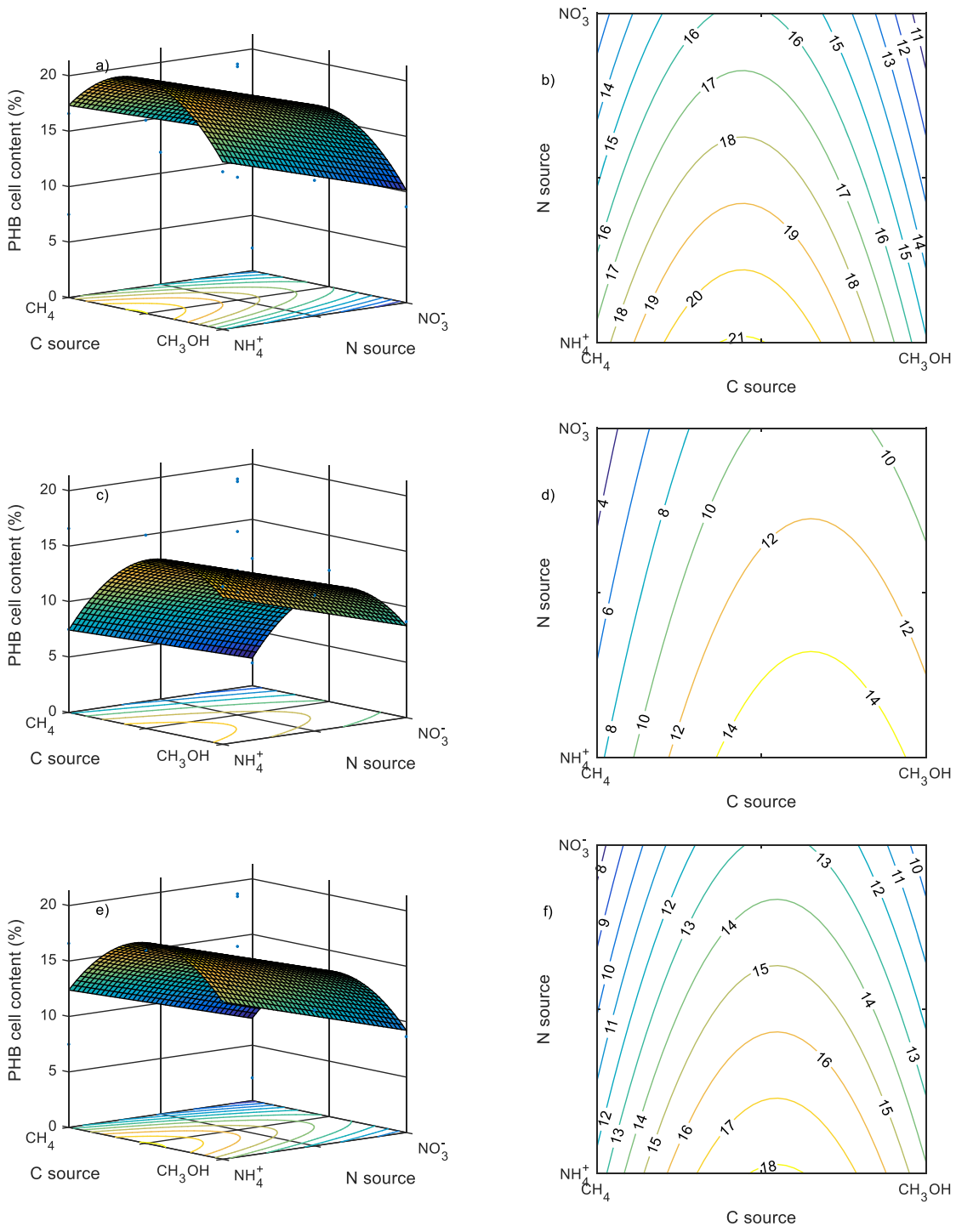

Figure C-3. Response surfaces (a, c, e) and contour plots (b, d, f) for PHB cell content for different values of x_3 (nitrogen-to-carbon ratio): 0.005, $x_3 = -1$ (a, b); 0.045, $x_3 = 1$ (c, d), and 0.025, $x_3 = 0$ (e, f).